5-8-2014

Bimodal Approach Using Spectroscopy and Digitial Imaging to Assist Otitis Media Diagnosis

Kaitlyn M. Longo
University of Connecticut - Storrs, klongo91@gmail.com

Bimodal Approach Using Spectroscopy and Digital Imaging to Assist Otitis Media Diagnosis

Kaitlyn Longo

B.S., University of Connecticut, Biomedical Engineering, May 2012

A Thesis

Submitted in Partial Fulfillment of the

Requirements for the Degree of

Master of Science

at the

University of Connecticut

May 2014

APPROVAL PAGE

Master of Science Thesis

Bimodal Approach using Spectroscopy and Digitial Imaging to Assist Otitis Media Diagnosis

Presented By

Kaitlyn Longo, B.S.

Major Advisor_____
Dr. Donald R. Peterson

Associate Advisor_____
Tulio A. Valdez, MD

Associate Advisor_____
Martin G. Cherniack, MD

University of Connecticut

2014

Acknowledgments

This work was made possible thanks to Tulio A. Valdez, Dr. Donald Peterson, and Dr. Martin Cherniack. I would like to thank each of them for their time and assistance in making this project possible.

Table of Contents

List of Figures

List of Tables

Abstract

Otitis Media is defined as inflammation of the middle ear region associated with middle ear fluid. This condition typically follows an upper respiratory infection, is commonly misdiagnosed by physicians and can potentially lead to the inappropriate use of antimicrobial agents. [1] This thesis describes the design of a novel medical device that utilized spectroscopy and digital imaging to provide physicians with a unique representation of the middle ear. Published literature has been reviewed to assess the different approaches that researchers have studied to improve the diagnosis of otitis media, where, for example, research conducted by Thorton et al. and Boppart et al. used fluorescence to identify bacteria contained in biofilms.[12,13] In addition, a population study conducted by Jensen et al. determined what the level of diagnostic certainty is in pediatric patients and determined that general practitioners had a diagnostic certainty of 58% in patients under one year of age and 73% certainty in patients over two and a half years of age.[9]

Eleven subjects, each with a history of recurrent acute otitis media and requiring myringotomy and ear tube placement, were selected for study in this thesis. All subjects received a digital imaging and spectroscopy examination using the device at the time of surgery. Five excitation and illumination wavelengths were used, including white light, 385-420 nm, 450-470 nm, 520-535 nm, and 640-650 nm as well as fluorescence imaging using 425 nm and 450 nm filters. Each of the chosen wavelengths were emitted into the ear canal and tympanic membrane during a typical otoscopic examination. Signal processing techniques were also applied to isolate various regions of the tympanic membrane using MatLAB to increase the resolution of the anatomical and physiological properties of the tympanic membrane.

The spectral readings between the wavelengths of 560 nm and 760 nm were plotted for each subject and were classified according to fluid retention, consistency, and vascularity. In this subject population, eight of the 22 ears were identified to be a noneffusion normal. Reflectance of keratin, cerumen, and bone, with well defined blood vessels and contrast, allowed for better characterization of the middle ear. [8] Reflectance spectra were classified according to fluid consistency and trends were determined for non effusion and effusion patients. Class one spectra were defined as tympanic membrane and canal spectra with a rapid increase in percent reflection between 575 nm and 650 nm and a rapid decrease in percent reflection between 650 nm and 750 nm. Class two spectra were defined as tympanic membrane and canal spectra with a gradual decrease in percent reflection between 575 nm and 800 nm. This novel device was successfully used to detect effusion consistency and color and it will continue to aid in the development of a new diagnostic procedure. It provides a means for the creation of a new diagnostic procedure that may be useful in assisting a physician in making an accurate diagnosis, and as a result, increase the diagnostic certainty.

1.0 Introduction

Otitis Media is characterized by the presence of fluid in the middle ear often following an upper respiratory infection and commonly affects infants and toddlers between ten months and four years of age. Physicians and ear, nose, and throat (ENT) specialists consistently misdiagnose otitis media, potentially leading to the inappropriate use of microbial agents which could hinder the well-being of the child .[1] Studies show that Acute Otitis Media resulted in 8.8 million cases; costing $2.8 billion on health care costs, $1.8 billion on ambulatory visits, and $.4 billion on over the counter prescriptions in 2006. [2] The number of acute otitis media cases justifies development of a method capable of assisting physicians to determine the diagnosis with increased diagnostic certainty. A new diagnostic method to facilitate in the diagnosis of otitis media in pediatric patients is presented to provide physicians with a tool that will assist otitis media diagnosis.

Red and swollen tympanic membranes are not the only characteristics of infection that should be considered for diagnosis of otitis media. The novel design of an otoscope presented in this thesis entailed the design of a device that utilized spectroscopy and fluorescence imaging to provide physicians with a tool that uniquely represents the middle ear to enhance the infection's characteristics. The enhanced characteristics of the tympanic membrane could potentially allow the user to determine whether or not there is infected fluid present which requires antibiotics due to the fluorescence and spectroscopy functions of the otoscope design.

There are three types of otitis media that are typically diagnosed in the pediatric population. Acute otitis media (AOM) is a condition that is characterized by inflammation of the middle ear and diagnosed after an upper respiratory infection or fever. Acute otitis media is characterized by

infected fluid behind the tympanic membrane and is commonly associated with otalgia, otorrhea, headache, and vomiting. Otitis media with effusion (OME) often follows a case of acute otitis media and is associated with sterile fluid retained in the middle ear region. [5] This type of otitis media is very hard to diagnose and is often mis diagnosed by practitioners due to the lack of acute symptoms. Otitis media with effusion can also lead to hearing loss, tinnitus, vertigo, and otalgia. [5] The fluid retained in the middle ear region may drain on its own over the course of a few weeks but will result in conductive hearing loss if the condition continued. [5]

Acute otitis media can benefit from the prescription of antibiotics; however, antibiotic treatment is not indicated for otitis media with effusion. Physicians must be capable of distinguishing between acute otitis media and otitis media with effusion because each condition does not have the same treatment when diagnosed correctly. General practitioners may diagnose a red, swollen tympanic membrane as otitis media; however, the determination of infected or non infected fluid is required to confirm the specific diagnosis. A whiteish-yellow bulging tympanic membrane is generally observed with acute otitis media due to the presence of pus and is more frequently correctly diagnosed by physicians.

The anatomical structure of the middle ear and Eustachian tube provides insight as to why otitis media is most commonly found in pediatric patients rather than an older population. The Eustachian tube is horizontally positioned allowing for inadequate pressure equalization and possible fluid retention in the middle ear during the first years of life. An initial respiratory infection and disruption of the Eustachian tube may lead to fluid retention due to the horizontal position. A swollen Eustachian tube may act as a suction to retain viral or bacterial fluid in the middle ear space when an effusion is present. The Eustachian tube will mature to a vertical

position to allow for better pressure equalization and fluid drainage as a child's internal anatomy matures.

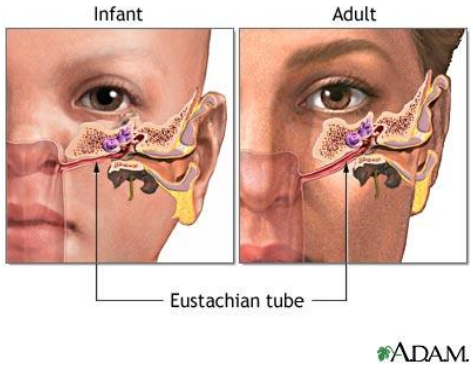

Figure 1: Comparison of an Infant and Adult Eustachian Tube [6]

Patients that have recurrent acute otitis media or persistent OME affecting speech or hearing loss receive a myringotomy and tubes. The myringotomy and tubes procedure is completed for pressure equalization and fluid drainage in the middle ear region. The procedure begins with the insertion of an ear tube through an incision in the tympanic membrane as in Figure 2. The ear tube will allow air to enter the middle ear region and subsequently prevent additional fluid from accumulating. The ear tubes fall out after approximately six to twelve months. [7]

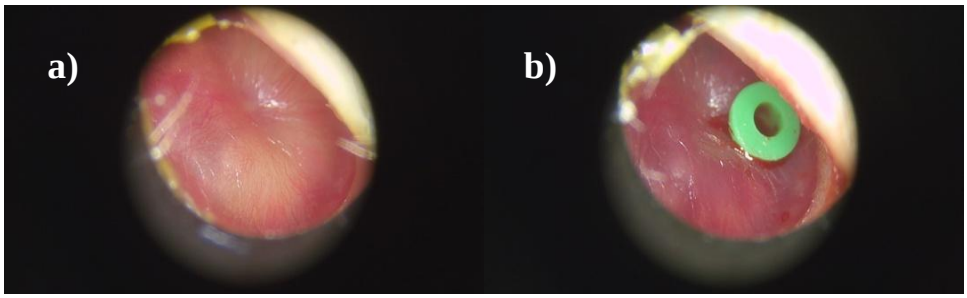

Figure 2: (a) Tympanic membrane before insertion is made **(b)** Tympanic membrane after ear tube insertion

An otoscope primarily consists of a head, handle, magnifying lens and a light source. A plastic interchangeable speculum is attached to the tip of the otoscope for insertion into the

auditory canal as in Figure 3. The otoscope is used by pulling on the pinna to subsequently straighten the ear canal for direct insertion into the ear. The physician can observe the middle ear through a magnifying lens. The interpretation of the findings in the middle ear with an otoscope is dependent on the experience of the physician at the time of diagnosis and has proven to often lack diagnostic certainty. This may lead to the wrongful prescription of antibiotics to the patient.

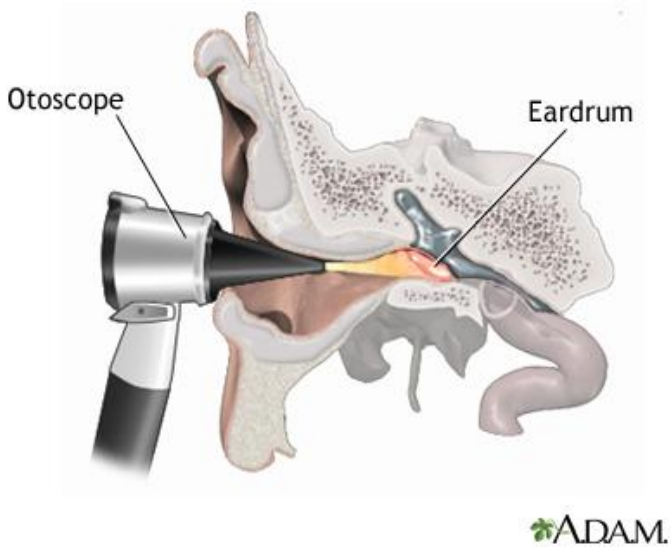

Figure 3: Otoscope inserted into the ear canal [3]

Many modern otoscopes also include an optical system that is more complex than a traditional otoscope and result in a better field of view, magnification and manual focus of the lens for patients with various ear canal lengths and for users with nearsightedness. [4]

The development of the otoscope described in this paper for fluorescence and digital imaging was developed to explore the possibility of distinguishing between acute otitis media and otitis media with effusion and subsequently increase the reliability of an accurate diagnosis. Various bones and regions behind the tympanic membrane were visualized with the otoscope's varying

wavelengths of light. The differences between ears with an effusion and non effusion were also investigated for the same purpose. The combination of spectroscopy with digital imaging was investigated to determine whether there were spectral differences between different wavelengths. Specifically, the spectral graphs demonstrated the light reflected or absorbed from a fluid as a function of the associated wavelength. Signal processing techniques were also applied to isolate various regions of the tympanic membrane using MatLab to increase the resolution of the anatomical and physiological properties of the tympanic membrane. Furthermore, the signal processing techniques were investigated to compare the recorded images and spectra for each patient. The design was more effective than a traditional otoscopy due to the reflectance of keratin, ceruem and bone with well-defined blood vessels and contrast visualized between the malleus and the rest of the tympanic membrane. [8] The newly developed otoscope, along with digital or fluorescence imaging, and spectroscopy had the potential to be an effective approach to diagnose pediatric patients with otitis media with increased diagnostic certainty.

1.1. Background

A study performed by Jensen et al. was conducted to determine what the acute otitis media diagnostic certainty was in pediatric patients. [9] The study determined that general practitioners were certain of the diagnosis in patients less than one year of age 58% of the time. It was also determined that there was a 73% certainty in patients over two and a half years of age. The diagnostic uncertainty was influenced by the diagnostic equipment, diagnostic criteria, the general practitioners knowledge, the presence of cerumen, and the behavior of the child. [9]

Similar studies have been completed to differentiate between acute otitis media and otitis media with effusion. One of the main reasons for carrying out this study was that the certainty of a diagnosis by primary care physicians in patients under the age of 0 to12 months was 58%, 66%

in children 13 to 30 months and 73.3% in children over 30 months. [10] There were two hundred and fifty eight patients that were categorized with acute otitis media, otitis media with effusion, and normal ears. The study required a skilled physician to examine each patient with an otoscope and diagnose them as either having acute otitis media, chronic otitis media, or a normal ear. The otoscope for the experiment incorporated an optical fiber and spectrometer. The diagnoses for each patient according to the physician and the raw spectra were compared and demonstrated that a skilled physician is capable of frequent misdiagnoses, resulting in unnecessary prescriptions to patients. This study has also proven that an otoscope that uses a spectroscopic method can quickly and noninvasively determine whether an individual has Otitis Media.

Armengol et al. performed a study to determine how often acute otitis media occurred in pediatric patients between six months and three years of age. [11] The patients were asked to return to their pediatrician for photographic and tympanometry readings of the ear before a cold and six to ten times during the cold. They determined that acute otitis media occurred in 55% of the colds, in 100% of patients with preexisting middle ear effusions, and in 5% of colds with no preexisting middle ear effusions. The investigators were able to determine that acute otitis media is a direct effect of the common cold in children, especially in cases when the children were previously diagnosed with middle ear effusions.

Research has been performed to determine what classifications of bacteria involved in acute otitis media do not respond to antibiotics. Thorton et al. investigated the effects of biofilm on otitis media diagnostics and determined that certain active bacteria that are unable to be cultured and are eradicated by antibiotic treatment are present in otitis media. [12] A biofilm is a colony of bacteria that forms on tissues to protect various bacteria from responding to antibiotics. This study aimed to determine whether the presence of a biofilm or intracellular bacteria may

play a role in the in-effectiveness of current treatments that are used for acute otitis media. The identification of the bacterium embodied in biofilm may determine the diagnosis of otitis media and the appropriate antibiotic prescription. Twenty patients that underwent surgery were recruited in the study. Each of these patients received a mucosal ear biopsy to determine whether pathogenic bacteria was contained intracellular or in a bacteria culture of biofilm.[12] A transmission electron microscope, and species fluorescent in situ hybridization and a confocal scanning microscope were used to complete the observations. The FISH technique was earlier developed to track DNA sequences on chromosomes.[12] In this case, it was used to determine the DNA sequences on middle ear mucosa to identify the presence of specific bacteria. The transmission electron microscope allowed the determination of the presence of intracellular bacteria and within cells; however the investigators were unable to identify the classification of the bacteria. The FISH and confocal scanning microscope allowed the determination of bacteria in fifteen of the total seventeen biopsies. Additionally, biofilm was observed in eleven biopsies and twelve were determined to have intracellular bacteria. [12] The use of the FISH technique and confocal scanning microscope enabled the investigators to determine a distinctive pattern between the DNA and associated bacteria involved with the reoccurring diagnosis of otitis media.

Boppart et al. studied the effects of biofilms on otitis media diagnosis and stated that "biofilms are thick adherent, glue-like material formed by polymicrobial communities of bacteria that act as protective microenvironments where bacteria can reside and colonize". [13] The findings that the bacteria formed in biofilms were resistant to antibiotics led to increased administration of antibiotics to children. They also studied the use of optical coherence tomography on otitis media biofilms using near infrared light. The researchers determined that

the noninvasive use of near infrared light has been known to capture ten to one hundred times better resolution than ultrasound waves noninvasively for otitis media biofilms. An otoscope with an optical coherence tomography scanner capable of providing optical coherence tomography images for visual representation on a laptop was presented in this paper as well.

Previous research has identified different techniques to facilitate the diagnosis of otitis media. Spector et al. investigated the noninvasive fluorescent identification of bacteria using fluorescence spectroscopy.[14] A mechanism of determining the type of bacteria using fluorescence spectroscopy was determined by identifying Streptococcus pneumoniae, Haemophilus influenzae, and Staphylococcus aureus using excitation wavelengths on the tympanic membrane. Sundberg et al. determined that the use of reflectance spectroscopy defined differences in effusion fluid in pediatric patients. [15] They also determined that otitis media with serous effusion was distinguished from otitis media with mucous effusion. Further research by Van der Jeught et al. has studied the thickness of the tympanic membrane, to create three-dimensional surface generation using optical coherence tomography. [16] The average thickness of the tympanic membrane was determined across various regions with similar regions of increased thickness. The reflectance and fluorescence spectroscopy methods and the average thickness of the tympanic membrane will be used in this study to facilitate the diagnosis of otitis media.

1.2. Commercial Products

Different commercial products currently used in the ear nose and throat industry are presented. Each of the devices described were presented because they contribute traditional technology as well as functionality new to the field. Typical otoscopes, such as the Welch Allen Macroview otoscope, were described due to its ability to record video in real time. Devices that

have recently been developed, such as the Cellscope otoscope, were included to provide an example of the recent technological advances in the ear, nose and throat industry.

The Welch Allen Digital Macroview otoscope is a commercial otoscope capable of providing digital recorded images in a medical setting. The device allows the physician to visualize a clear view of the tympanic membrane in the office which allows for additional communication between the patient and the physician. The otoscope enables the physician to save the images to a patient's file and to serve as an educational reference as in Figure 4. This tool can also be used as an educational training aid as high resolution images can be visualized from a laptop. Additionally, the high resolution of the camera also allows for the distinction between objects of very fine detail.

Figure 4: Welch Allen Digital Macroview otoscope [17]

Various video otoscopes are currently sold commercially for use in a medical environment. The Aurical OTOcam 300 video otoscope combines the traditional otoscope with high power light sources and OTOsuite software to enhance the characteristics of otitis media and to improve the diagnosis. [18]Additionally, the firefly DE550 handheld digital wireless video otoscope has

been developed with additional components that are not incorporated on traditional otoscopes. The firefly otoscope in Figure 5 features wireless connectivity to a laptop with variable magnification between fifteen and one hundred and fifty times digitally. The otoscope operates in real time with thirty frames per second using firefly pro software. Images are recorded via the button on the otoscope and can transmit the images to a computer up to thirty feet away. [19]

Figure 5: Firefly wireless otoscope and software demo [19]

Cellscope otoscope is a commercial device that took a unique and modern approach to otitis media diagnosis. The cellscope provided a quick mechanism to diagnose an ear infection directly from an iphone for immediate diagnosis by an untrained or trained individual. The purpose of the cellscope design as seen in Figure 6, was to provide a high quality diagnosis without taking a trip to a physician's office. A speculum attachment and iphone app was all that was required to record an image of the ear canal, middle ear and tympanic membrane with high resolution and visibility. A study found on the distributor's website recruited sixty three patients who visited the

emergency room between May and December of 2012. The patients were diagnosed with the Cellscope Oto and a traditional otoscope at the time of the visit. Forty nine of the patients were diagnosed with acute otitis media and there was no difference in the quality or diagnosis between the traditional otoscope and the Cellscope Oto when shown to physicians. Parents also felt comfortable taking additional images at home that would be sent to the physician for continued diagnostic treatment.

Figure 6: Cellscope otoscope [20]

2.0 Methods

An otoscope for fluorescence and digital imaging was developed to increase the reliability of an accurate diagnosis of otitis media. The combination of spectroscopy with digital imaging was investigated to determine whether there were spectral differences between different wavelengths using a multi-wavelength light source. More specifically, reflectance spectroscopy and digital imaging were performed independently to identify similarities between middle ear fluid properties and the two procedures were also used to determine whether or not the detection of an effusion could be non-invasively identified by a physician.

Reflectance spectroscopy was included to identify the light reflected or absorbed from a fluid as a function of the associated wavelength. Differences in intensity and percent reflection as a function of wavelength were recorded for the tympanic membrane and canal spectra. A criterion was developed to differentiate between different spectral properties patients with and without an effusion as a function of the associated wavelength. Class one was defined as tympanic membrane and canal spectra with a rapid increase in percent reflection between 575 nm and 650 nm and a rapid decrease in percent reflection between 650 nm and 750 nm. Class two was defined as tympanic membrane and canal spectra with a gradual decrease in percent reflection between 575 nm and 800 nm. Class three and four spectra were defined to group spectra that deviated from the typical waveforms of class one and two.

This otoscope was designed to be used either for surgical procedures or routine patient visits. Accordingly a disposable spectrum was changed between patients and the otoscope was disinfected with an alcohol cloth after each patient. Necessary precautions were taken into account to prevent the spread of bodily fluids and bacteria during the procedure. Electrical safety precautions needed to be considered to ensure electrical safety. The device was approved by the

clinical engineering department at Connecticut Children's Medical Center and the procedure was approved by the Institutional Review Board at Connecticut Children's Medical Center. [4]

2.1.Design

The otoscope design, pictured in Figure 7, included two high power light emitting diodes (LEDs) intended to illuminate the tympanic membrane. A high power red, green, blue, white (RGBW 625 nm, 523 nm, 455 nm, white) and high power Ultraviolet (UV 400-405nm) LED were integrated into the design.

Figure 7: Complete otoscope design

The electrical design in Figure 8 featured an LED constant current source and AC power source for maximum power and light intensity. The high power LEDs were mounted on thermal heat sinks designed to hold both LEDs in a stable enclosure using a spring locking mechanism for maximum efficiency. Five pushbutton switches and a power switch were mounted on a switch box for easy activation of each excitation wavelength.

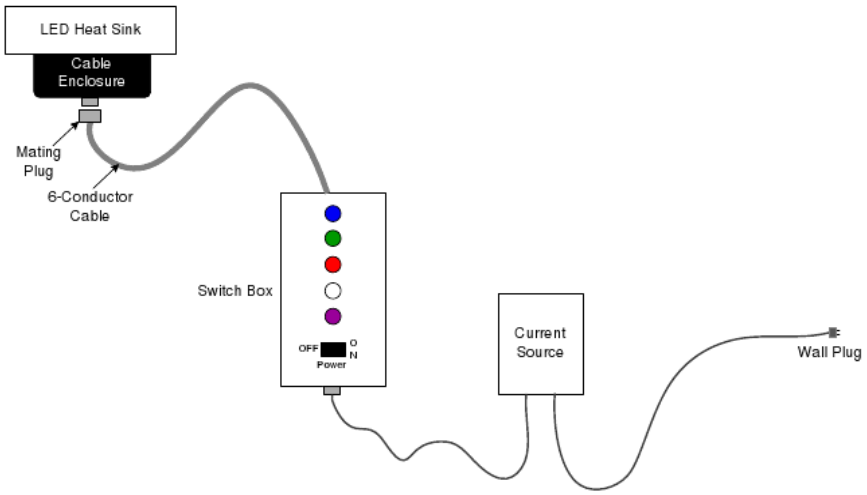

Figure 8: Electrical LED design implemented in the otoscope.

2.1.1. Mechanical Assembly

The otoscope was designed to feature a traditional Welch Allen otoscope head combined with components useful for Fluorescence and Digital Imaging Analysis of the tympanic membrane. The aluminum frame was built into three separate pieces including the base, handle, and heat sink. The base was designed to align the CMOS camera, filter wheel, optical insert and Welch Allen otoscope head on a center optical axis. Light from the heat sink cavity was directed into the ear through the Welch Allen otoscope head from the heat sink as pictured in Figure 9. The excitation and emission wavelengths both reflected off of the tympanic membrane directly into the otoscope's optical axis. The filter wheel was designed to pass the emission wavelength along the axis into the camera to record an image on a laptop through USB.

Emission wavelength is initiated in the Tympanic Membrane.

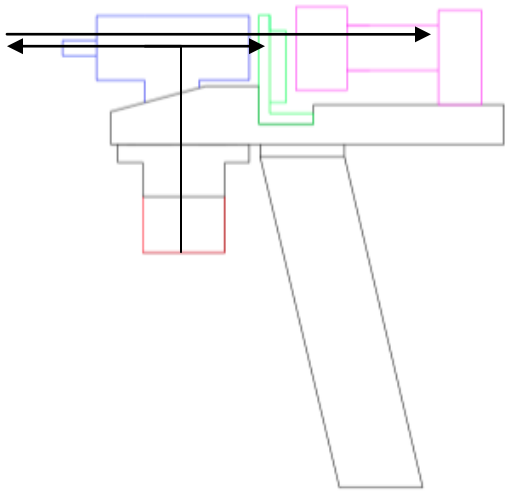

Figure 9: Mechanical design of the otoscope

The top, bottom and front view of the base of the otoscope in Figures 10 through 12 represented the 7.222 x 1.8 x 0.726 in. dimensions of the frame.

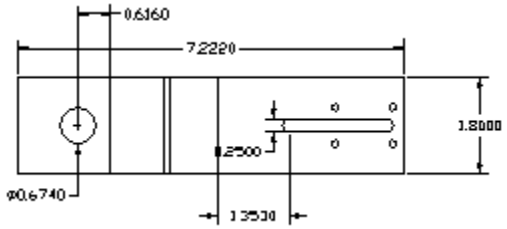

Figure 10: CAD drawing of the top view of the base of the frame (units in inches)

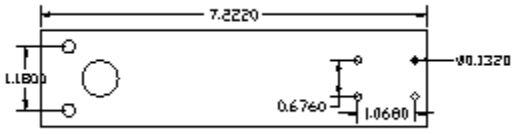

Figure 11: CAD drawing of the bottom view of the base of the frame (units in inches)

The Welch Allen otoscope head was designed to fit securely into the base of the frame on a 165 degree angle. This was designed to provide a direct optical path from the LEDs to the CMOS camera.

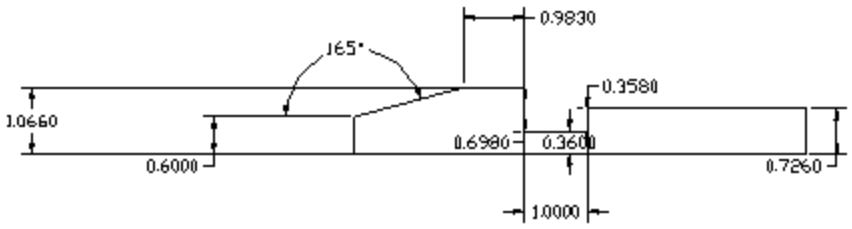

Figure 12: CAD drawing of the front view of the base of the frame (units in inches)

2.1.1.1. Optical Insert

An aluminum optical insert was designed to secure the filter wheel into the base of the frame. This piece filtered light that passed from the filter wheel to the camera through the insert. A screw was fastened to the optical insert to mate the filter wheel to the bottom of the frame. It was built out of a block of aluminum and cut to a height of 2.00 in., length of 1.00 in. and width of 1.8 in. The insert was 0.125 inches thick and sat flush with the base of the frame. Additionally, the diameter of the filter wheel hole was 0.3940 inches and was designed to sit 1.408 inch from the base of the frame. The mounting screws in Figure 13 were positioned 1.5 inches apart.

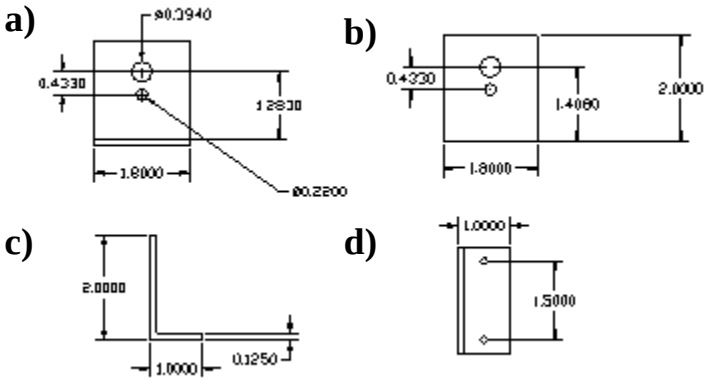

Figure 13: CAD drawing of the **(a)** front **(b)** back **(c)** right **(d)** top view of the optical insert (units in inches)

2.1.1.2. Heat Sink

The heat sink in Figures 14 through 16 was designed to dissipate heat evenly for maximum electrical efficiency and measured 2.6 in. x 2.4 in. x 0.8561 inch. It was mounted directly beneath the Welch Allen Otoscope head and featured two recessed one inch by one inch compartments to house the LEDs. The LEDs were mounted inside of the heat sink in mounting holes with M3 #4-40 mounting screws. The component was designed to move in perpendicular alignment to the otoscope for use of each LED. It was positioned so that the top of the LED was flush or below the height of the compartment to protect the LEDs when the heat sink was repositioned. This was completed using a screw, washer, and spring to facilitate the perpendicular movement.

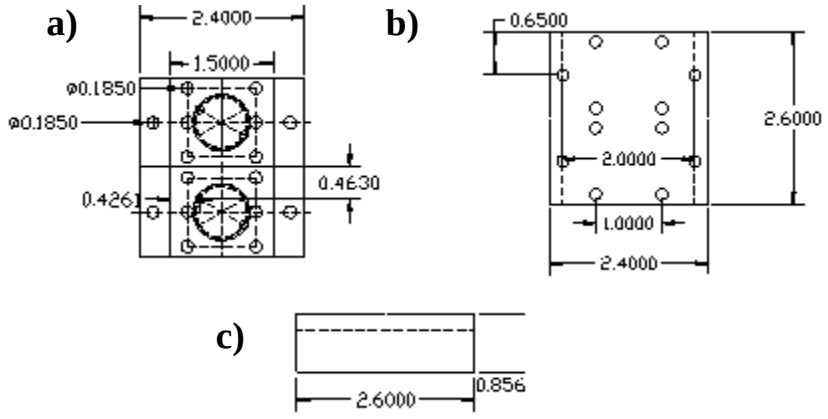

Figure 14: (a) Top, **(b)** bottom and **(c)** side view of the otoscope

The mounted heat sink was designed to move perpendicular to the otoscope's frame using a spring locking mechanism as seen in Figure 15 and 16. The washer was positioned with its curvature facing the hear sink to eliminate friction between the heat sink and the frame. The spring assembly was mounted to the base of the frame for structural and ergonomic stability.

Figure 15: Spring locking mechanism implemented on the heat sink.

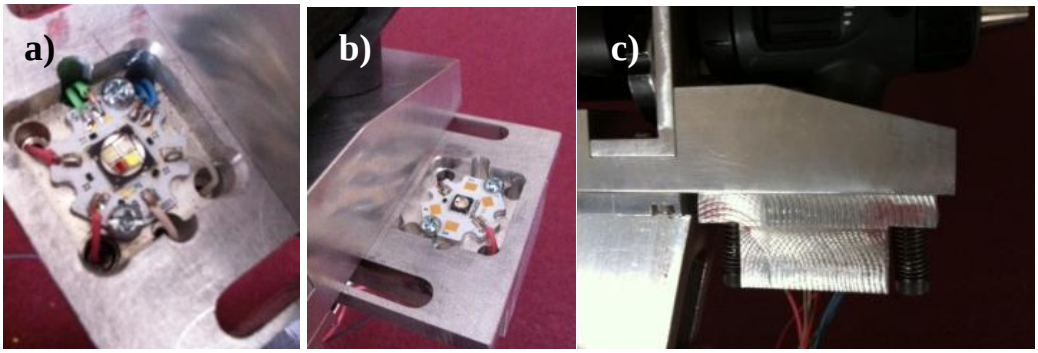

Figure 16: Four color LED **(a)** and single color UV LED **(b)** used for fluorescence imaging and illumination. Pictured on the otoscope **(c)**

2.1.1.3. Filter wheel

The filter wheel in Figure 17 was designed for the use of two 12.5 mm individual filters during the diagnostic procedure. A single filter compartment was left empty to provide a traditional otoscopic exam. A 12.5 mm PVC ring was inserted over the filter to prevent movement and to provide stability.

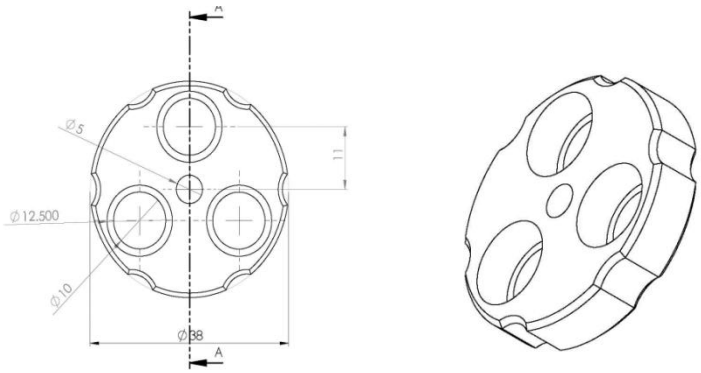

Figure 17: CAD drawing of the three-hole filter wheel (units in millimeters) [21]

Figure 18: Three-hole filter wheel pictured on the otoscope frame

2.1.1.4. Camera

The Thorlabs DCC1645C CMOS camera seen in Figure 19 was incorporated to capture high resolution fluorescence and illumination images of the tympanic membrane. The camera features a 1.88 in. x1.68 in. x 1.00 in. frame with a ¼ - 20 tap on the bottom of the camera as seen in Figure 21. The ¼ - 20 tap was used to mount the camera to the otoscope frame and allow the user to define the position of the camera along the axis. The camera had a frame rate of 25 fps and resolution of 1280 x 1024 pixels. [22] It was USB compatible for visual representation on a laptop.

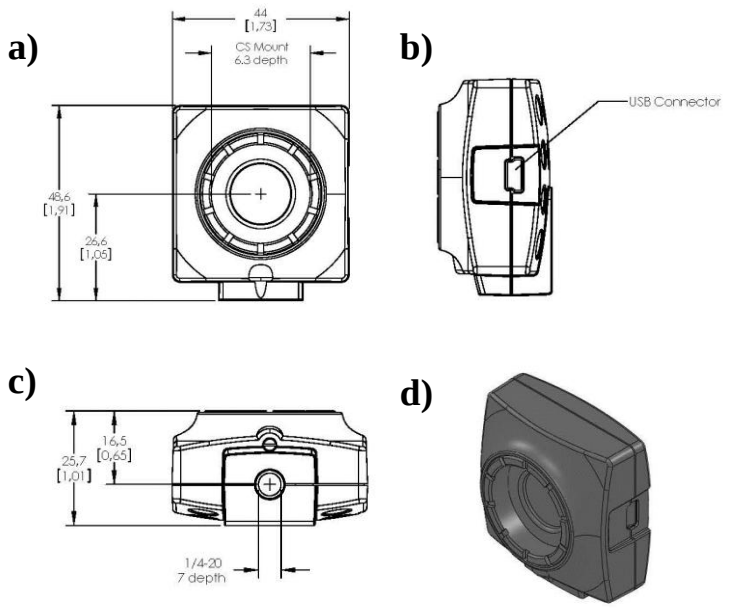

Figure 19: (a) Front **(b)** side **(c)** bottom and **(d)** 3-dimensional Thorlabs CMOS DC1645C dimensions [22]

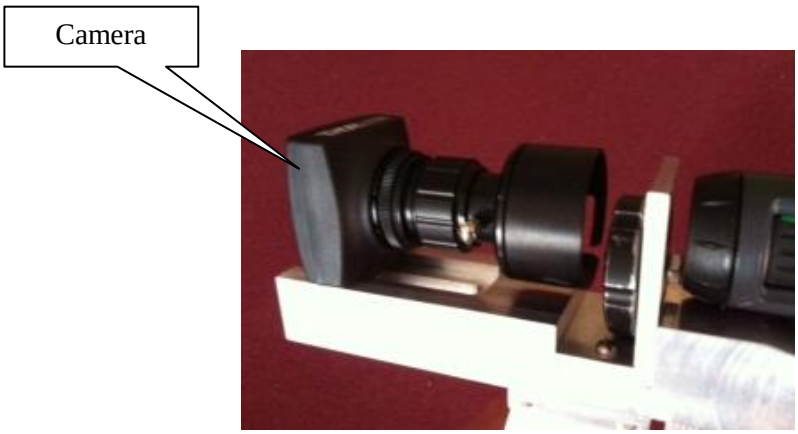

Figure 20: Thorlabs CMOS DCC1645C high-resolution camera used in the design

2.1.2. Electrical Design

The electrical design featured the combination of high power LEDs and circuitry to illuminate the tympanic membrane. The combination of high power LEDs and LED driver constant current source was incorporated to input 95-250 VAC and output 4-12 VDC for high power excitation wavelengths.

2.1.2.1. Light Emitting Diodes

The high power Red, Green, Blue, white (625 nm, 523 nm, 455 nm, white) and high power Ultraviolet (400-405nm) LED in Figure 21 were integrated into the design for maximum efficiency, where the LZ4-00MD00 high luminous efficacy LED featured a 625 nm, 523 nm, 455 nm and 5500K white LED.

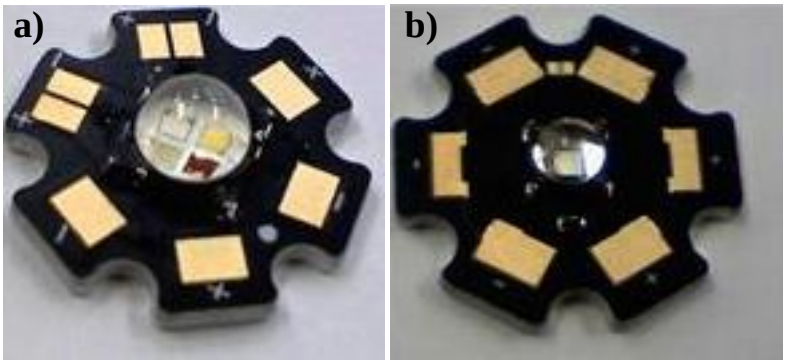

Figure 21: (a) LZ4-00MD00 High Luminous Efficacy RGBW LED Emitter and **(b)** LZ1-00UA00 High Efficacy Violet LED Emitter by LED Engin [23,24]

Table 1 displays the maximum forward current of 700 mA and the forward voltage which varied between 2.2 and 3.35 V for each wavelength.

Table 1: Forward Voltage and Current for the RGBW LED [23]

Wavelength	**Forward Voltage (V)**	**Forward Current (mA)**
625	2.2	700
523	3.35	700
455	3.2	700
5500K White	3.2	700
Power Rating: 10W	95 Degree Viewing Angle	

The LZ1-000A00 high efficacy UV LED featured a 400-405 nm wavelength. The forward current was 700 mA and the maximum forward voltage was 3.9V as seen in Table 2. The LED was set at an 85 degree viewing angle and the LED specifications can be seen in Table 2.

Table 2: Forward Voltage and Current for the UV LED [24]

Wavelength	400-405nm
Forward Voltage	3.9V
Forward Current	700mA
Power Rating	5W
Viewing Angle	85

2.1.2.2. LED Driver

The constant current source utilized in this design was the 3 Watt Magtech 20-4169 Constant Current LED Driver. The LED driver featured a 95-250 VAC Input and 4-12 VDC output and it was rated for 700 mA current output and 1-3 Watts Output Power.

Figure 22: MagTECH 20-4169 constant current source [25]

2.1.2.3. Switch

Five two pole SPST on-off push button switches as pictured in Figure 23 were used to maneuver between wavelengths. They were rated for 3A/125 VAC and each of the switches were mounted into the switch box for easy activation.

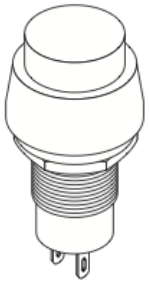

Figure 23: 103-1422-EVX SPST on-off switch [26]

2.1.2.4. Switch Box

A plastic enclosure was modified to mount five push button switches as in Figure 24. The power switch that was used to turn the power on and off was also mounted onto the plastic enclosure.

Figure 24: Plastic LED switch box and enclosure

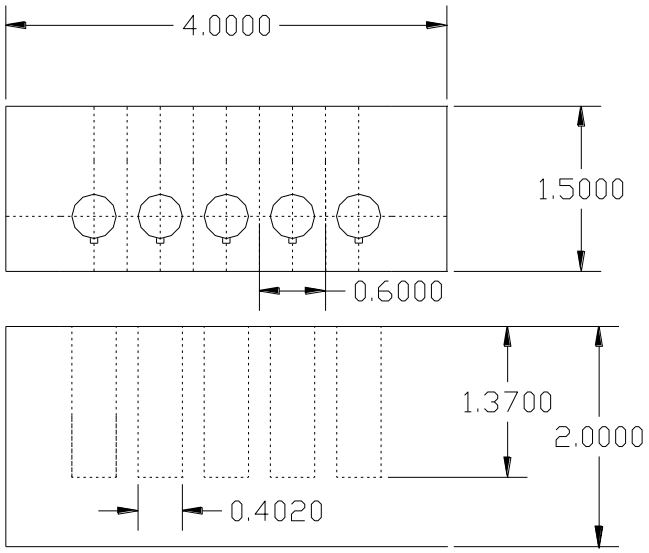

Figure 25: CAD drawing of the plastic LED switch box and enclosure (units in inches)

2.1.2.5. Circuitry

The electrical portion of the device was designed to transmit power from an AC power source as seen in Figure 26. The LED driver constant current source was incorporated to input 95-250 VAC and output 4-12 VDC. A 700 mA constant current rating was determined to be ideal for the LEDs. The constant current source was wired to the five SPST on-off switches. The on-off pushbutton switches were connected to a six-pin mating plug and conductor cable. The six-pin mating plug receptacle allowed current to transfer from the SPST switches to each LED. The high power LEDs were wired according to the wiring detail provided by the manufacturer as noted in Tables 3 and 4. Each of the nine pads associated with the high power RGBW LED functioned as the anode or cathode for a given wavelength as noted in Figure 27.

Table 3: Pin out of the RGBW LED [23]

Pad	Die	Color	Function
1	A	White	Anode
2	A	White	Cathode
3	B	Red	Anode
4	B	Red	Cathode
5	C	Green	Anode
6	C	Green	Cathode
7	D	Blue	Anode
8	D	Blue	Cathode
9	n/a	n/a	Thermal

Table 4: Pin Out for LZ1-00UA00 High Power LED [24]

Pad	Function
1	Cathode
2	Anode
3	Anode
4	Cathode
5	Thermal

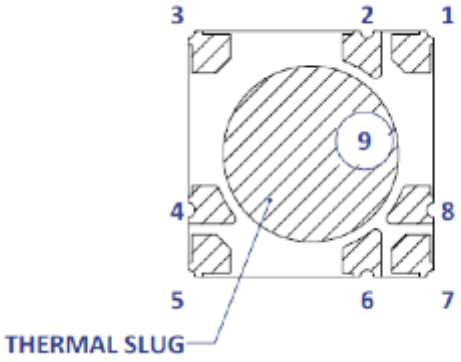

Figure 26: Plastic LED Thermal heat sink pad layout [24]

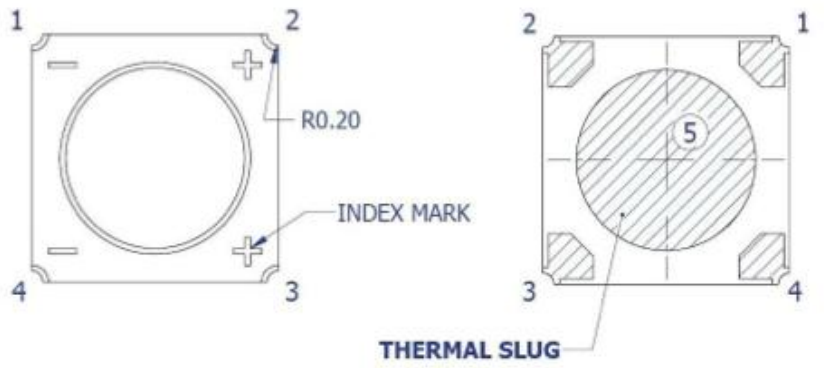

Figure 27: LZ1-00UA00 thermal pad distribution as seen in the manufacturer Data Sheet [24]

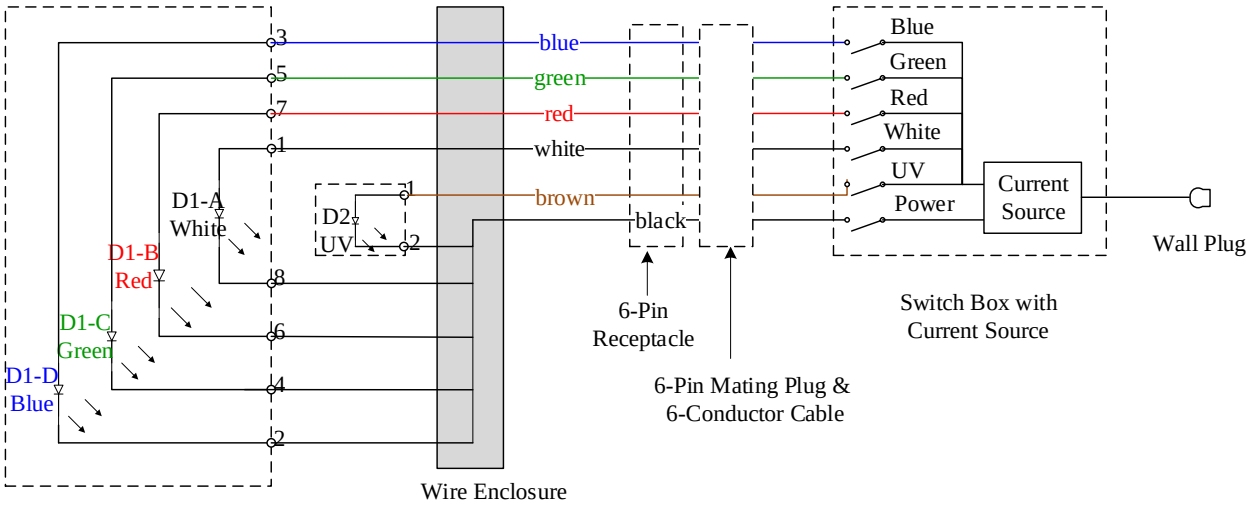

Figure 28: Electrical design of the otoscope including the LEDs, switches, mating conductor, constant current source and power source

2.2. Calibration

Reflectance measurements were collected using a USB4000 spectrometer from Ocean Optics. The wavelengths of the spectrometer were calibrated using a Mercury Argon Calibration Source to ensure accurate wavelengths during the spectral and medical imaging components of the procedure. The wavelength of the spectrometer was calibrated by determining the coefficients for a third order regression. The predicted wavelength was determined by algebraic manipulation of the experimental wavelength. The predicted and actual wavelengths in table 5 were determined to calculate the calibration coefficients for the regression of the form

$$\lambda_p = I + C_1\rho + C_2\rho^2 + C_3\rho^3, \qquad (1)$$

.

where λ is the wavelength of the pixel, *p*, *I* is the wavelength of pixel 0, C_1 is the first calibration coefficient in (nm/pixel), C_2 is the second calibration coefficient in (nm/pixel^2), and C_3 is the third calibration coefficient in (nm/pixel^3). [27]

Table 5: Spectrometer Calibration Regression Data

True Wavelength (nm)	Pixel #	Pixel # ^2	Pixel #^3	Predicted Wavelength	Difference
365.09	91	8281	753571	364.944564	0.145436039
404.36	276	76176	21024576	404.4668686	0.106868638
407.54	290	84100	24389000	407.4405272	0.099472759
435.43	424	179776	76225024	435.7786166	0.348616648
491.4	690	476100	328509000	491.3561655	0.04383449
546.26	958	917764	879217912	546.4210355	0.161035476
577.47	1108	1227664	1360251712	576.8234751	0.646524879
593.36	1190	1416100	1685159000	593.3146516	0.045348425
625.88	1354	1833316	2482309864	626.0201744	0.140174354
696.2	1713	2934369	5026574097	696.2991784	0.099178441
706.43	1766	3118756	5507723096	706.5189304	0.088930355
726.95	1873	3508129	6570725617	727.0271654	0.077165394
729.81	1888	3564544	6729859072	729.888814	0.078814004
738	1931	3728761	7200237491	738.073936	0.073936016
749.95	1994	3976036	7928215784	750.0169857	0.066985665
763.35	2064	4260096	8792838144	763.2182081	0.131791897
771.99	2111	4456321	9407293631	772.0410044	0.05100443
794.56	2232	4981824	11119431168	794.6027855	0.04278546
800.68	2264	5125696	11604575744	800.5326509	0.147349074
811.2	2322	5391684	12519490248	811.2409539	0.040953944
826.44	2404	5779216	13893235264	826.2927881	0.147211899
842.3	2492	6210064	15475479488	842.3311876	0.031187588
852.09	2546	6482116	16503467336	852.1137052	0.023705238
871.7	2655	7049025	18715161375	871.7216517	0.021651736
912.63	2885	8323225	24012504125	912.4825553	0.147444667
922.77	2944	8667136	25516048384	922.8028695	0.032869513
965.84	3194	10201636	32584025384	965.9085512	0.068551229

The intercepts for the linear regression were calculated in Table 6.

Table 6: Experimental calculation of the calibration regression coefficients

Intercept	345.3503
X Variable 1	0.215872
X Variable 2	-6E-06
X Variable 3	-2.3E-10

The regression was performed after determining the difference between the true wavelength and predicted wavelength. Table 7 summarizes the r square values for the regression.

Table 7: Regression Statistics

Multiple R	0.999999491
R Square	0.999998983
Adjusted R Square	0.99999885
Standard Error	0.182709533
Observations	27

Table 8: Experimental calculation of the calibration regression statistics

	Df	**SS**	**MS**	**F**	**Significance F**
Regression	3	754700.3946	251566.7982	7535826.8	4.8143E-69
Residual	23	0.767803787	0.033382773		
Total	26	754701.1624			

Table 9: Experimental calculation of the calibration regression statistics

	Coefficients	**Standard Error**	**P-value**	**Lower 95%**	**Upper 95%**	**Lower 95.0%**	**Upper 95.0%**
Intercept	345.3502937	0.157994463	1.2E-62	345.02346	345.6771	345.0235	345.68
X 1	0.215872347	0.000430991	6.1E-48	0.2149808	0.216764	0.214981	0.2168
X 2	-6.0309E-06	3.00212E-07	4.4E-16	-6.652E-06	-5.4E-06	-6.7E-06	-5E-06
X 3	-2.27504E-10	5.93957E-11	0.00086	-3.504E-10	-1E-10	-3.5E-10	-1E-10

The reflectance probe and spectrometer in Figure 32 were calibrated before reflectance measurements were taken for each patient using the following procedure. The probe was placed

in a dark environment and a dark and light spectrum were taken as demonstrated by Ocean Optics every time SpectraSuite was opened, (Figures 30 and 31). The calibration process was as follows:

1. The calibration process was performed after all spectroscopy equipment was connected to the computer.
2. Run Spectrasuite.
3. Place the probe (Figure 34) in a dark environment and collect the dark spectrum. The dark spectrum was collected by clicking on the dark spectrum option on the tool bar.
4. Light source was turned on.
5. Reflection calibration environment was set up appropriately.
    a. A reflectance tool (Figure 31) was placed inside of a dark environment. The probe was placed inside of the dark environment and the light source was turned on. A light spectrum was collected at this time.

Figure 29: Reflectance source used for calibration

    b. The light spectrum was collected by clicking on the light calibration option on the tool bar.
6. The reflectance option on the tool bar was chosen once the calibration measurements were completed.

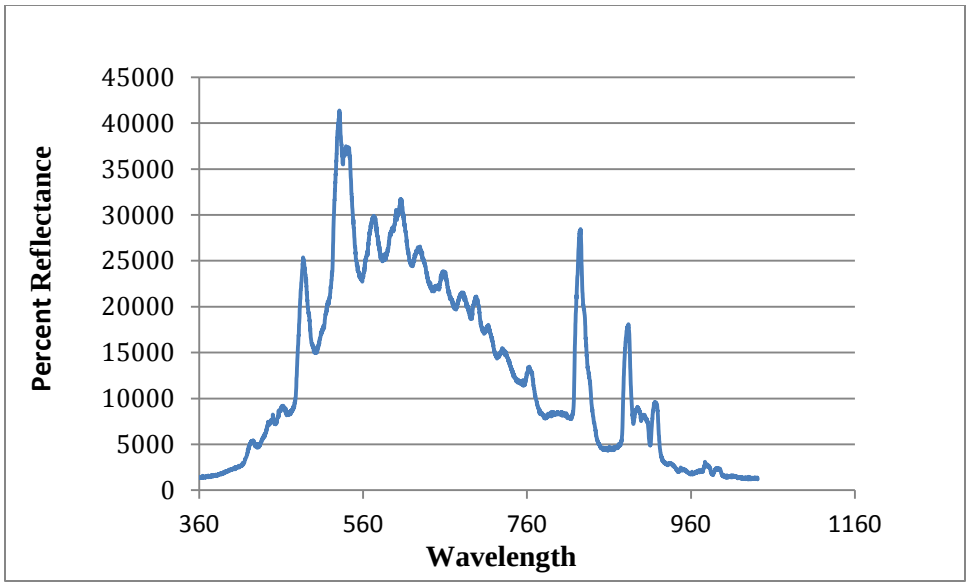

Figure 30: Light Calibration using Spectra Suite

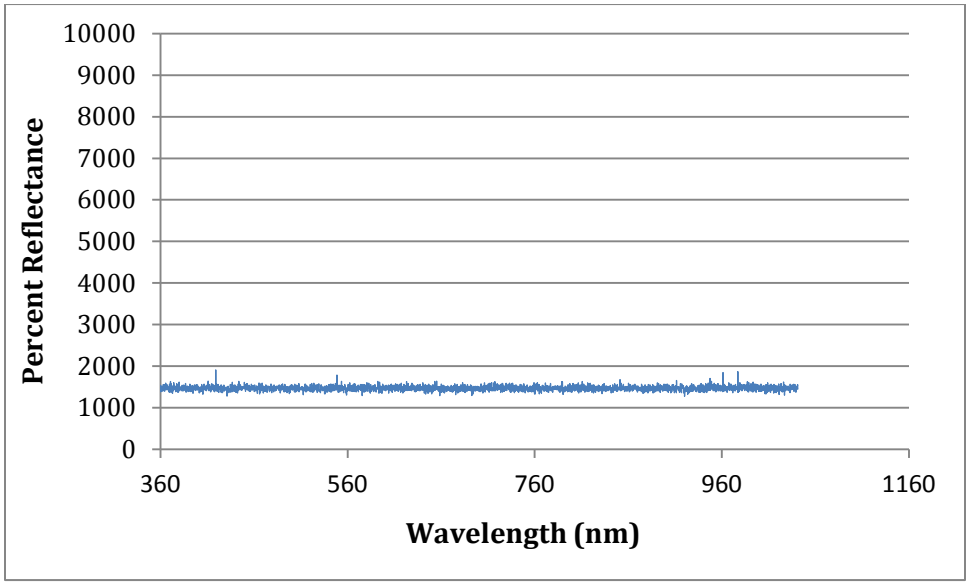

Figure 31: Dark Calibration using Spectra Suite.

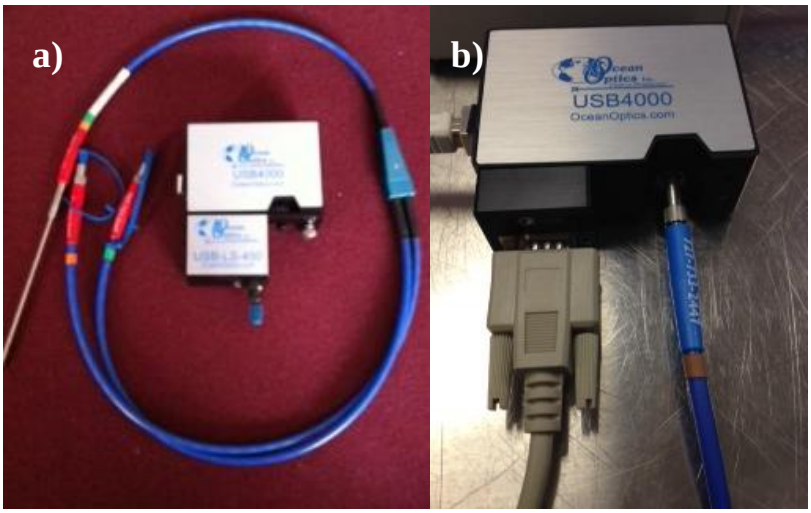

Figure 32: (a) Ocean Optics spectrometer and **(b)** reflectance probe

2.3. Clinical Testing

The following procedure was written according to the Connecticut Children's Medical Center's protocol approved by the Institutional Review Board for the study numbered 09-113. Patients that participated in this study were recruited for myringotomy and PE tube placement for standard treatment of recurrent otitis media or persistent middle ear effusion. [28] Digital images and spectra were recorded during the initial examination regardless of whether an effusion was present. Patients that had no effusion at the time of surgery had spectroscopy and digital images recorded and served as the "non-effusion normals" for the study. Patients that were determined to have a normal otoscopy with a white light otoscope at the time of surgery served as the control group since there was no available information for spectral or imaging analysis. [28] Patient information was removed from the results and were retained for further subsequent studies. Study duration depended on timing of specimen collection, lasted approximately one year. [28]

The procedure began with the removal of debris and cerumen from the ear canal to improve the visual clearance of the tympanic using the test set-up in Figure 33. A spectral signal was recorded with a reflectance probe once in the canal and tympanic membrane. A total of four

reflectance spectra were recorded for each patient. The four reflectance spectra included a canal and tympanic membrane spectra for the right and left ear for each patient. The spectral examination took approximately one minute and involved illuminating the auditory canal with a UV-Visual Xenon Px-2 light source and reflectance probe. The spectral output of the Xenon light source can be seen in Figure 33. Wavelengths between 200 nm and 800 nm were illuminated by the emitted by the light source. The resulting spectra ranged between 300 nm and 700 nm and was recorded by SpectraSuite over several seconds.

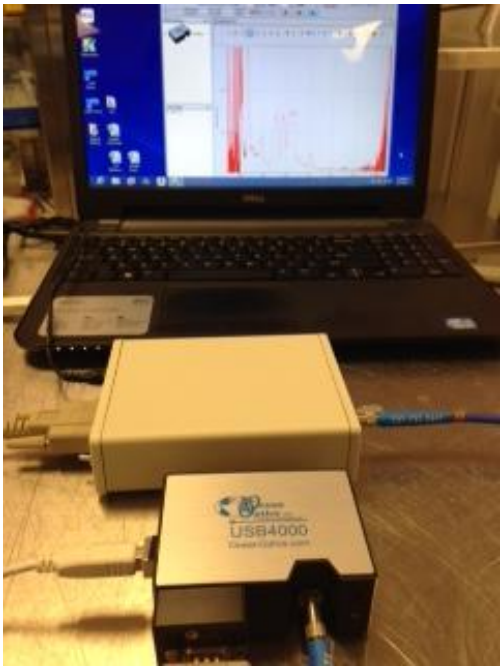

Figure 33: Experimental spectroscopy set-up

A sample of middle ear fluid was suction removed from patients with an observed effusion after the myringotomy incisions had been made. [28] The spectral output as a function of wavelength for the Xenon Px-2 uv-visual light source, as pictured in Figure 34, verified that wavelengths between 200 nm and 800 nm illuminated the tympanic membrane.

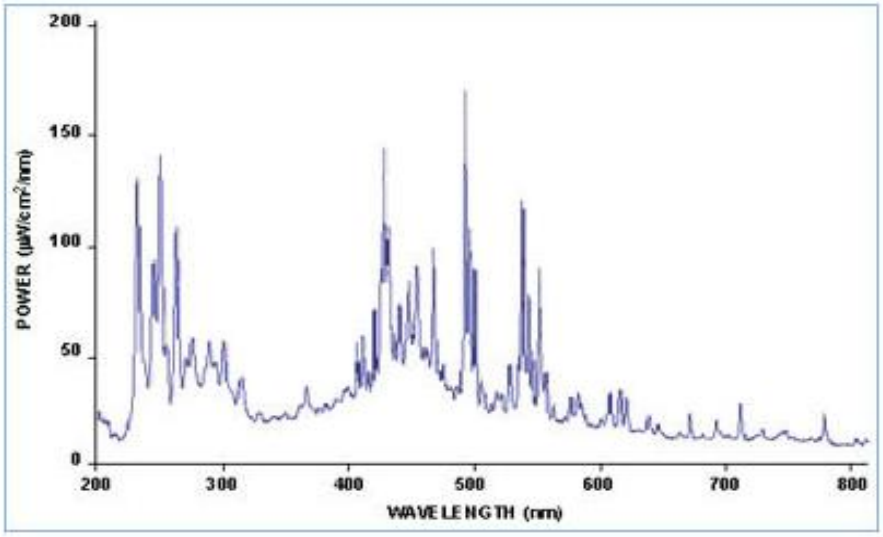

Figure 34: Spectral Output of the PX-2 UV-Visual Light Source [29]

Five excitation and illumination wavelengths were studied for fluorescence imaging including: white light, 385-420 nm, 450-470 nm, 520-535 nm and 640-650 nm. Each of the chosen wavelengths were emitted into the ear canal and tympanic membrane as in a typical otoscopic examination. A 425 nm and 500 nm filter were used to attenuate the excitation wavelengths. The emission wavelength passed through a CMOS camera and an image was recorded of the tympanic membrane. Fluorescence and illumination images of the tympanic membrane were recorded and compared for "effusion" and "non-effusion" patients. This was done for each wavelength and prolonged the surgery an additional three to five minutes. There was no additional associated risk to the patient. [28]

3.0 Results

The results include two separate sets of data: design validation and clinical trials. The design validation was performed to ensure appropriate functionality of the otoscope before clinical trials. The validation procedure required that the device be tested on one individual with no signs of otitis media. A normal tympanic membrane was imaged at each wavelength and the initial benefits of the newly designed otoscope in comparison to a traditional otoscopy were identified.

The clinical trials were defined as an experimental procedure attached to a routine myringotomy and PE tube placement procedure. Here, the newly designed otoscope was used in a routine surgical procedure and not in a controlled setting.

3.1.Design Validation

The newly developed otoscope was tested before clinical trials to compare differences between a normal tympanic membrane with various wavelengths, in order to establish a normal control group prior to recruiting patients. This served as the device validation. The wavelengths chosen for the procedure were a 625 nm, 523 nm, 455 nm, 5500 K and their LEDs were located on a heat sink for thermal stability and conductivity. Figure 35 graphically represented the power spectrum and bandwidth for each wavelength.

a)

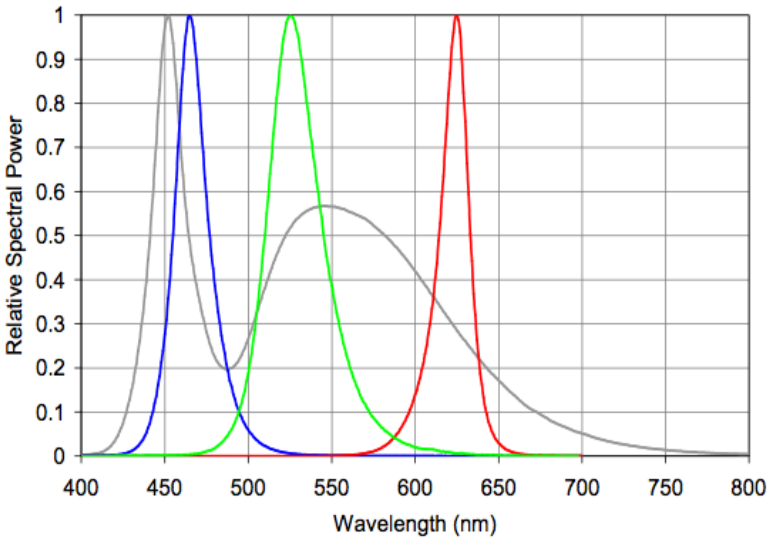

b)

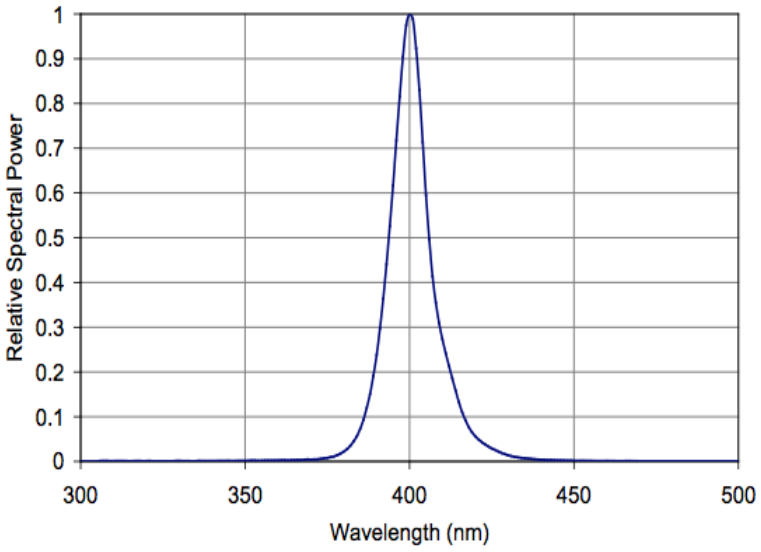

Figure 35: Relative Spectral Power vs. Wavelength for the **(a)** 4 color LED and **(b)** Single Color UV LED [23,24]

The images below were captured with a high resolution CMOS camera when the LEDs were tested in a normal tympanic membrane with a 450 nm and 500 nm longpass filter. These filters captured the emission wavelengths that originated at wavelengths longer than 450nm and 500 nm, respectively (Figure 36). Preliminary results were recorded as a standard for a normal tympanic membrane to ensure accuracy of the device before patients were recorded for the study. Additionally, the preliminary image presented the reflectance of keratin, cerumen, and bone in

the tympanic membrane with well defined blood vessels and contrast between the malleus and the rest of the tympanic membrane. [8]

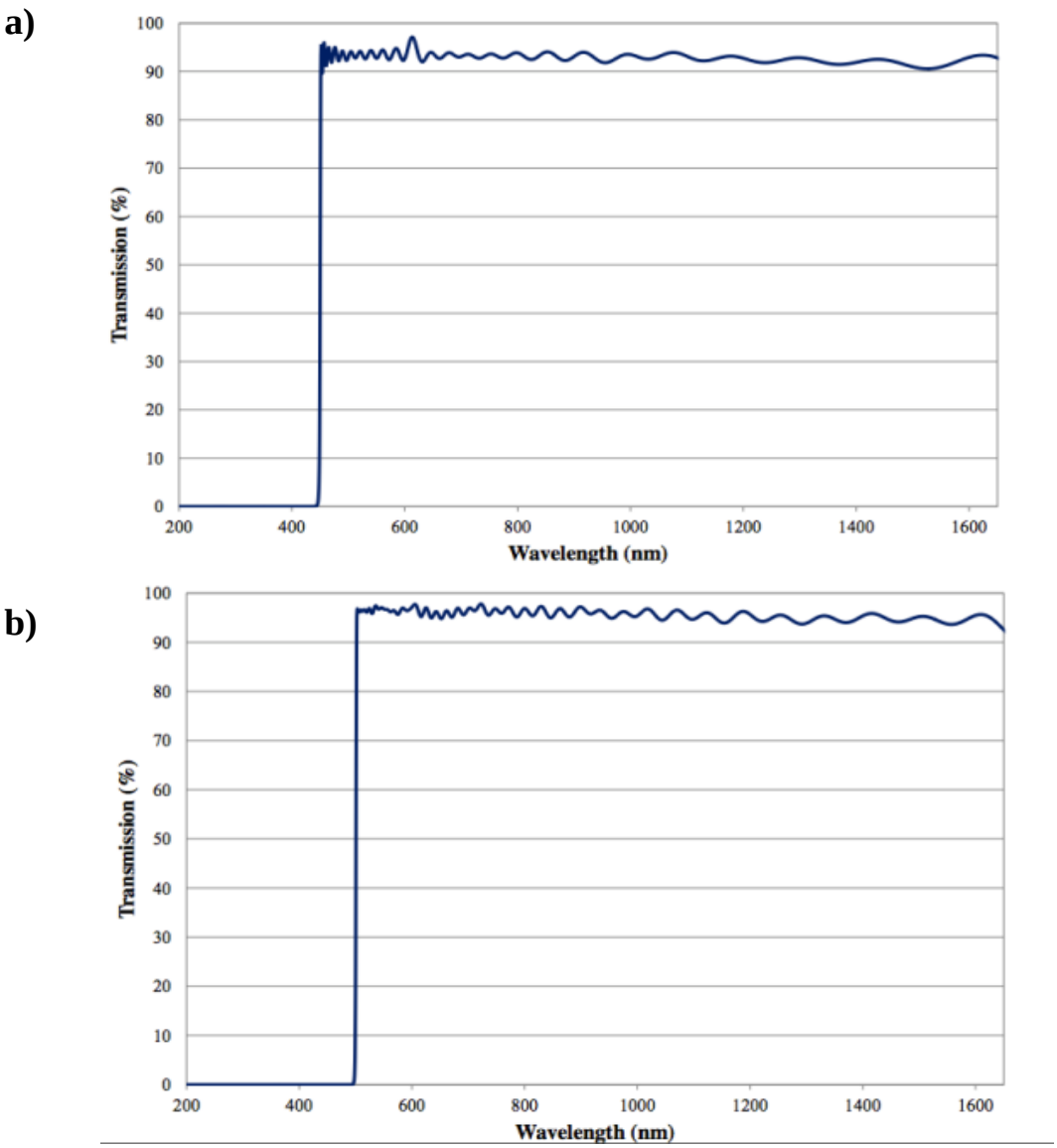

Figure 36: Longpass **(a)** 450nm and **(b)** 500nm filter [30,31]

The images presented below focused on a clear transparent tympanic membrane that centered on the malleus bone with high contrast. The ear showed no signs of otitis media and was considered normal in all diagnostic aspects. It was proposed that the excitation wavelengths aided in the determination of an effusion behind the tympanic membrane regardless of the

tympanic membrane thickness. Therefore, the excitation wavelengths would potentially penetrate the tympanic membrane with enough power that structures and effusions behind it would fluoresce. The detection of an effusion allowed for a highly accurate diagnosis of otitis media and provided a proof of concept of the otoscope design. Further fluorescence and reflectance measurements may provide additional bacterial properties as well.

An image was recorded for a normal tympanic membrane with the 5500K white LED pictured in Figure 37. The white LED was determined to enhance the presence of vascularity and contrast of the malleus bone. The white light was also determined to provide increased contrast, magnification, and resolution in comparison with a traditional otoscopic visual representation as seen in Figure 37.

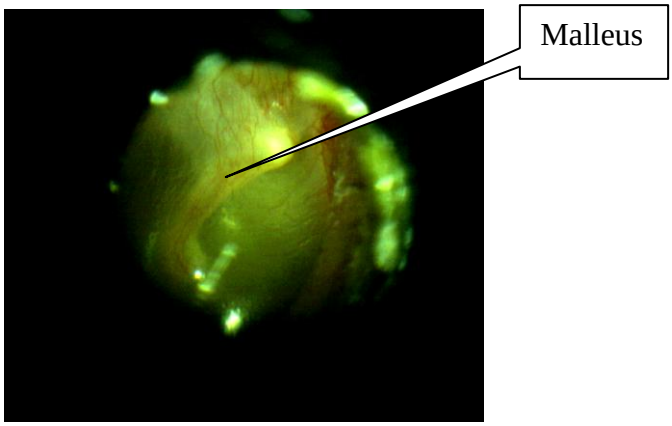

Figure 37: Tympanic membrane using white light

Blue and ultra-violet wavelengths were investigated to excite photons in the tympanic membrane. Images that were recorded for emission wavelengths between 425 nm and approximately 1000 nm were passed using a 425 nm and 500 nm longpass filter for 400 nm through 405 nm and 455 nm excitation sources. It was hypothesized that this wavelength will show wax, bacteria, and keratin fluorescence in the ear based on the preliminary images. Figure 38 displays an image of a normal tympanic membrane using a 455 nm blue LED.

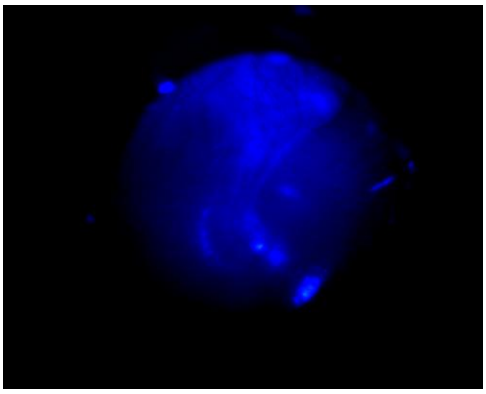

Figure 38: Tympanic membrane using blue light

The 523 nm LED was incorporated into the design to obtain illumination images. The chosen LED spectrum ranged from 475 nm to approximately 590 nm with a dominant wavelength at 523 nm. It was proposed that this wavelength will show wax, keratin, and fluorescence of the effusion located behind the tympanic membrane with enhanced resolution and contrast of the middle ear region based on the preliminary results. Figure 39 displays an image of a normal tympanic membrane recorded using the 523 nm light source.

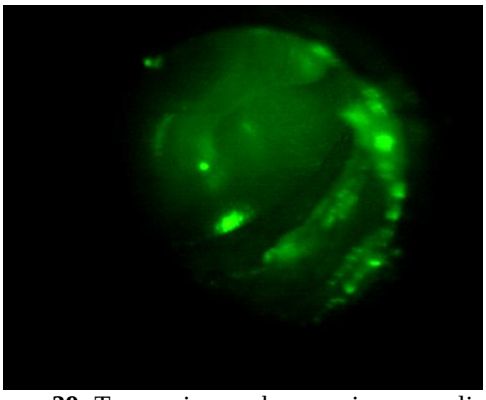

Figure 39: Tympanic membrane using green light

The 625 nm LED in Figure 40 was incorporated into the design for illumination of the tympanic membrane. Regions that absorb light may appear darker in specific areas of interest but fluorescence is not expected due to the wavelength. There were differences in light intensity in comparison to a normal ear when the 625 nm LED was illuminated in an ear with otitis media.

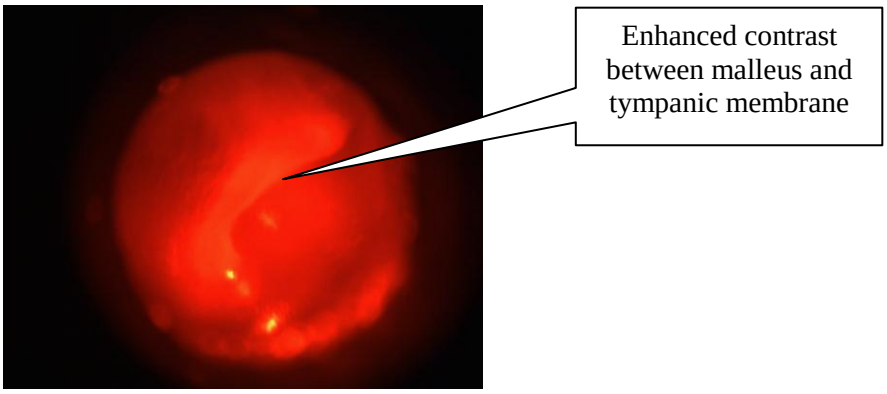

Figure 40: Tympanic membrane using 645nm light

The preliminary image results showed the reflectance of keratin, cerumen, and bone in the tympanic membrane and well-defined blood vessels and contrast between the malleus and the rest of the tympanic membrane were observed.

3.2. Signal Processing

Signal processing developed by Trinity College enhanced the contrast of the malleus and the tympanic membrane for better identification of structures. The signal processing techniques were applied to isolate various regions of the tympanic membrane using MatLAB to increase the resolution of the anatomical and physiological properties of the tympanic membrane. The signal processing techniques were investigated to compare the recorded images and spectra for each patient.

The signal processing algorithms implemented for each of the images were capable of removing an artifact by isolating specific regions of the tympanic membrane and subtracting the artifact of interest. Additionally, an algorithm capable of enhancing the images was used to increase the contrast and definition of the identified structures. [8] Figure 41 displayed an example of an enhanced white light image of the tympanic membrane.

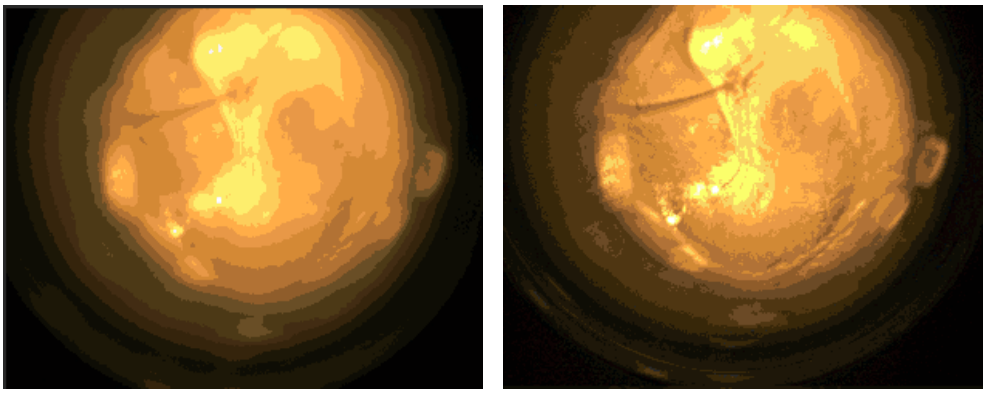

Figure 41: Enhanced white light image using signal processing algorithms [8]

3.3. Effusion Spectra

Fourteen of the 22 ears were determined to have otitis media with effusion due to the presence of fluid in the middle ear region. The patient descriptions and the classification of effusion spectra for each patient were displayed in Tables 10 and 11. Each of the spectra were classified according to percent reflection as a function of wavelength as defined in the Methods and Table 11. Tympanic membrane spectra were characterized by a gradual decreasing slope between 560 nm and 800 nm, while the canal spectra were characterized by rapid increase in percent reflection between 575 nm and 750 nm.

Table 10: Experimental Observations and Patient Descriptions

Date	Patient	Ear	Description	Additional Comments
09/25/13	P1	Right	Thin pus	Moderate vascularity
09/25/13	P1	Left	Thin pus	Thick TM
09/25/13	P2	Right	No fluid	Normal vascularity
09/25/13	P2	Left	No fluid	Normal vascularity
09/25/13	P3	Right	Thick fluid	Moderate vascularity
09/25/13	P3	Left	Thin Fluid	Retracted ear drum
10/09/13	P1	Right	Thin Fluid	Moderate vascularity
10/09/13	P1	Left	No Fluid	Normal vascularity
10/16/13	P2	Right	No Fluid	Myringosclerosis, Thin TM, Normal vascularity
10/16/13	P2	Left	No Fluid	Thin TM, retracted thin TM, high vascularity
10/30/13	P1	Right	No Fluid	NA
10/30/13	P1	Left	No Fluid	NA
11/06/13	P2	Right	Thick purulent fluid	NA
11/06/13	P2	Left	Thin Fluid	NA
11/13/13	P1	Right	Thick mucoid fluid	Moderate vascularity in the TM. Some vascularity in the canal
11/13/13	P1	Left	Thick mucoid fluid	Moderate vascularity in the TM. Some vascularity in the canal
11/13/13	P2	Right	Fluid	NA
11/13/13	P2	Left	Fluid	NA
12/04/13	P1	Right	Purulent fluid	Thick TM and high vascularity
12/04/13	P1	Left	No Fluid	Myringosclerosis
01/08/14	P1	Right	Thick Fluid	Moderate-high vascularity
01/08/14	P1	Left	Thick pus	Moderate vascularity

Table 11: Experimental effusion classification for each patient

Subject/Ear	Non Effusion Normal Spectra Classification		
	Effusion Consistency	***TM Class***	***Canal Class***
9-25-13 P1 L	Thin	2	2
9-25-13 P1 R	Thin	2	2
9-25-13 P3 L	Thin	2	2
9-25-13 P3 R	Thick	2	2
10-09-13 P1 R	Thin	2	3
11-06-13 P2 L	Thin	3	4
11-06-13 P2 R	Thick	3	1
11-13-13 P1 L	Thick	1	1
11-13-13 P1 R	Thick	1	1
11-13-13 P2 L	Thin	2	4
11-13-13 P2 R	Thin	2	4
12-04-13-P1 R	Thick	1	1
01-08-14 P1 L	Thick	1	1
01-08-14 P1 R	Thick	1	1

3.3.1. Tympanic Membrane

There were two predominant spectral trends determined for the tympanic membrane effusion spectra that were characterized by percent reflection as a function of wavelength and effusion consistency as seen in Figures 42 through 45. Tympanic membrane spectral waveforms were determined to be consistent with the thin and thick spectra trends .

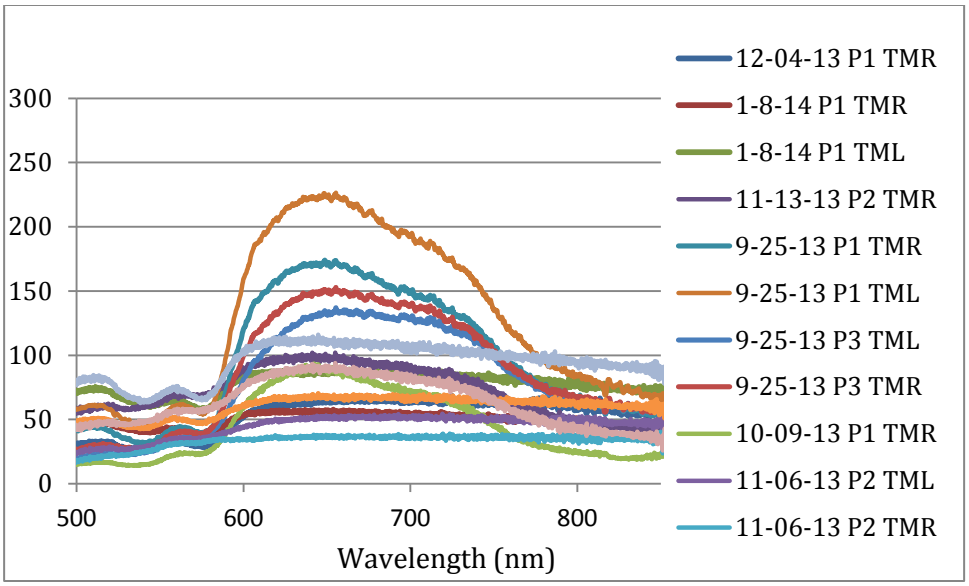

Figure 42: Tympanic membrane reflectance spectra for patients with an effusion at the time of surgery

Class one tympanic membrane effusion spectra resulted in the following waveform and was predominatly characterized by thick effusion consistency. The initial peak at 550 nm can be attributed to hemoglobin and is present in all tympanic membrane spectra. The tympanic membrane spectra varied between 30 and 110 percent reflection.

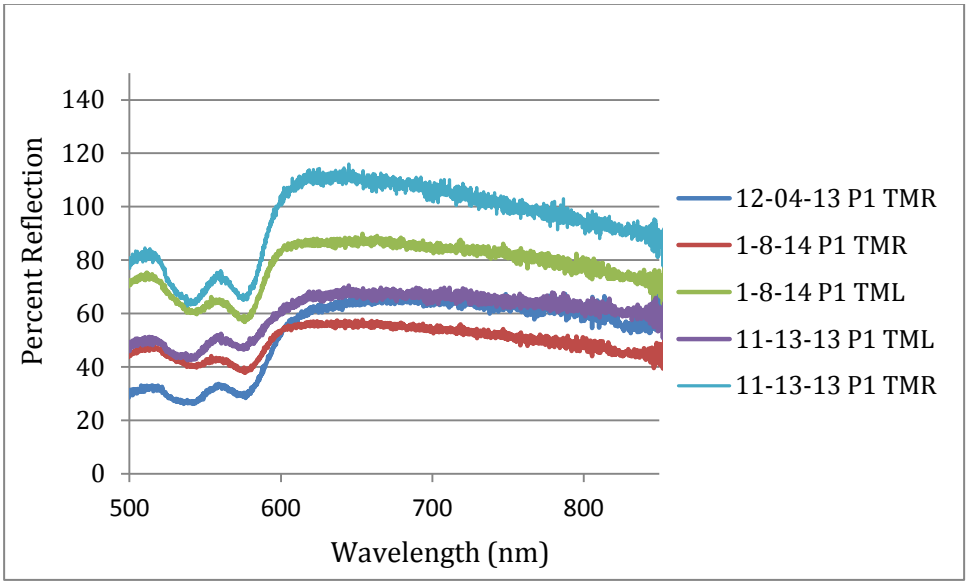

Figure 43: Class 1 Tympanic Membrane Thick Effusion Spectra

The second class of TM effusion spectra was characterized by thin fluid and a rapid increase in percent reflection between 575 nm and 650 nm and a rapid decrease in percent reflection between 650 nm and 750 nm. Percent reflection varied between 50 and 225 percent. The initial peak occurred at 555 nm, which was also attributed to hemoglobin.

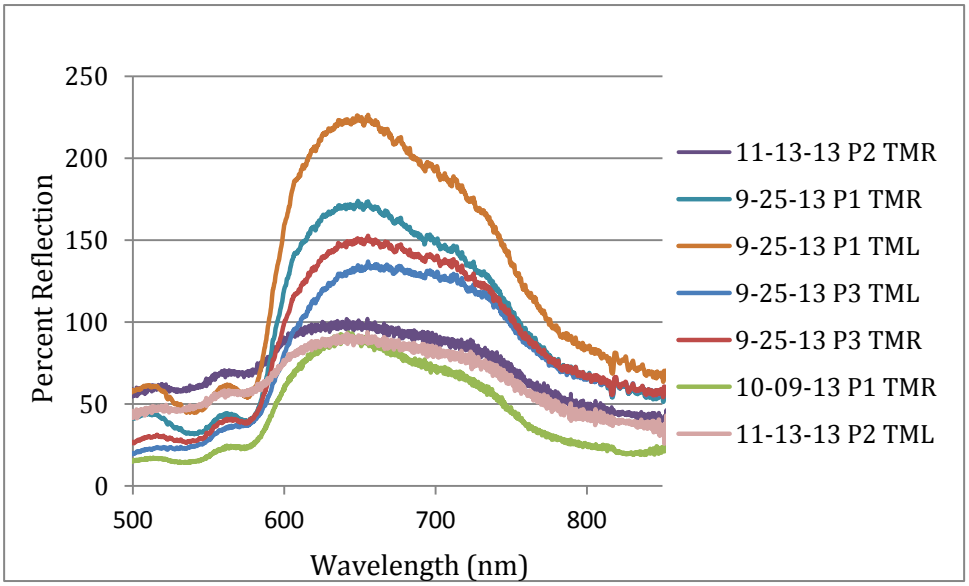

Figure 44: Class Two Tympanic Membrane thin effusion spectra

Class three tympanic membrane effusion spectra were determined to be inconsistent with the thick and thin effusion consistency spectra. Percent reflection varied between 35 and 50 percent. The characteristic peak at 550 nm due to the presence of hemoglobin was present in both reflectance spectra.

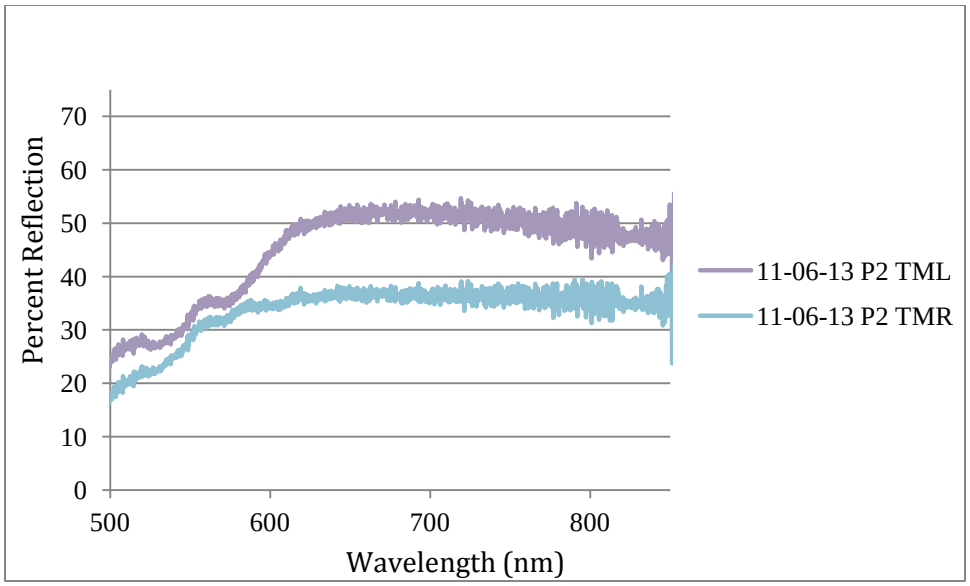

Figure 45: Class three tympanic membrane reflectance spectra inconsistent with effusion and non effusion classifications

3.3.2. Canal Spectra

The two dominant tympanic membrane spectra classifications were also used to classify the canal spectra. The spectra were classified according to the tympanic membrane effusion consistency to determine whether there was a correlation between the canal and tympanic membrane spectra for effusions with specific consistencies. The fluid was located behind the tympanic membrane and no fluid was present in the canal. Canal spectra for ears with a predominantly thick effusion were categorized into the predetermined Class one spectra. They were similar in waveform to Class one TM effusion spectra with a higher percent reflection. The same was identified for the Class two canal effusion spectra in respect to thin effusion consistency. Class three and four effusion canal spectra were characterized by unique waveforms potentially due to the medical condition or disturbance. It was determined that most of the canal spectra shapes were similar to their tympanic membrane effusion spectra shapes. All of the canal reflectance effusion spectra can be seen in the following plot.

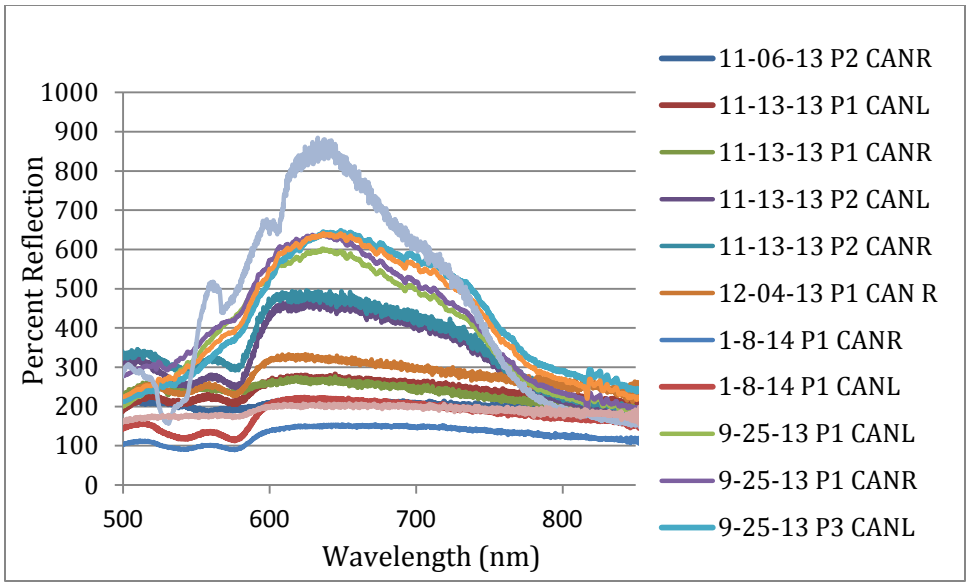

Figure 46: All canal reflectance spectra with an effusion

The canal reflectance spectra were categorized in terms of the spectral waveform in Figures 46 through 50. The first classification of canal spectra shape was dominated by the same shape as tympanic membrane spectra for effusions with thick consistency and a decreasing slope between 600 nm and 850 nm. All of the spectra had a percent reflection under 350 percent.

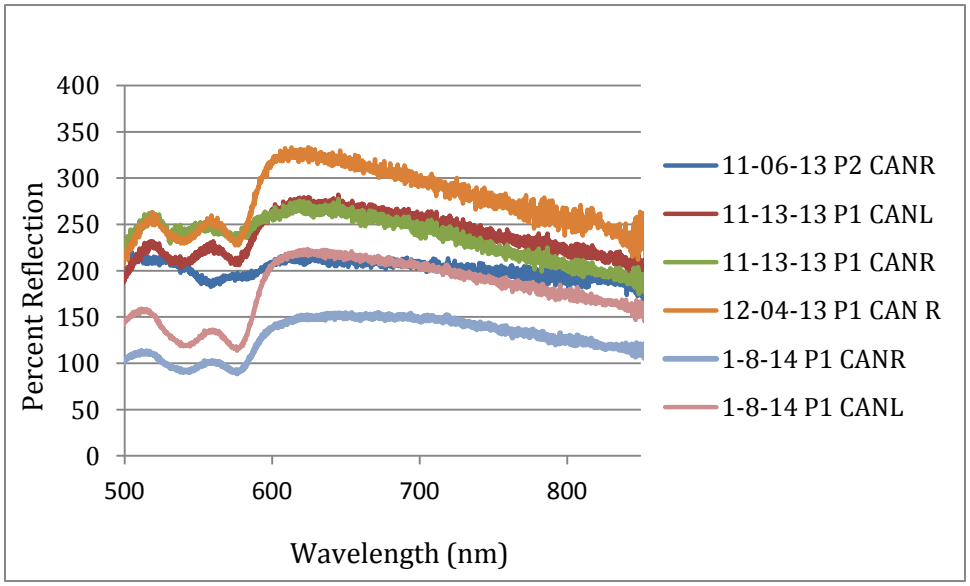

Figure 47: Class one canal reflectance spectra for ears with a thick effusion

The second class of canal effusion spectra was characterized by the same shape as tympanic membrane spectra for thin effusion consistency. This class was characterized by rapid increase in percent reflection between 575 nm and 650 nm and a rapid decrease in percent reflection between 650 nm and 750 nm.

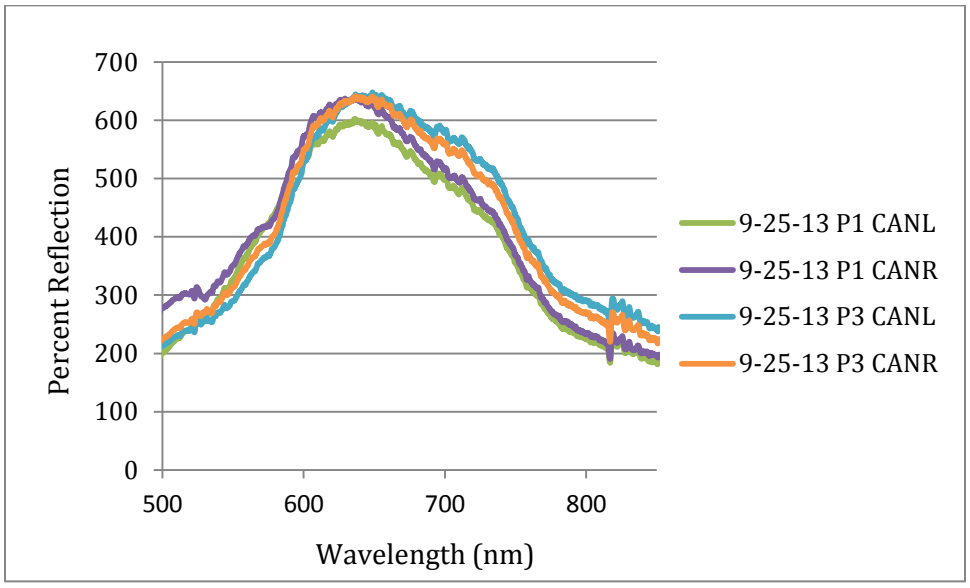

Figure 48: Class two canal reflectance spectra for ears with a thin effusion

The third class of canal spectra was determined because it did not follow the same waveform as the thick and thin spectra. This spectrum may be attributed to a disturbance of the probe during the procedure. The fourth classification of canal spectra for ears with an effusion resulted in a curve that combined characteristics of Class one and Class two waveforms. The characteristic hemoglobin spike was also present in these spectra.

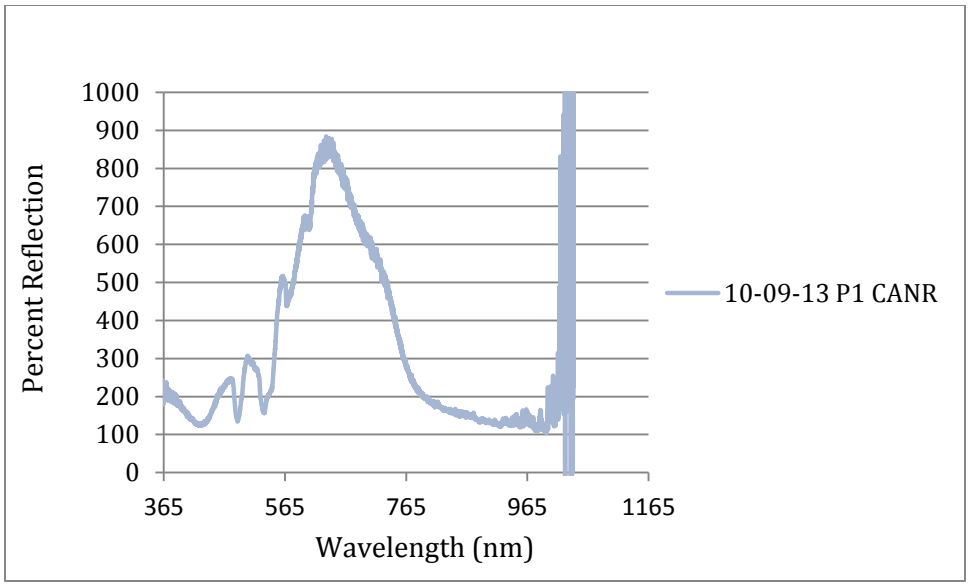

Figure 49: Class three canal reflectance spectra for ears with a thin effusion

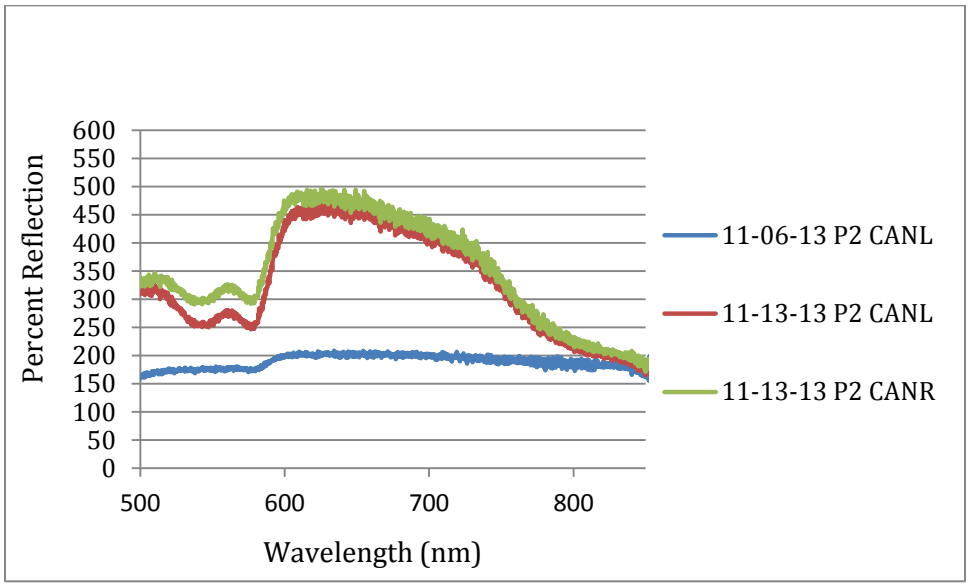

Figure 50: Class four canal reflectance spectra for ears with an effusion

3.3.3. Effusion Statistics

A chi square distribution was performed to determine the goodness of fit between the number of effusions that were observed as having class one or two effusion spectra and the number of effusions that were expected to have class one or two effusion spectra. Table 12 displays the expected and observed values for each of the dominant effusion classifications for

the tympanic membrane characterized by thick and thin fluid, respectively. The chi square was determined using equation 2. [33]

$$\sum \frac{(\boldsymbol{Observed - Expected})^{\mathbf{2}}}{\boldsymbol{Expected}} \qquad (2)$$

The degrees of freedom, n-1, where n is the number of classifications was determined to be 1. The chi square value was determined to be 0.2917 where p= 0.7. Therefore, p>0.05 and insignificant. It was determined that there was no statistical difference between the number of observed and expected fluid consistencies based on this test. The chi square distribution was only determined for tympanic membrane spectra since there was no effusion in the canal. It was however, determined that the canal effusion spectra followed the same classifications as the tympanic membrane.

Table 12: Chi Square Values

	Class 1	**Class 2**	**Total**
Observed	5	9	14
Expected	6	8	14
Total	11	17	28
Chi Square			0.291667

3.4.Noneffusion Spectra

The TM and canal noneffusion results were also characterized into the predetermined Class one and two spectra as seen in Table 13. There was no effusion present in the canal, however the classifications followed waveforms similar to the tympanic membrane and canal.

Table 13: Non Effusion Normal Spectra Classification

Subject/Ear	Non Effusion Normal Spectra Classification	
	TM Class	Canal Class
9-25-13 P2 L	*2*	*2*
9-25-13 P2 R	*2*	*2*
10-9-13 P1 L	*2*	*2*
10-16-13 P2 L	*1*	*1*
10-16-13 P2 R	*1*	*1*
10-30-13 P1 L	*1*	*1*
10-30-13 P1 R	*1*	*1*
12-04-13 P1 L	*1*	*1*

3.4.1. Tympanic Membrane

Percent reflection was determined to be between 30 and 50 percent for the first classification of tympanic membrane spectra with no effusion. There was a gradual decrease or no variance in percent reflection. The characteristic peak at 550 nm was present in all patients.

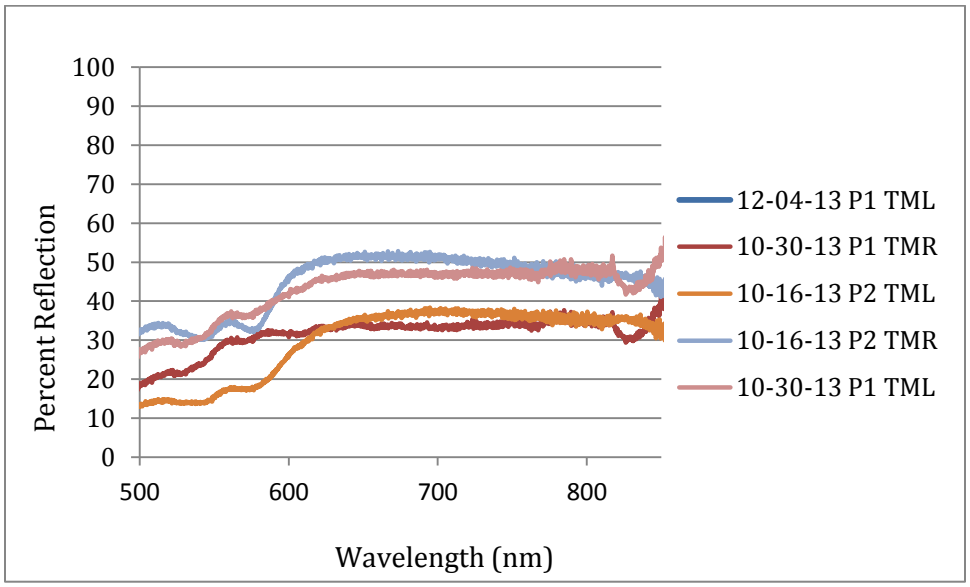

Figure 51: Class one tympanic membrane spectra in the presence of no effusion

Class two noneffusion spectra were characterized by a rapid increase in percent reflection between 600 nm and 620 nm and rapid decrease in percent reflection between 620 nm and 750 nm as in Figure 52. A peak at 550 nm was present in these spectra due to hemoglobin.

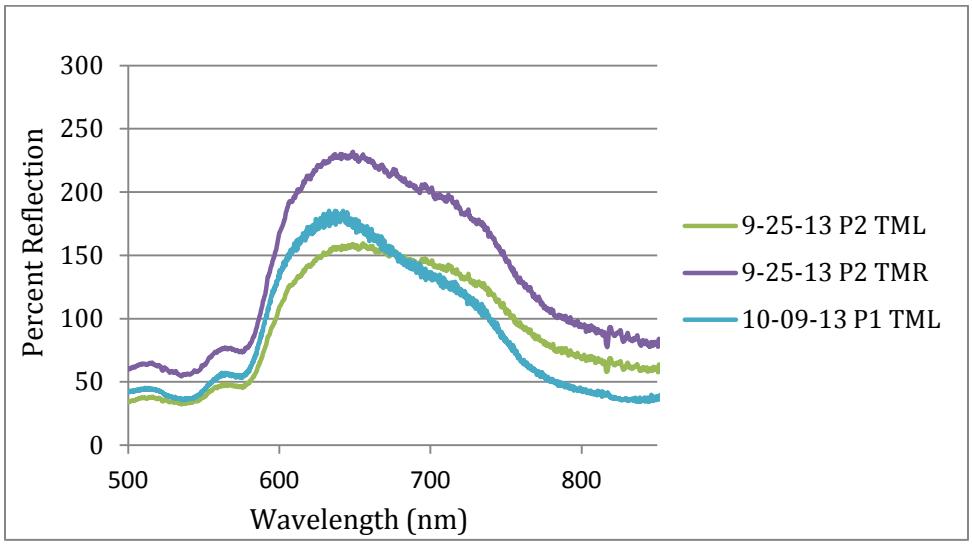

Figure 52: Class two tympanic membrane spectra in the presence of no effusion

3.4.2. Canal Spectra

Four ears were characterized by a decreasing slope between 600 nm and 800 nm for the first classification of canal spectra with no fluid retention in Figure 53. A characteristic hemoglobin peak around 600 nm was also present.

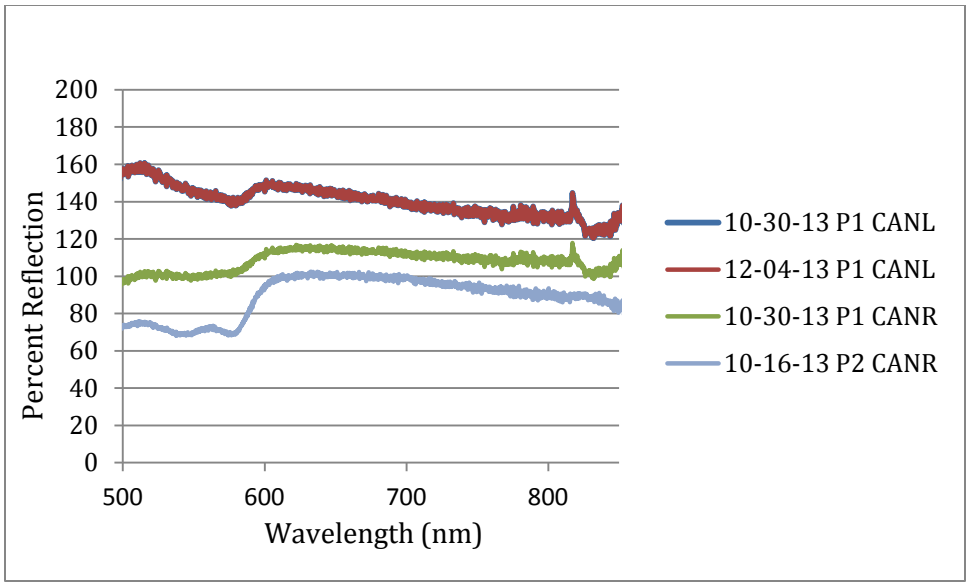

Figure 53: Class one canal spectra in the presence of no effusion

The second class of canal spectra for ear with no fluid retention was displayed in Figure 54. The spectra was characterized by an increase in percent reflection between 520 nm and 620 nm. There was also a decrease in percent reflection between 620 nm and 750 nm. A spike in percent reflection was not expected due to the absence of fluid in this region. The disruption of the spectra between 525 nm and 600 nm may be attributed to a disturbance during the procedure.

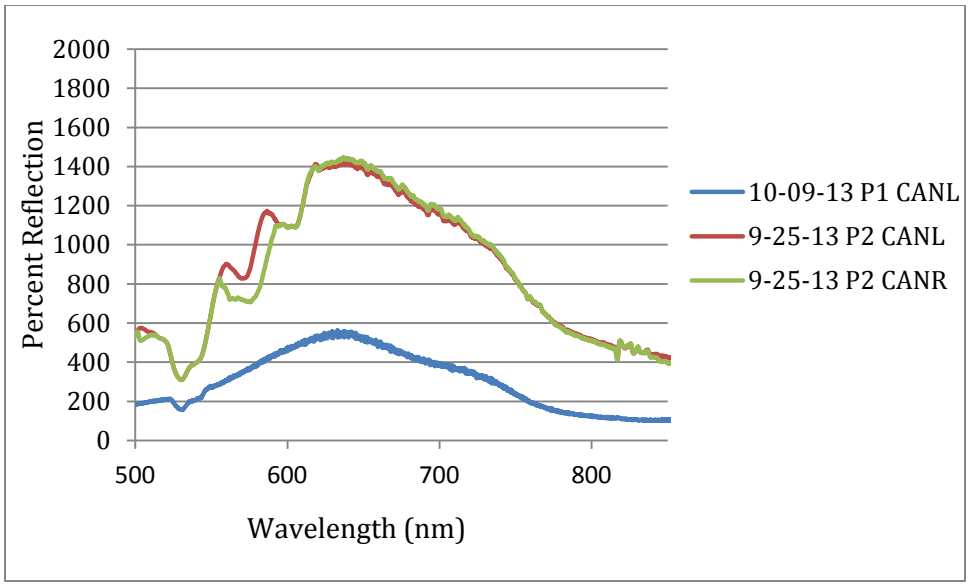

Figure 54: Class two canal spectra in the presence of no effusion

The third class of canal spectra in the presence of no effusion was displayed in Figure 55. Extra spikes between 525 nm and 625 nm may be attributed to a physical disruption during the reading.

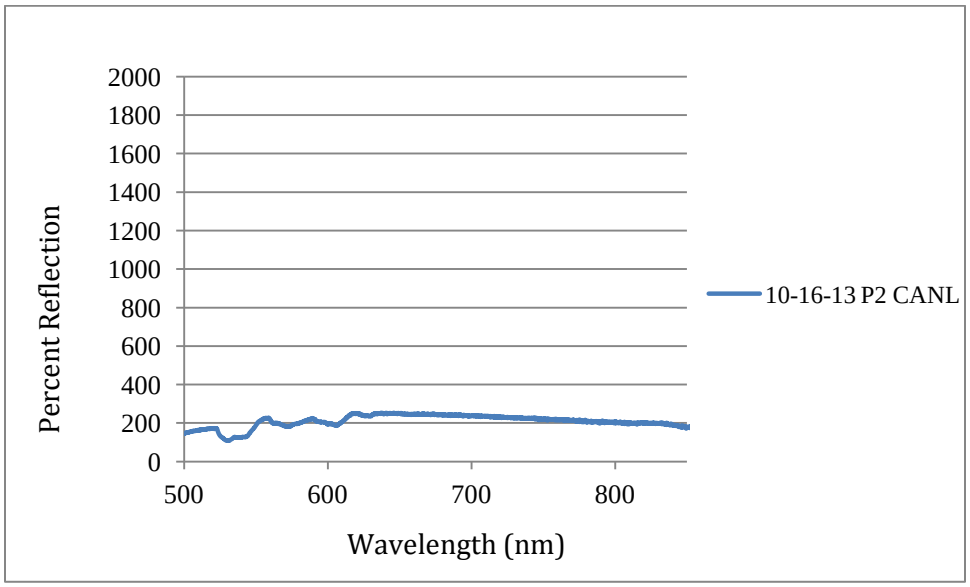

Figure 55: Class three canal spectra in the presence of no effusion

Similarities between fluid consistencies were determined from this study. There were also trends between the waveforms of TM and canal spectra for patients with an effusion and no effusion with a couple deviations. This finding may lead to further investigation to determine whether the bacteria causing otitis media has characteristic spectral properties. The images were enhanced through signal processing to improve resolution and contrast in the middle ear region.

3.5.Digital Imaging

Images were recorded by a Thorlabs camera for each patient. A white, white-blue, blue, green, red, and uv-visual images were recorded. A 500 nm filter was applied to the blue wavelength and an image was recorded. An image of a 425 nm and 500 nm filter with the UV wavelength was also recorded for each patient. Figures 58 through 62 displayed some of the images recorded for 12-04-14 P1 R. An effusion and swollen tympanic membrane were observed. Figure 56 was recorded with a white-blue excitation source. The original image can be seen in the upper left corner of the image. Signal processing algorithms were used to enhance the characteristics of the image. Blue and green wavelengths had the same effect.

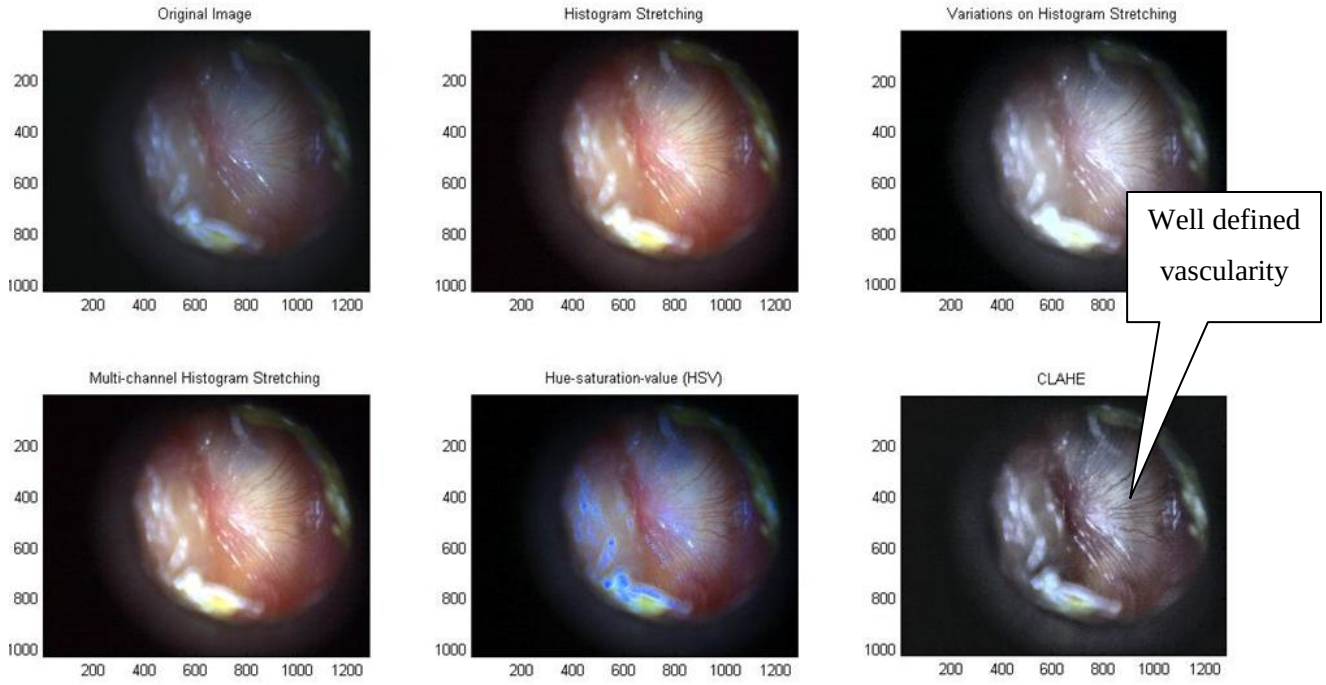

Figure 56: Tympanic membrane image recorded using White and blue wavelengths.

The UV light source was emitted into the ear and Figure 57 was recorded without a filter.

Enhanced contrast and vascularity resulted from this wavelength.

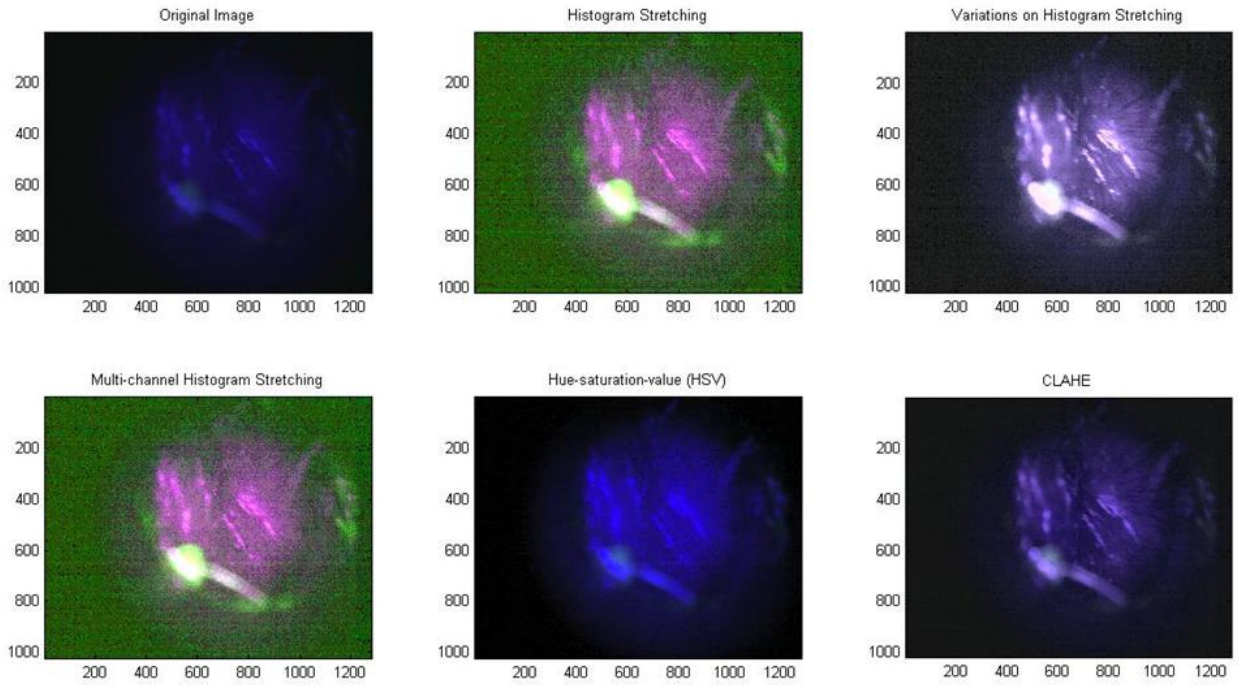

Figure 57: Tympanic membrane image recorded using a UV 405nm wavelength.

The UV light source and a 425 nm filter were emitted into the ear and Figure 58 was recorded.

Blue Fluorescence was observed an enhanced through signal processing.

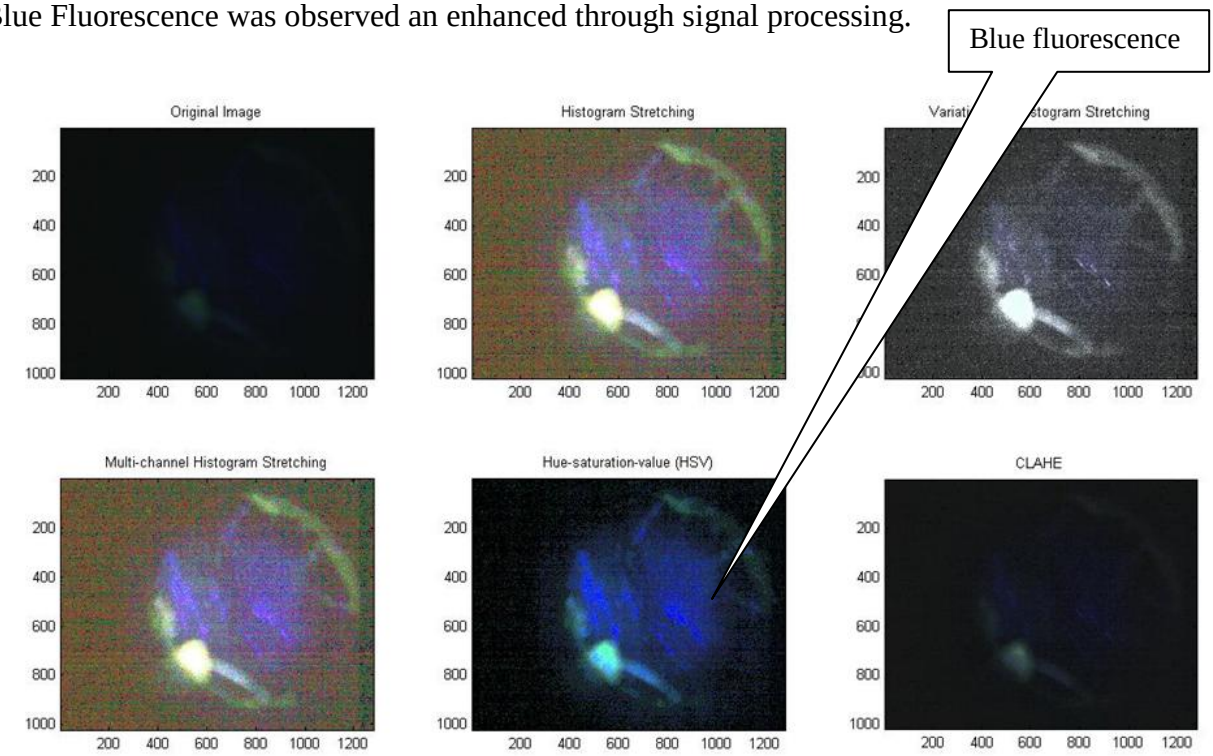

Figure 58: Tympanic membrane image recorded using a UV 405nm wavelength and 425nm filter.

The UV light source and a 500 nm filter emitted into the ear and Figure 59 was recorded. Cerumen and green fluorescence was observed.

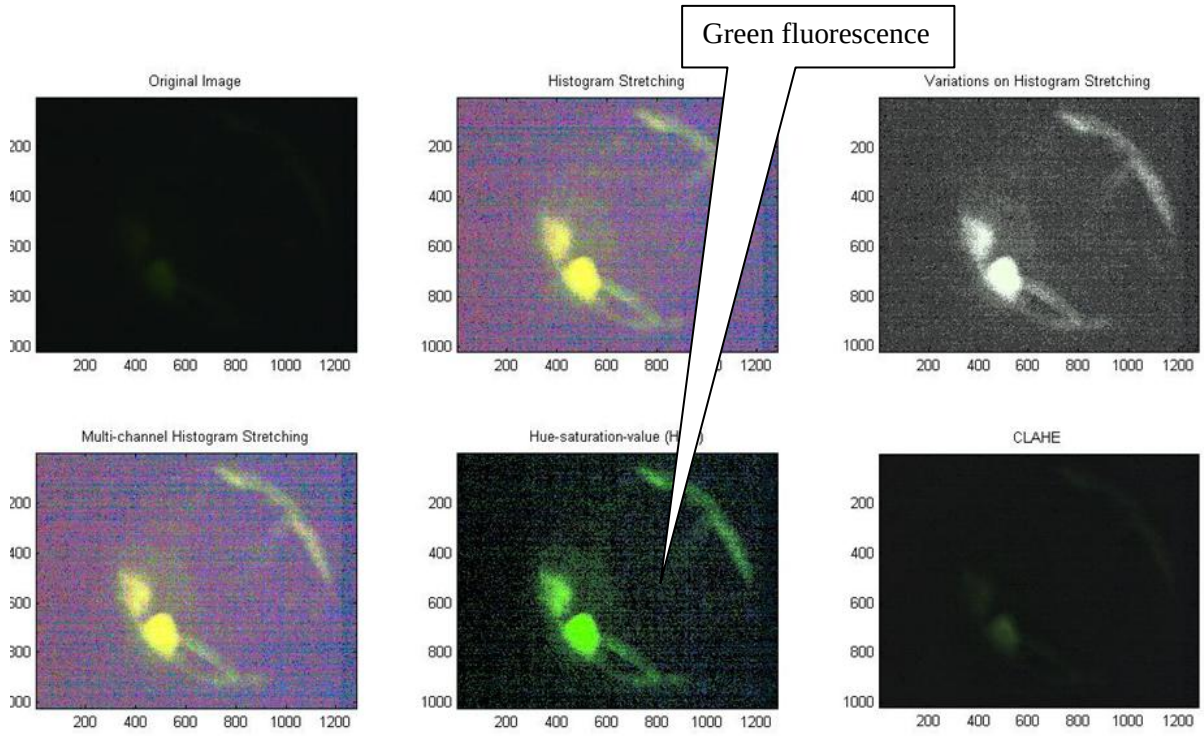

Figure 59: Tympanic membrane image recorded using a UV 405 nm wavelength and 500 nm filter

The red light source was emitted into the ear and Figure 60 was recorded. This wavelength provided contour observations not observed with the other wavelengths.

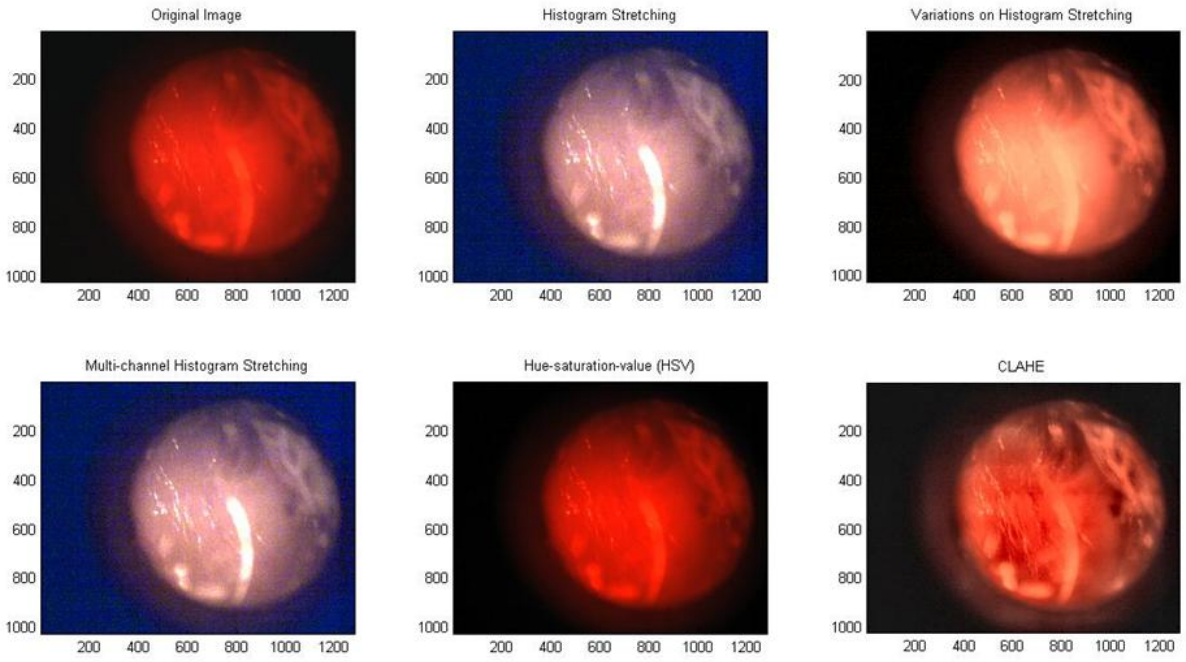

Figure 60: Tympanic membrane image recorded using a red wavelength

The results show that there is no obvious difference between images with and without an effusion. Figure 61a is an image of the tympanic membrane using blue and white light in the presence of an effusion. Figure 61b is an image of the tympanic membrane with no effusion. Enhanced resolution and magnification are observed in both.

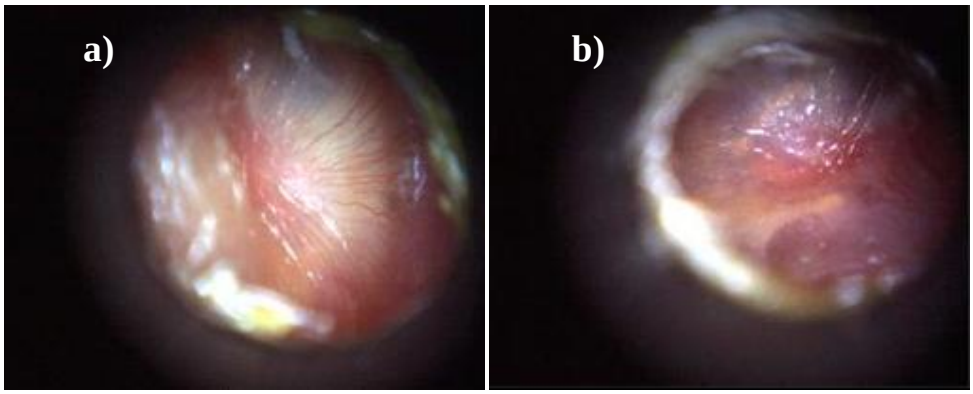

Figure 61: (a) Tympanic membrane image recorded using blue and white light in the presence of an effusion. **(b)** Tympanic membrane image recorded using blue and white light in the absence of an effusion

It was also determined that the presence and absence of an effusion each resulted in the observation of fluorescence as seen in Figure 62a and 62b.

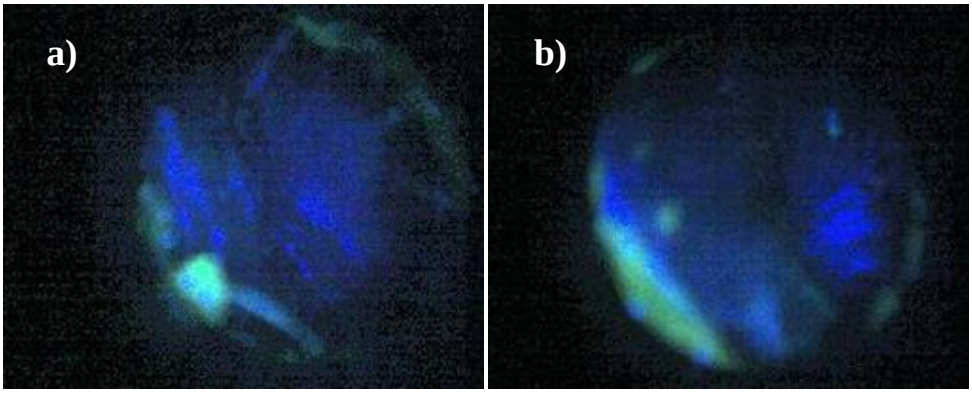

Figure 62: (a) Tympanic membrane image recorded using a 405nm excitation source and 425nm longpass filter in the presence of an effusion. **(b)** Tympanic membrane image recorded in the absence of an effusion

4.0 Discussion

This study investigated the novel design of a device that utilized spectroscopy and fluorescence imaging to provide physicians with a tool to present a unique representation of the middle ear to enhance an infection's characteristics. The design, along with medical imaging and spectroscopy has shown to be an effective approach to diagnose otitis media with increased diagnostic certainty. Various factors that typically led to the inaccurate diagnosis of otitis media by a general practitioner and otolaryngologist due to the difficulty of differentiating between the various types of otitis media were considered.

Acute otitis media is a condition that is characterized by inflammation of the middle ear in the presence of an infected effusion and was typically diagnosed after an upper respiratory infection or fever. General practitioners diagnose a red, swollen tympanic membrane with acute otitis media without further investigation; however, more information is required to confirm the diagnosis. A whiteish-yellow swollen tympanic membrane was generally the observation of

acute otitis media due to the presence of pus behind the tympanic membrane. Furthermore, otitis media with effusion was resistant to antibiotics and was characterized by a non-infected effusion. It was important that a highly accurate approach was applied when a diagnosis is made because not all classifications of otitis media were receptive to antibiotics.

Currently the Welch Allen otoscope is commercially available to induce movement within the tympanic membrane through an insufflation port. Activation of the insufflation port was a potential benefit to many modern day otoscopes due to its capabilities. Specifically, an effusion was present in the middle ear region if there was no movement of the tympanic membrane when air was forced through the port into the ear. The tympanic membrane movement, in addition to the expertise of a specialist, was one of the most efficient mechanisms to determine an accurate diagnosis without intraoperative care to date.

The otoscope was designed to build off of traditional otoscope components to provide a comfortable, easy to use device. The design incorporated a unique combination of fluorescence and illumination components as well as a traditional otoscope head and basic aluminum structure. The Welch Allen head incorporated into this design is widely used by practitioners and otolaryngologists to efficiently emit light into the tympanic membrane. A new otoscope head was not included in the design because of the simplicity of the structure and the time allotted for the project. The otoscope head contained a light pipe, magnifying lens, and additional magnification and focus settings to view the tympanic membrane.

The device design incorporated components that are not traditionally featured on commercial otoscopes. Traditional otoscopes primarily rely on white light and a physician's trained eye to determine whether there was presence of otitis media and an effusion. The new

design incorporated five different wavelengths across the spectrum that had unique individual characteristics to enhance the reliability of an accurate diagnosis. Specifically, the UV, blue, and combination of UV and Blue light served to enhance the internal anatomy around the tympanic membrane as in Figure 63. The combination of blue and green also enhanced the tympanic membrane with better visibility for certain patients. Figure 63 was not processed through the signal processing algorithm.

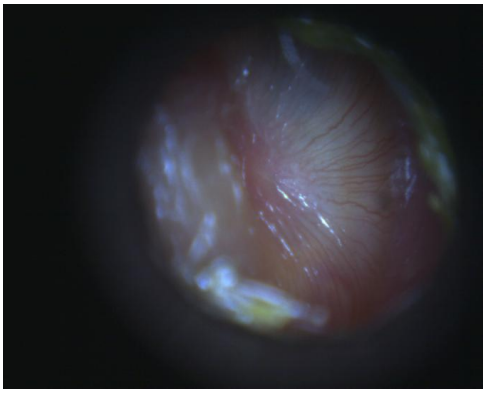

Figure 63: Tympanic membrane image recorded using a white and blue combination light source

Contrast between the malleus and the rest of the tympanic membrane was observed with these wavelengths in normal patients. Enhanced definition of the swollen tympanic membrane and vascularity were observed in patients with otitis media. The surgeon was also capable of determining whether or not an effusion was present from the medical images. The characteristics in the presence and absence of an effusion were not obvious; however, a physician was able to determine whether or not the fluid was present from the images. Furthermore, the results showed that additional research is necessary accurately determine what is responsible for fluorescence the middle ear region. Fluorescence was observed in the presence and absence of an effusion potentially due to fluid or the anatomical characteristics of the tympanic membrane. Conditions such as myringosclerosis, a condition that is characterized by calcium deposits and dense

connective tissue due to persistent acute otitis media, were also enhanced with each wavelength. myringosclerosis typically resulted in a thicker nontransparent tympanic membrane due to the collection of cells on the surface. The ultraviolet and white/blue combination wavelengths enhanced these features as pictured in Figure 64.

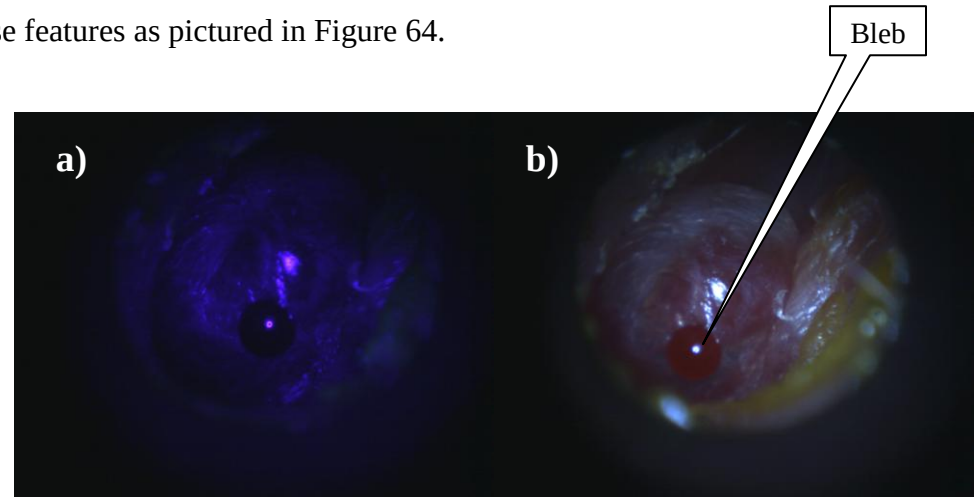

Figure 64: (a) Ultraviolet and **(b)** white/blue combination image of myringosclerosis before signal processing

Fluorescence spectroscopy is the study of the interaction of electrons with a photon or other type of electromagnetic radiation. A high-energy photon is absorbed during the fluorescence process and results in the promotion of an electron to an excited, higher energy, vibrational state as in Figure 65. The electron energy is subsequently transferred to a lower vibration state and relaxed back to ground state with lower energy. A longer wavelength of light is emitted as a result of the process. The emitted color of fluorescence light is dependent on the vibrational states that the electron is promoted to. [32] Blue and Ultraviolet wavelengths were investigated as part of this study and found to enhance characteristics of otitis media, where blue and green fluorescence were detected.

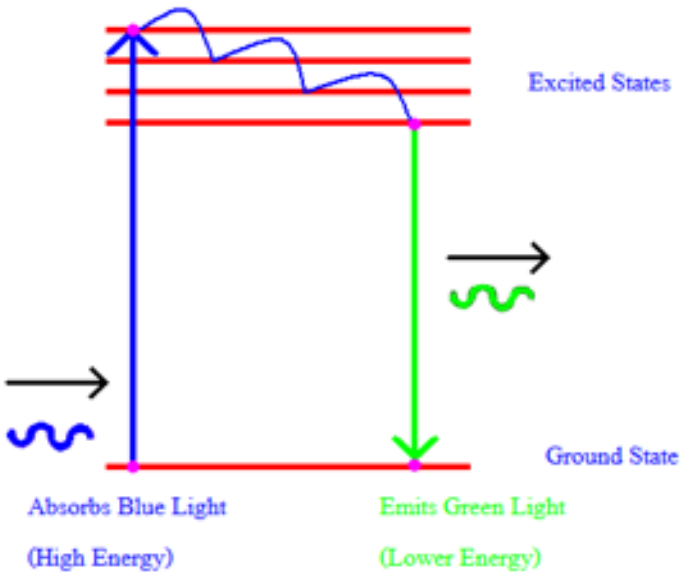

Figure 65: Fluorescence energy level diagram [32]

Fluorescence was observed from the UV and Blue wavelengths using a 425 nm and 500 nm filter. Excitation wavelengths were emitted into the ear canal using the otoscope speculum. The excitation light reached the tympanic membrane and was reflected back into the otoscope with the corresponding longer emission wavelength. The excitation wavelength was filtered out and the emission wavelength was allowed to pass for observation as demonstrated in the Figure 66.

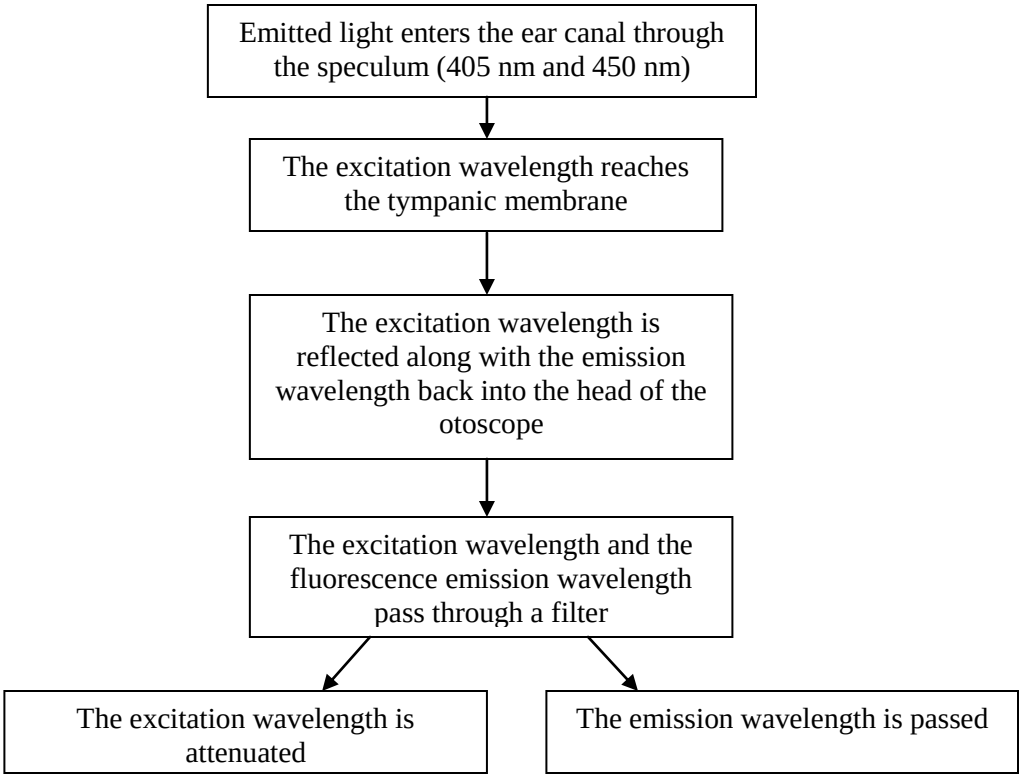

Figure 66: Fluorescence flow chart

The 425 nm longpass filter paired with a 405 nm excitation source resulted in fluorescence images. Additionally, the 500 nm filter paired with the 405 nm filter also resulted in fluorescence images. Fluorescence was observed for patients with an effusion and no effusion. This may lead to the conclusion that all forms of otitis media fluoresce including, acute otitis media, and otitis media with or without effusion, and chronic otitis media. Further research to determine the effect of different bacteria species may also help to determine a relationship between the detection of fluorescence and the type of bacteria causing the infection. Additional techniques such as optical coherence tomography in addition to fluorescence spectroscopy may also lead to the determination of biofilms in otitis media mucosa. The determination of the type of bacteria and response to antibiotics would enable physicians to prescribe antibiotics based on an accurate bacterial diagnosis instead of visual observation.

The reflectance spectroscopy procedure resulted in two dominant waveforms between 550 nm and 800 nm. The results for a thin effusion accurately represented the percent reflectance as a function of wavelength as expected. The tympanic membrane results in the case of an effusion were represented by a waveform that rapidly increased prior to a rapid decrease in percent reflection as a function of the associated wavelengths. This was expected due to the presence of an effusion; however, further research is required to validate the reason. The tympanic membrane results in the case of a thick effusion were also consistent with the original hypothesis because there was a gradual decrease in the percent reflectance as a function of wavelength. Initially, it was hypothesized that the spectra was characteristic of the consistency of the effusion fluid. A chi square statistical distribution validated that this was a valid observation for the tympanic membrane spectra.

Two dominant canal classifications were consistent with the two dominant tympanic membrane classifications. It was originally hypothesized that class one and two waveforms were characteristic of the effusion consistency; however, there was no effusion present for the canal spectra that were consistent for these results. This leads to the conclusion that there are other factors in addition to effusion consistency that influence the reflectance spectra. Factors such as bacteria identification and individual properties of the tympanic membrane should be considered.

Any additional inconsistencies in the data can be attributed to a variety of factors. The lights were dimmed during the myringotomy procedure for the spectra and fluorescence imaging collection. However, additional light from the operating room may have affected the spectra collection if the reflectance probe was not appropriately directed into the ear canal. Furthermore, variations in the spectra, as seen in the third class of canal spectra for patients with an effusion, can be attributed to a disruption of the probe during the procedure. It was possible that the

reflectance probe may have made contact with an internal structure during the process. Further inconsistencies may be attributed to the calibration method that was performed each day of data collection. A dark box was used to collect the dark measurements; however, a better calibration source may have provided a more efficient mechanism to collect the data.

The 455 nm blue wavelength was also used to detect fluorescence in the tympanic membrane. This wavelength served as a sufficient excitation source; however, the correct filter may not have been implemented for each reading. The 500 nm filter and the 455 nm light source resulted in a combination of fluorescence and faint blue light. The 455 nm excitation source had a broad bandwidth that interfered with the 500 nm filter. Faint blue light was not attenuated by the 500 nm filter as a result. A longpass filter capable of attenuating wavelengths below 500 nm should be considered in the future design for 455 nm excitation wavelengths.

Previous studies suggested that spectroscopy may provide reasonable evidence to suggest that the reflectance and absorption measurements of clinical data, in combination with other non-invasive devices, aided in diagnosis. [10] Further research and collaborative design could combine optical coherence tomography and fluorescent spectroscopy for commercial use in a pediatrics office. Furthermore, the research presented in this paper could be applied to differentiate acute otitis media and otitis media with effusion diagnosis in pediatric patients. Optical coherence tomography and the determination of bacteria biofilms may provide the reason that the biofilms are not susceptible to antibiotics in certain cases. Fluorescence spectroscopy was applied to this research to determine a comparison between effusion and non-effusion normal otitis media patients. Reflectance, absorption, and fluorescence spectroscopy combined with medical imaging during an otoscopic examination may provide insight to whether there is fluid in the middle ear

region. In addition, the fluorescent characterization of bacteria infected fluid would provide the correct treatment for the patient.

Antibiotics will continue to be prescribed medication without high diagnosis certainty if a new diagnostic criterion is not developed. The development of a new device will reduce over-diagnosis of otitis media in the pediatric community and increase the accuracy of a diagnosis by a general practitioner. An otoscope capable of fluorescence and high resolution imaging would allow the physician to make an interpretation based off of a detailed image of the tympanic membrane. Further classification of reflectance spectra would also allow the physician to link the visual interpretation to a series of data that would assist to make an appropriate diagnosis. An otoscope that combines the use of spectroscopy and fluorescence imaging would facilitate this process. A future otoscope would potentially combine a reflectance probe in the handle. The use of plastic and three dimensional printing would also enhance the design. Furthermore, fluorescence imaging and reflectance spectroscopy will determine an optimal otoscopic procedure to determine whether otitis media with effusion is present.

5.0 Conclusion

The development of a new device for fluorescence imaging and spectroscopy was investigated to increase the reliability of otitis media diagnosis. Distinct spectral and otoscopic images of the tympanic membrane were observed using the novel design of an otoscope. The reflectance spectroscopy portion of the research resulted in a characterization of ears with and without an effusion present in the middle ear region. Differences in effusion consistency were also characterized by distinct spectral waveforms between 560 nm and 800 nm using a UV-visual light source. There were trends between the waveforms of the tympanic membrane and canal spectra for patients with an effusion and no effusion may lead to further investigation to determine whether the bacteria causing otitis media has characteristic spectral properties.

The varying wavelengths of light emitted from the otoscope also aided in structural recognition and enhancement in the middle ear region. Specific wavelengths such as the UV-visual 405 nm and 455 nm excitation sources induced fluorescence in the blue and green spectrum. Fluorescence was detected for patients with an effusion that could potentially lead to the conclusion that specific bacteria in an effusion can produce fluorescence. The use of fluorescence imaging to assist the physician could potentially aid in increase of otitis media diagnostic certainty due to identification of fluorescence in the middle ear region. Further research is required to determine spectral and digital differences due to the fact that patients with no effusion also had faint fluorescence readings. The Methods described proved to initiate the development of criteria to increase the level of diagnostic certainty of otitis media that will reduce over-diagnosis of otitis media in the future.

6.0 References

1. Phillip H. Kaleida, MD[a,b], Dianna L. Ploof, EdD[a,b], Marcia Kurs-Lasky, MS[c], Nader Shaikh, MD[a,b], D. Kathleen Colborn, BS[a], Mary Ann Haralam, MSN[a], Sean Ray, BS[a], Diana Kearney, RN, CCRC[a], Jack L. Paradise, MD[a,b], Alejandro Hoberman, MD[a,b]
2. Mastering Diagnostic Skills: Enhancing Proficiency in Otitis Media, a Model for Diagnostic Skills Training Soni, A. Ear Infections (Otitis Media) in Children (0−17): Use and Expenditures, 2006. Statistical Brief #228. December 2008. Agency for Healthcare Research and Quality, Rockville, MD, http://www.meps.ahrq.gov/mepsweb/data_files/publications/st228/stat228.pdf
3. "Otoscopic Exam of the Ear: MedlinePlus Medical Encyclopedia Image." U.S National Library of Medicine. U.S. National Library of Medicine, n.d. Web. 17 Mar. 2014.
4. Longo, Kaitlyn., Kent, Amy., Frederick Wright. Senior Design Report. University of Connecticut
5. Otitis Media ." Otitis Media. N.p., n.d. Web. 18 Mar. 2014. http://emedicine.medscape.com/article/994656-overview
6. Productions, Visible. "Middle Ear Infection Images: Learning Center on Yahoo! Health."Yahoo! Health. Web. 15 Nov. 2011. <http://health.yahoo.net/channel/ear-disorders_images>.
7. "Otitis Media with Effusion (Serous Otitis Media)." *The Children's Hospital of Philadelphia*. N.p., n.d. Web. 18 Mar. 2014.
8. Valdez, Tulio. "Post Image Processing." PowerPoint presentation. Hartford, CT. 2013.
9. Jensen P, Lous J. Criteria, Performance and Diagnostic Problems in Diagnosing Acute Otitis Media. Family Practice 1999; 16(3):262--268.
10. "Spectrophotometric otoscope: A new tool in the diagnosis of otitis media". *Nong Lam University*. Web. <http://www2.hcmuaf.edu.vn/data/phyenphuong/J15_0209.pdf>.
11. Occurrence of Acute Otitis Media During Colds in Children Younger Than Four Years Armengol, Carlos Eladio MD*†; Hendley, J. Owen MD*; Winther, Birgit MD‡ Pediatric Infectious Disease Journal:June 2011 - Volume 30 - Issue 6 - pp 518-520http://journals.lww.com/pidj/Abstract/2011/06000/Occurrence_of_Acute_Otitis_Media_During_Colds_in.17.aspx
12. Multi-species bacterial biofilm and intracellular infection in otitis media. Ruth B Thornton12[*], Paul J Rigby3, Selma P Wiertsema12, Pierre Filion4, Jennifer Langlands2, Harvey L Coates156, Shyan Vijayasekaran156, Anthony D Keil7 and Peter C Richmond12 http://www.biomedcentral.com/1471-2431/11/94
13. Boppart, Stephen. Visualizing Middle Ear Biofilms in otitis Media: a new benchmark for successful treatment. http://biophotonics.illinois.edu/pubs/biophotonics_current/ENTSO12_Boppart.pdf
14. Spector BC, Reinisch L, Smith D, Werkhaven JA.Laryngoscope. 2000 Jul;110(7):1119-23. Noninvasive fluorescent identification of bacteria causing acute otitis media in a chinchilla model.Department of Otolaryngology, Vanderbilt University Medical Center, Nashville,

Tennessee 37232-2559, USA.

15. Sundberg M, Peebo M, Oberg PA, Lundquist PG, Strömberg T.Diffuse reflectance spectroscopy of the human tympanic membrane in otitis media. Department of Biomedical Engineering, Linköpings Universitet, SE-581 85 Linköping, Sweden. miksu@imt.liu.se
16. Van der Jeught S, Dirckx JJ, Aerts JR, Bradu A, Podoleanu AG, Buytaert JA. J Assoc Res Otolaryngol. 2013 May 15. [Epub ahead of print]Full-Field Thickness Distribution of Human Tympanic Membrane Obtained with Optical Coherence Tomography.Laboratory of Biomedical Physics, University of Antwerp, Groenenborgerlaan 171, B-2020, Antwerp, Belgium,
17. "Welch Allyn Digital MacroView Otoscope." *: Get Quote, RFQ, Price or Buy*. N.p., n.d. Web. 19 Mar. 2014. <http://www.news-medical.net/Welch-Allyn-Digital-MacroView-Otoscope>.
18. "AURICAL OTOcam 300 - Video Otoscope." Video Otoscopy. N.p., n.d. Web. 18 Mar. 2014.
19. Firefly DE550 Handheld Digital Wireless Otoscope - Oasis Scientific Inc." Oasis Scientific Inc. N.p., n.d. Web. 18 Mar. 2014. http://www.oasisscientific.com/firefly-de550-handheld-digital-wireless-otoscope.html
20. N.p., n.d. Web.http://www.mdtmag.com/news/2013/10/ear-infection-diagnosis-smartphone
21. Longo, KAitlyn, Wright, Fred, Kent, Amy. Senior Design Report.
22. "SM1 Thread Compatibility." Thorlabs. N.p., n.d. Web. 03 Mar. 2014. <http://www.thorlabs.com/newgrouppage9.cfm?objectgroup_id=4024&pn=DCC1645C>.
23. Mouser Electronics. http://www.mouser.com/ProductDetail/LedEngin/LZ4-20MD00/?qs=sGAEpiMZZMubXWjzskHvc%2fnbIuZUZtWA. Web.
24. Mouser Electronics. http://au.mouser.com/ProductDetail/LedEngin/LZ1-10UA00-U7/?qs=sGAEpiMZZMv/bGM7XKYHK8wl3wqjbvce. Web.
25. "MagTech - 3-Watt 700mA Constant Current LED Driver." *MagTech - 3-Watt 700mA Constant Current LED Driver*. N.p., n.d. Web. 28 Feb. 2014.
26. "103-1422-EVX." *Mouser Electronics*. N.p., n.d. Web. 28 Feb. 2014. <http://au.mouser.com/ProductDetail/Mountain-Switch/103-1422-EVX/?qs=%2fha2pyFaduiUT2Qxm9RKEUvtwZl%2frGbUKtmPPp7FY8A%252byKYj7Qtbtg%3d%3d>.
27. Calibrating the wavelength of the Spectrometer. Web. http://www.oceanoptics.com/Technical/wavelengthcalibration.pdf
28. Valdez Tulio, Roehm Corrie. Spectral Otoscopic Evaluation of the Tympanic Membrane and Middle Ear Effusions. 2013. Connecticut Children's Medical Center, CT.
29. "PX-2 Pulsed Xenon Light Source." PX-2 Pulsed Xenon Light Source. N.p., n.d. Web. 15 May 2013.
30. Edmund Optics.

http://www.edmundoptics.com/techsupport/resource_center/product_docs/curv_62975.pdf**. Web.**

31. Edmund Optics. http://www.edmundoptics.com/techsupport/resource_center/product_docs/curv_62976.pdf. Web.
32. "Fluorescence." Fluorescence. N.p., n.d. Web. 10 Mar. 2014. <http://www.st-andrews.ac.uk/seeinglife/science/imaging/fluorescence/fluorescence.html>.
33. Chi-Square Test. N.p., n.d. Web 29. Apr. 2014.

7.0 Appendix

9-25-13 P1 Left

Images: BGL2, BL, BL500, GBL2, GL, RL, UV500, UVL, UVL425, UVL500, W2L, WBL

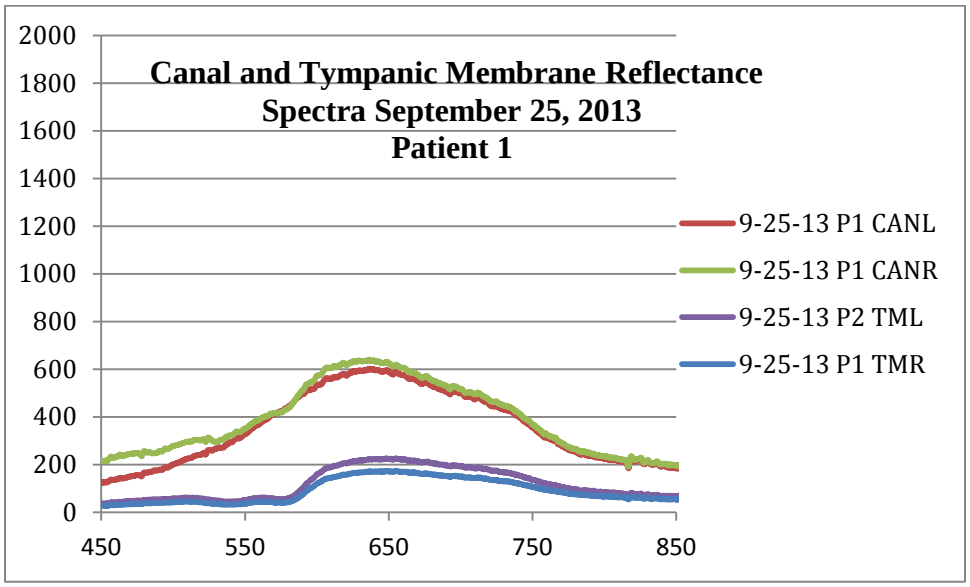

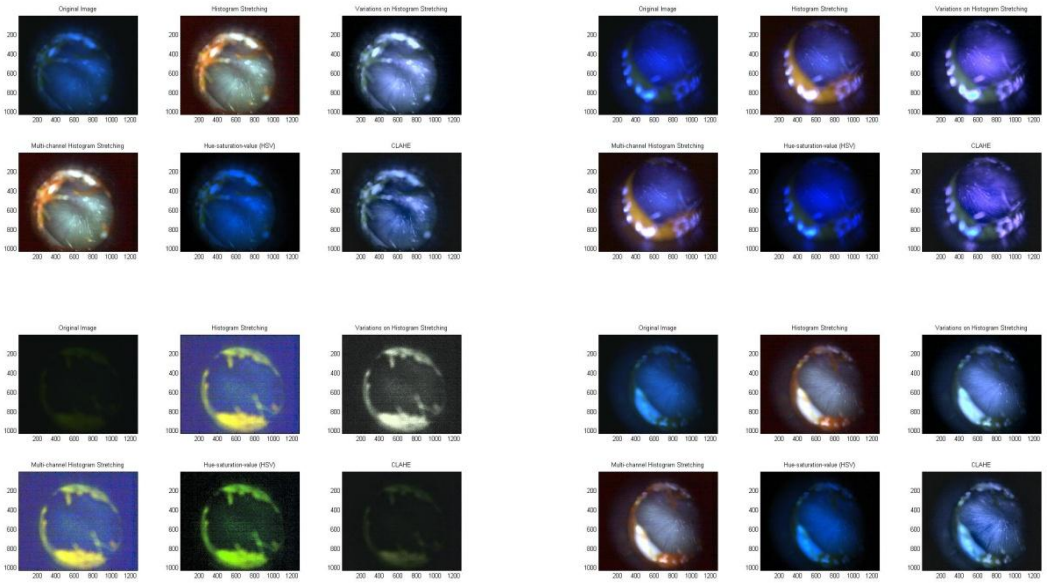

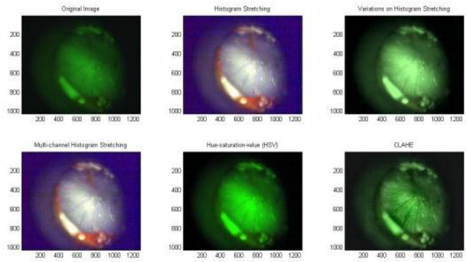
Original Image
Histogram Stretching
Variations on Histogram Stretching
Multi-channel Histogram Stretching
Hue-saturation-value (HSV)
CLAHE

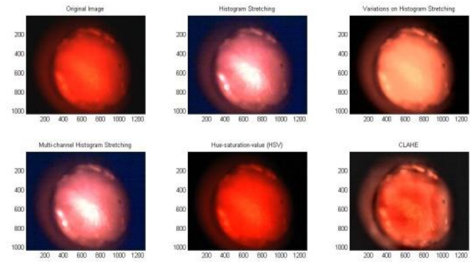
Original Image
Histogram Stretching
Variations on Histogram Stretching
Multi-channel Histogram Stretching
Hue-saturation-value (HSV)
CLAHE

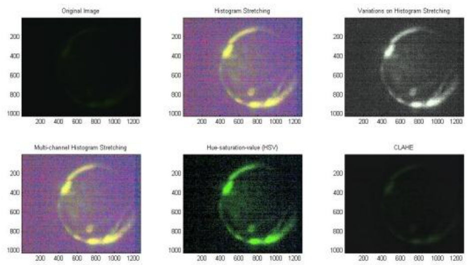
Original Image
Histogram Stretching
Variations on Histogram Stretching
Multi-channel Histogram Stretching
Hue-saturation-value (HSV)
CLAHE

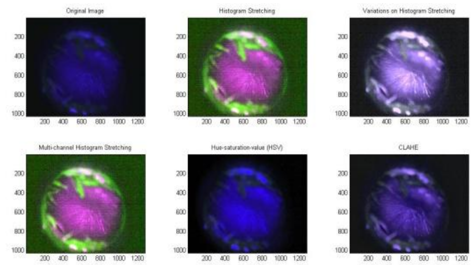
Original Image
Histogram Stretching
Variations on Histogram Stretching
Multi-channel Histogram Stretching
Hue-saturation-value (HSV)
CLAHE

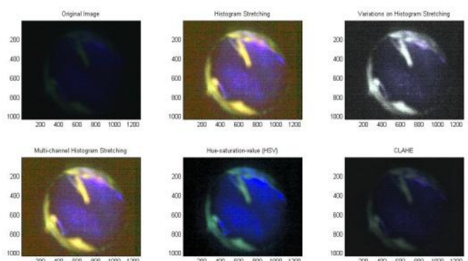
Original Image
Histogram Stretching
Variations on Histogram Stretching
Multi-channel Histogram Stretching
Hue-saturation-value (HSV)
CLAHE

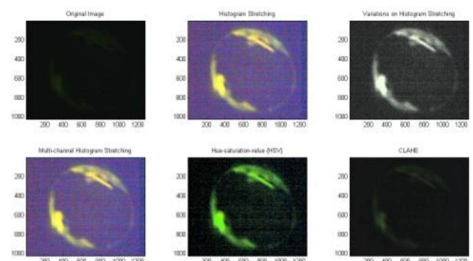
Original Image
Histogram Stretching
Variations on Histogram Stretching
Multi-channel Histogram Stretching
Hue-saturation-value (HSV)
CLAHE

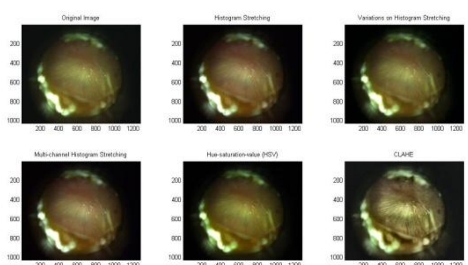
Original Image
Histogram Stretching
Variations on Histogram Stretching
Multi-channel Histogram Stretching
Hue-saturation-value (HSV)
CLAHE

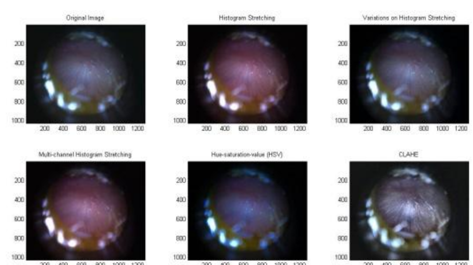
Original Image
Histogram Stretching
Variations on Histogram Stretching
Multi-channel Histogram Stretching
Hue-saturation-value (HSV)
CLAHE

9-25-2013 P1 Right

Images BGR, BR, BR500, GR, RR, UVR, UVR425, WBR, WR

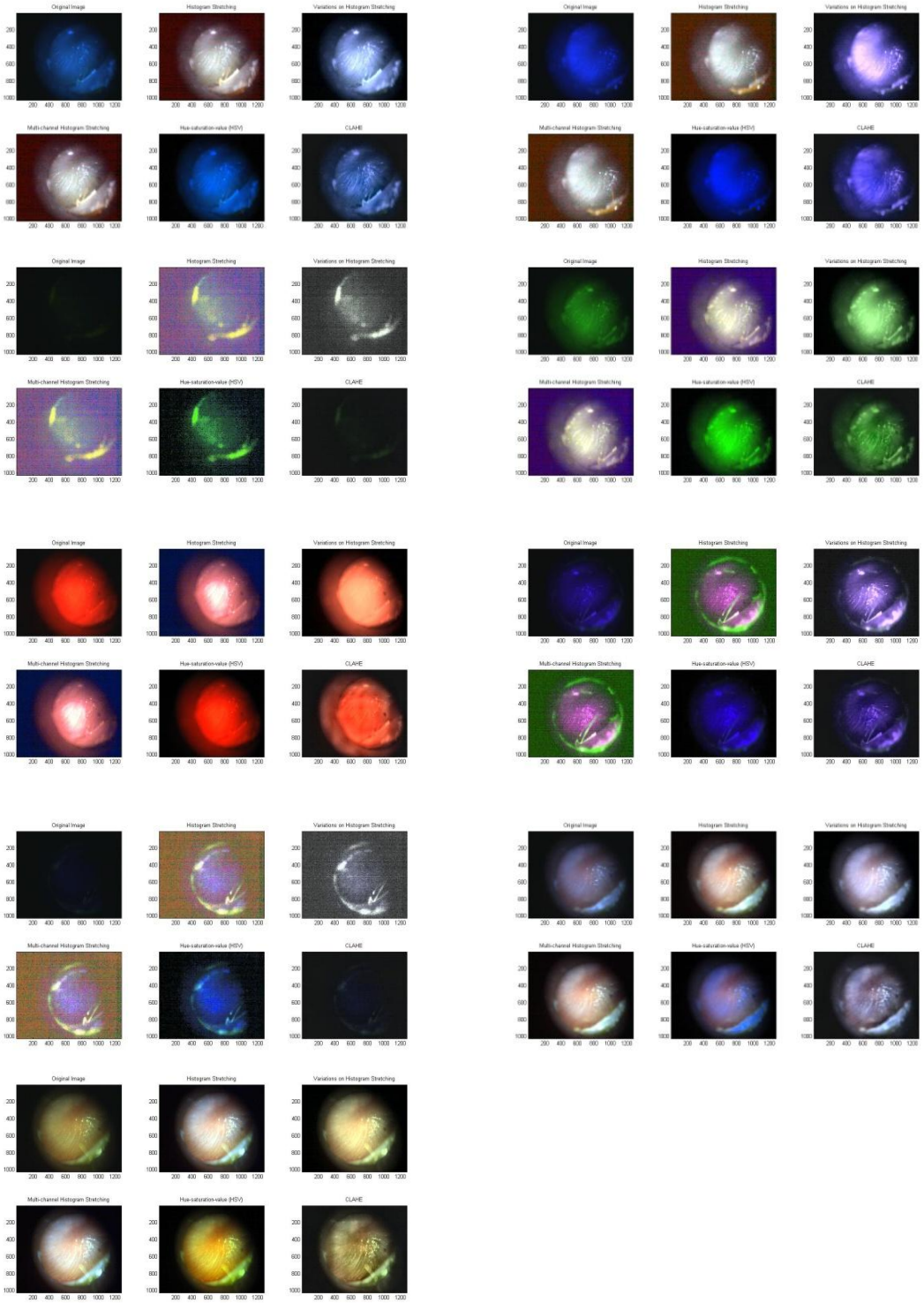

9-25-13 P2 Left

Images B500L, BGL, BL, GL, RL, UV425L, UV500L, UVL, WBL, WL

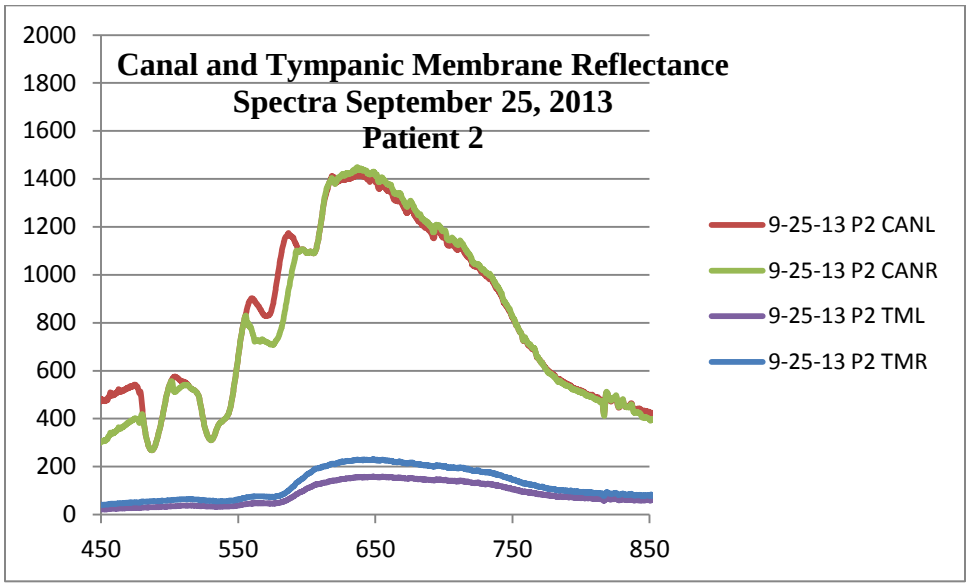

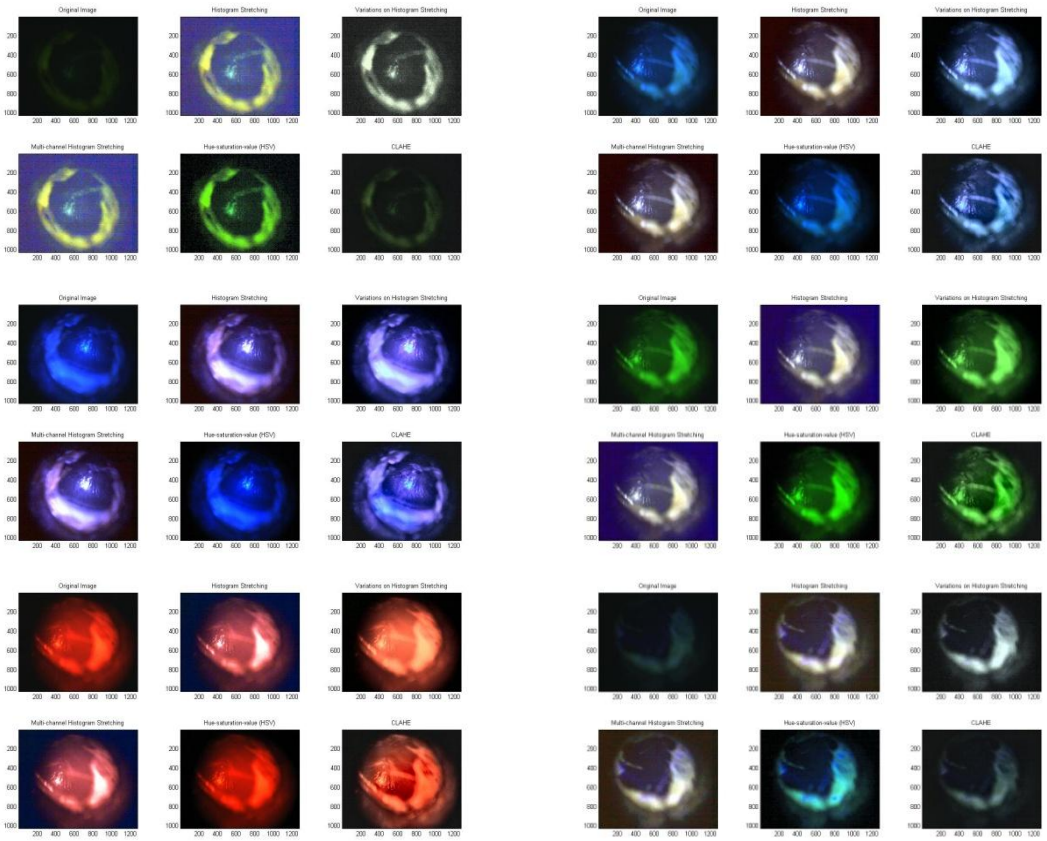

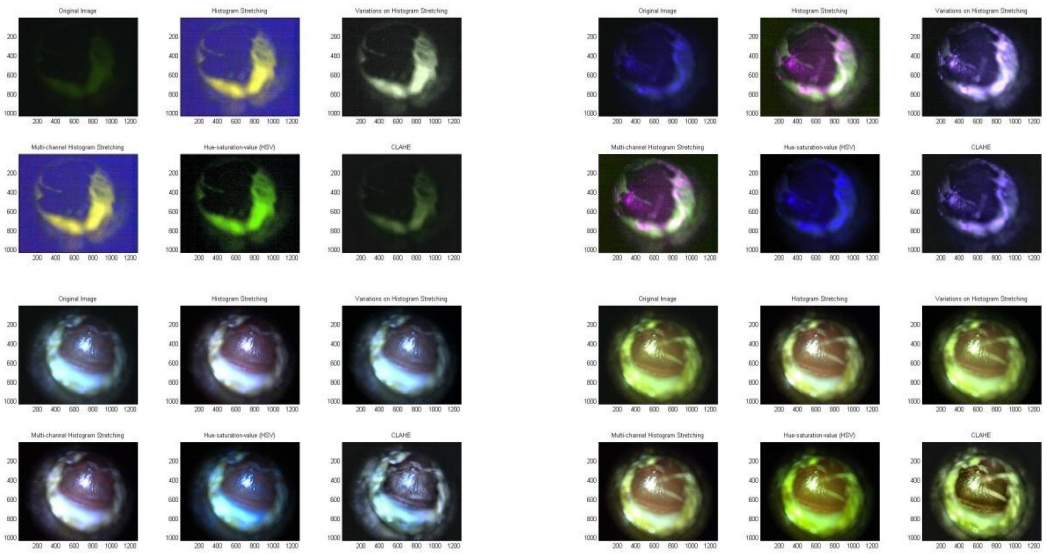
Original Image
Histogram Stretching
Variations on Histogram Stretching
Multi-channel Histogram Stretching
Hue-saturation-value (HSV)
CLAHE
Original Image
Histogram Stretching
Variations on Histogram Stretching
Multi-channel Histogram Stretching
Hue-saturation-value (HSV)
CLAHE
Original Image
Histogram Stretching
Variations on Histogram Stretching
Multi-channel Histogram Stretching
Hue-saturation-value (HSV)
CLAHE
Original Image
Histogram Stretching
Variations on Histogram Stretching
Multi-channel Histogram Stretching
Hue-saturation-value (HSV)
CLAHE

9-25-2013 P2 Right

Images: BGR, BR, BR500, GR, RR, UVR, UVR425, UVR500, WBR, WR

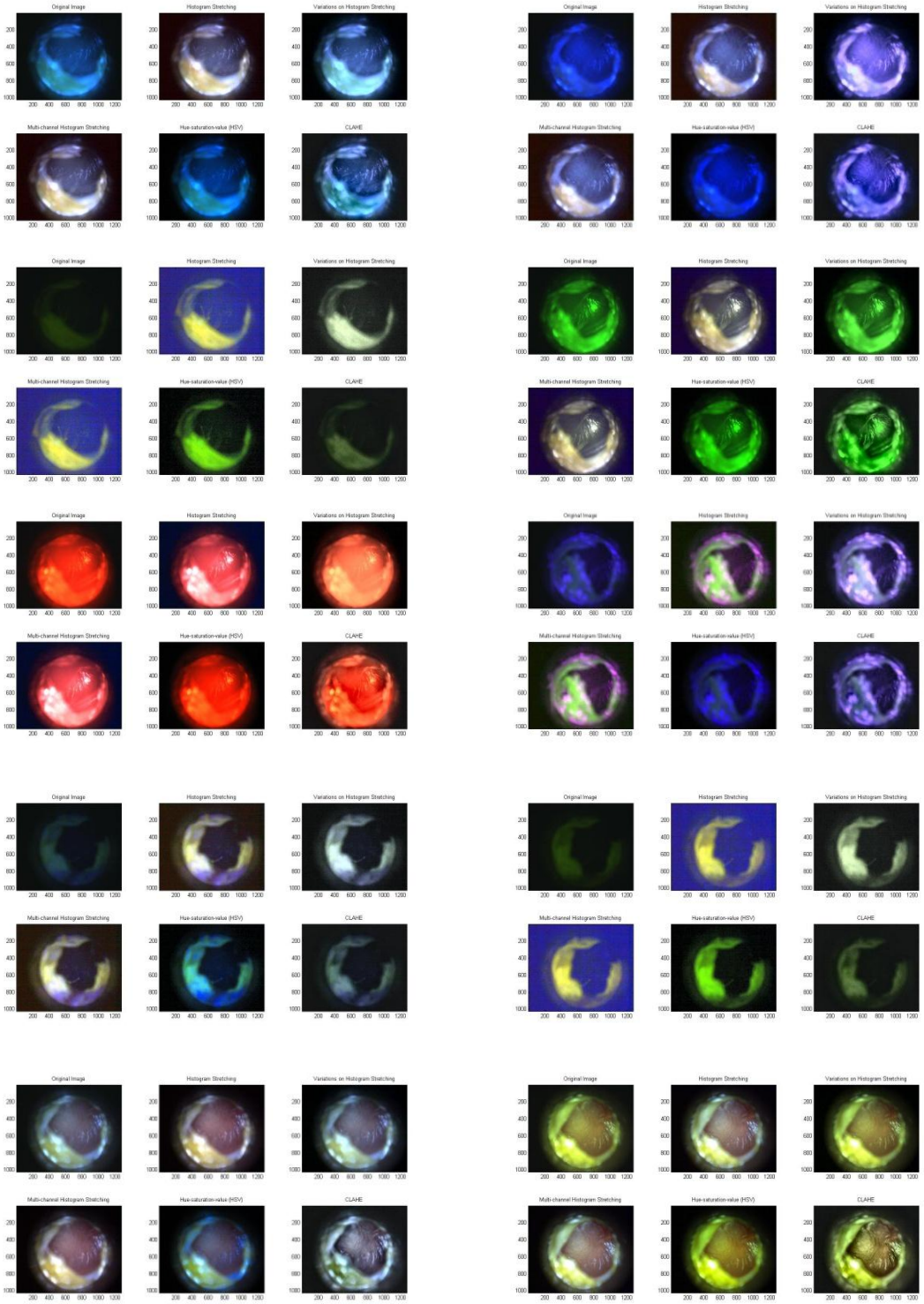

9-25-2013 P3 Left

Images: BL,BL500, GL, RL, UVL2, UVL425, UVL500, WBL WL

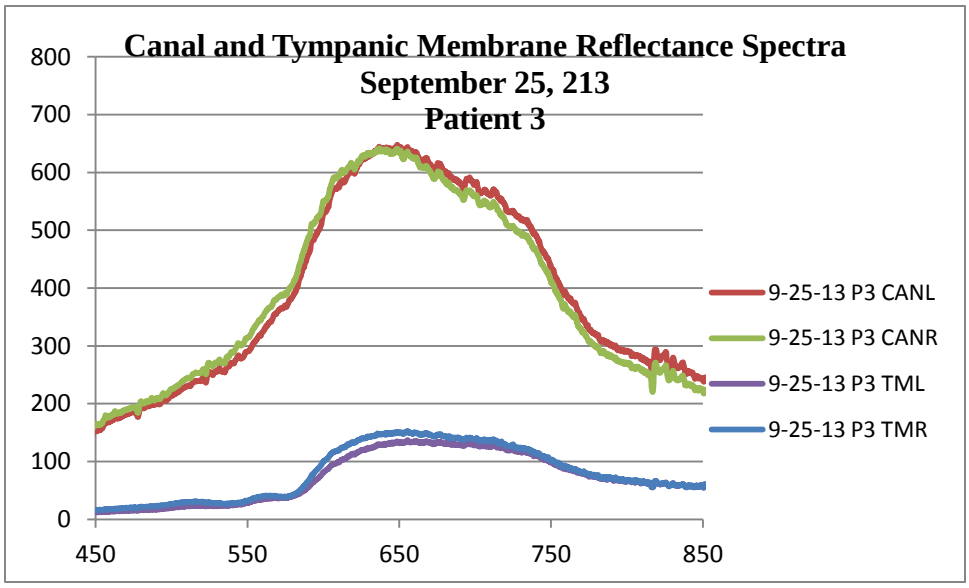

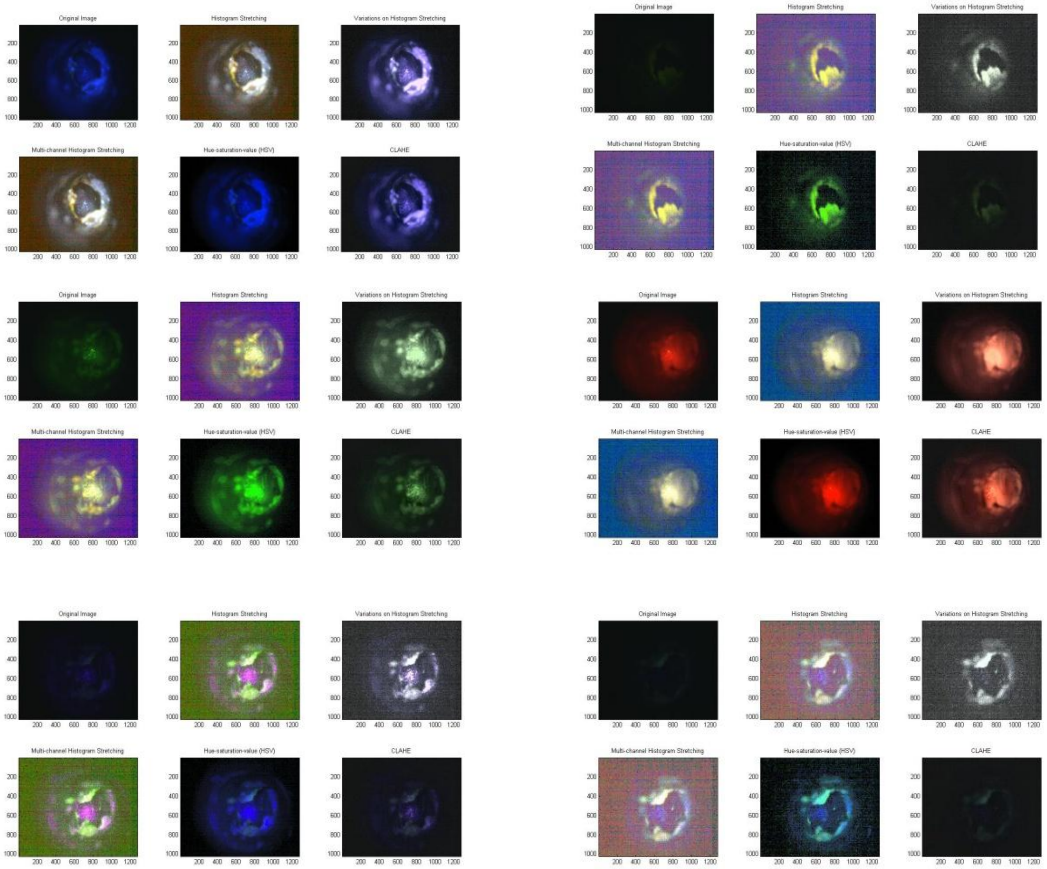

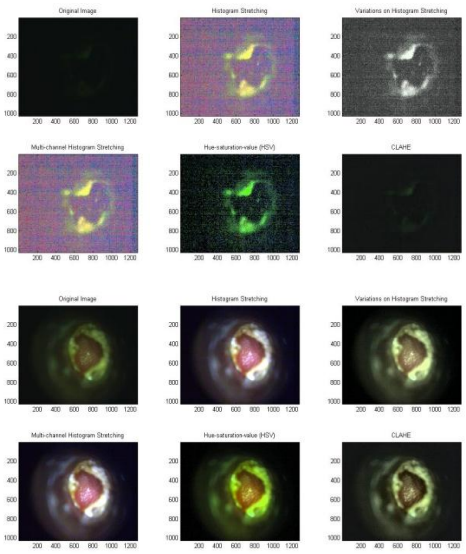
Original Image
Histogram Stretching
Variations on Histogram Stretching
Multi-channel Histogram Stretching
Hue-saturation-value (HSV)
CLAHE
Original Image
Histogram Stretching
Variations on Histogram Stretching
Multi-channel Histogram Stretching
Hue-saturation-value (HSV)
CLAHE

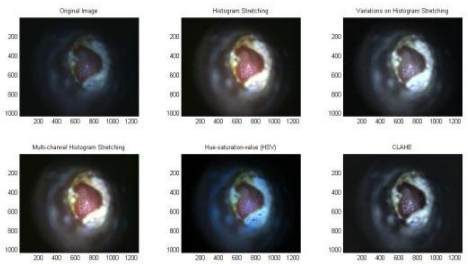
Original Image
Histogram Stretching
Variations on Histogram Stretching
Multi-channel Histogram Stretching
Hue-saturation-value (HSV)
CLAHE

9-25-2013 P3 Right

Images BGL, BGR, BR, BR500, GR, RR, UVR, UVR500, WBR, WR

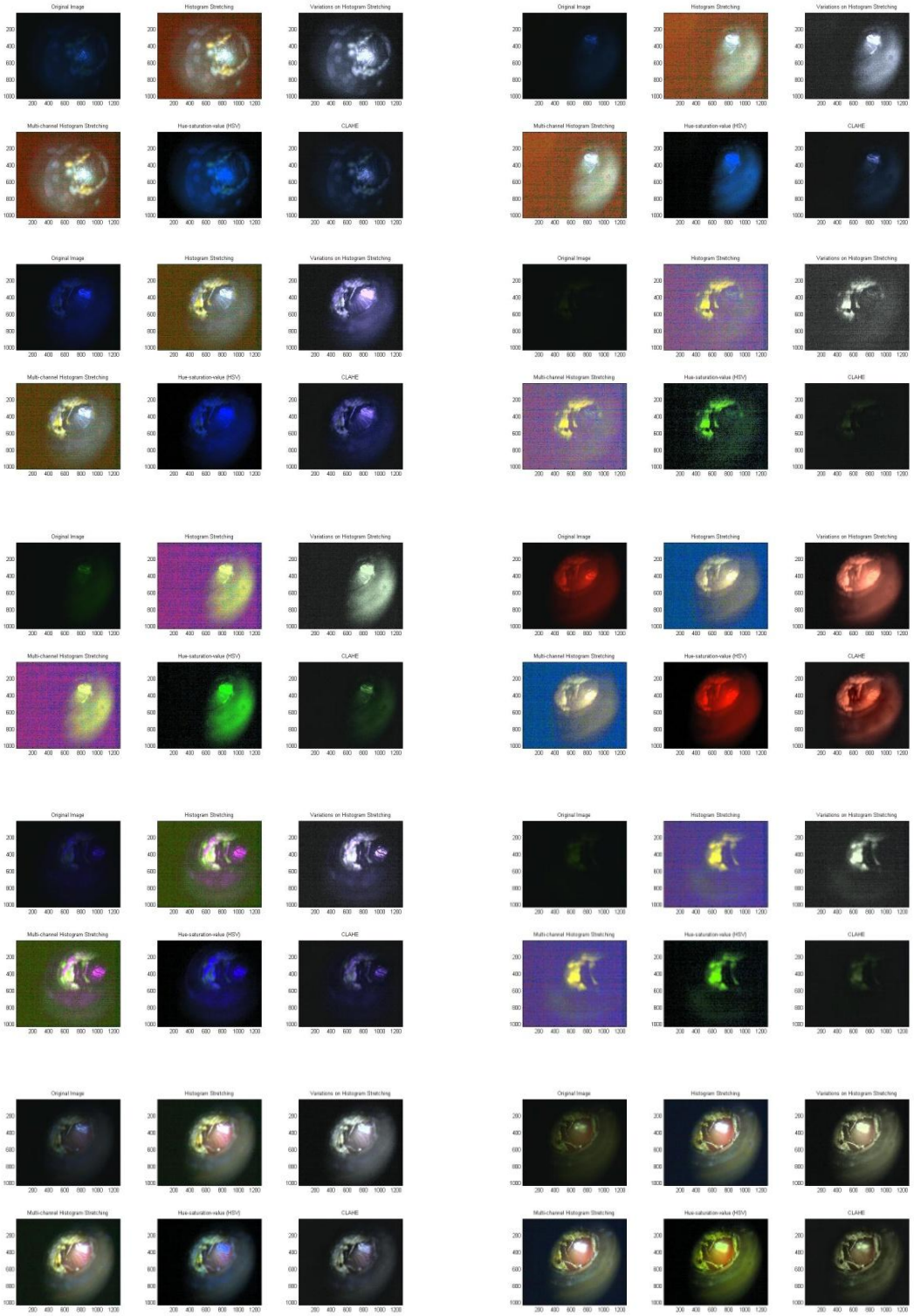

10-9- 2013 P1 Left

Images: B500L, GBL, BL, GL, RL, UV425L, UV500L, UVL, WBL, WL

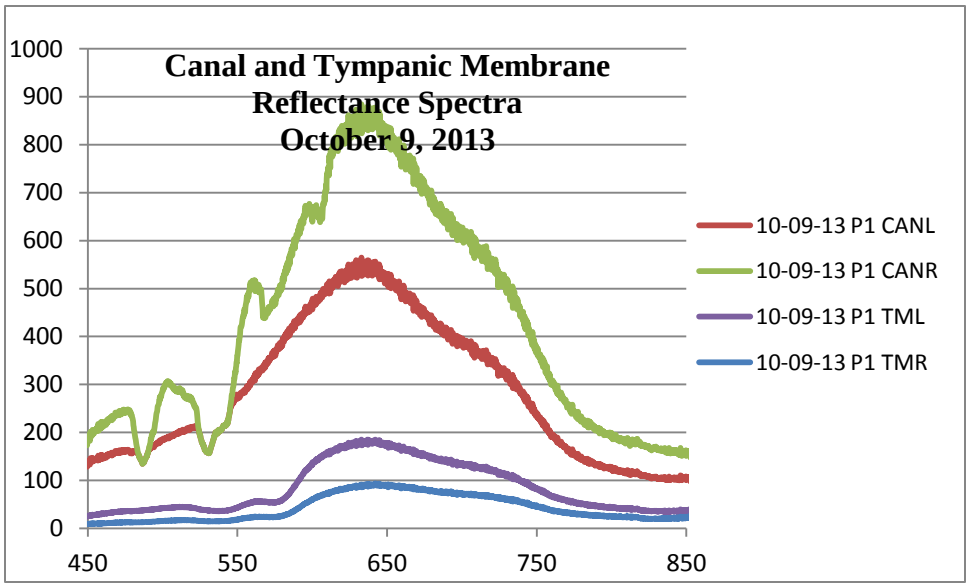

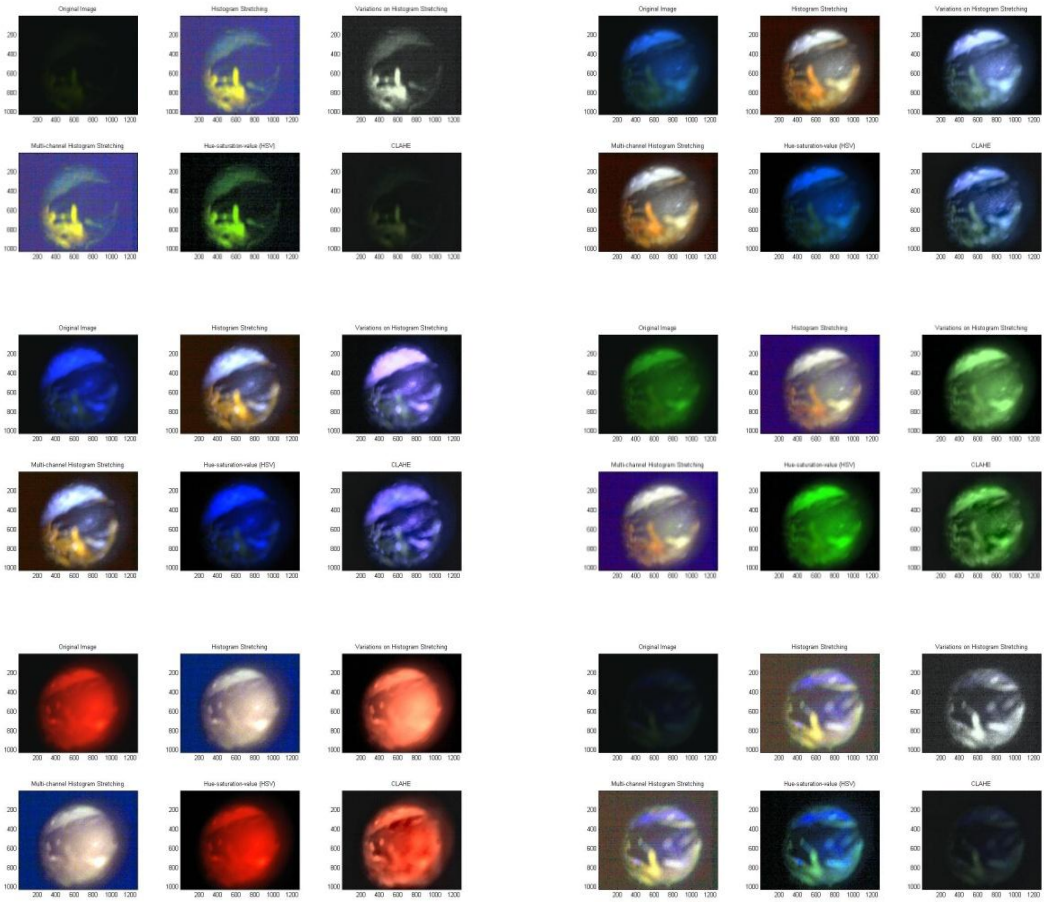

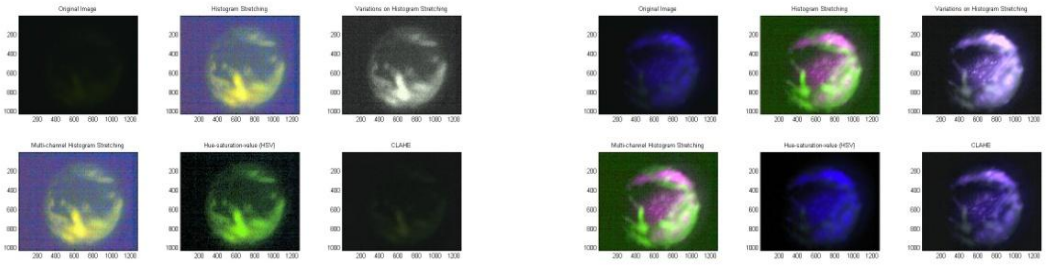
Original Image
Histogram Stretching
Variations on Histogram Stretching
Multi-channel Histogram Stretching
Hue-saturation-value (HSV)
CLAHE

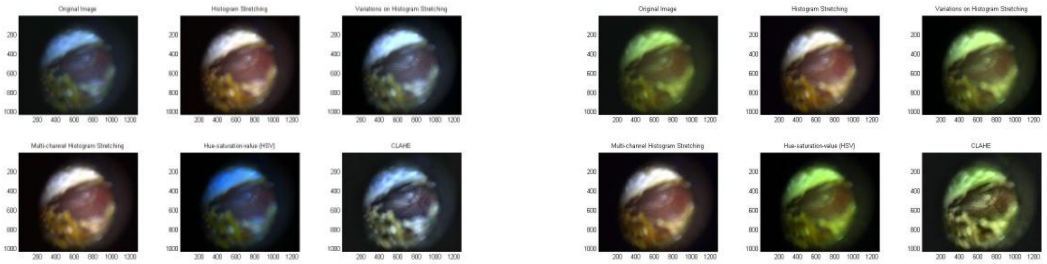
Original Image
Histogram Stretching
Variations on Histogram Stretching
Multi-channel Histogram Stretching
Hue-saturation-value (HSV)
CLAHE

10-9-2013 P1 Right

Images: 2BR, BGR, BR, BR500, BR5002, GR2, RR, UV425R2, UVR, WBR, WBR2, WR2

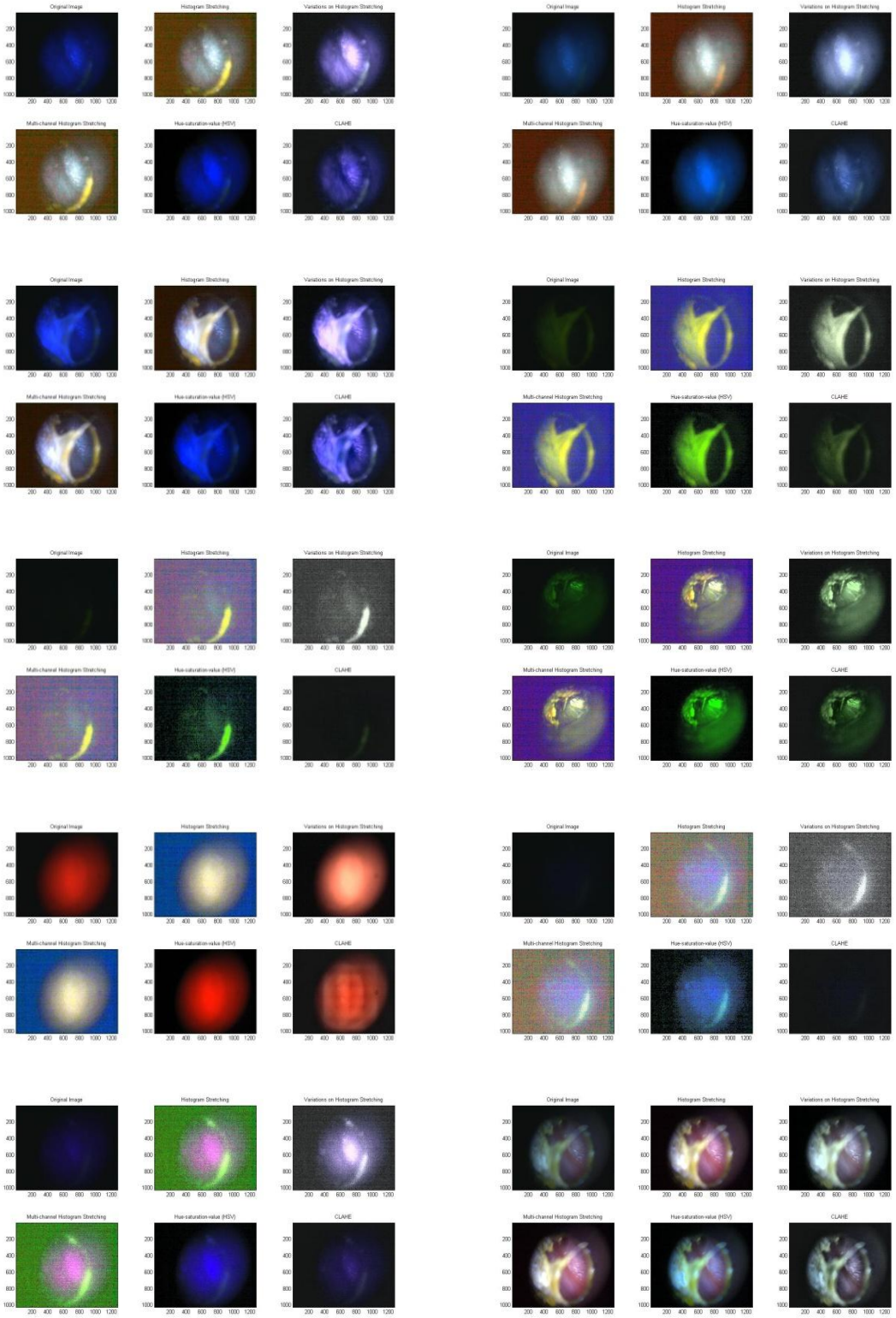

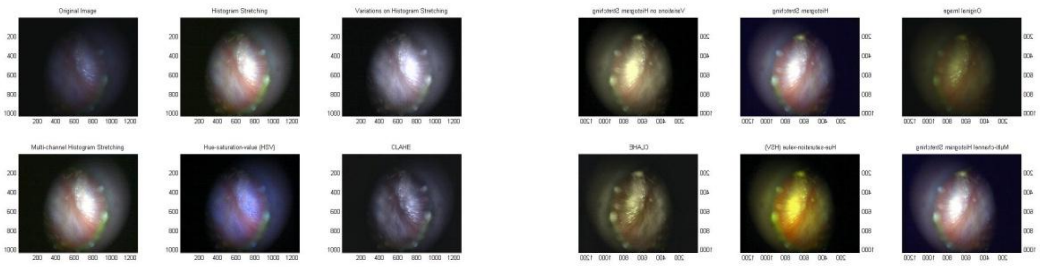
Original Image
Histogram Stretching
Variations on Histogram Stretching
Multi-channel Histogram Stretching
Hue-saturation-value (HSV)
CLAHE
BHAJO

10-16-2013 P1 Left

Images: BGL, BL, BL500, GL, RL, UVL, UVL425, UVL500, WBL, WL

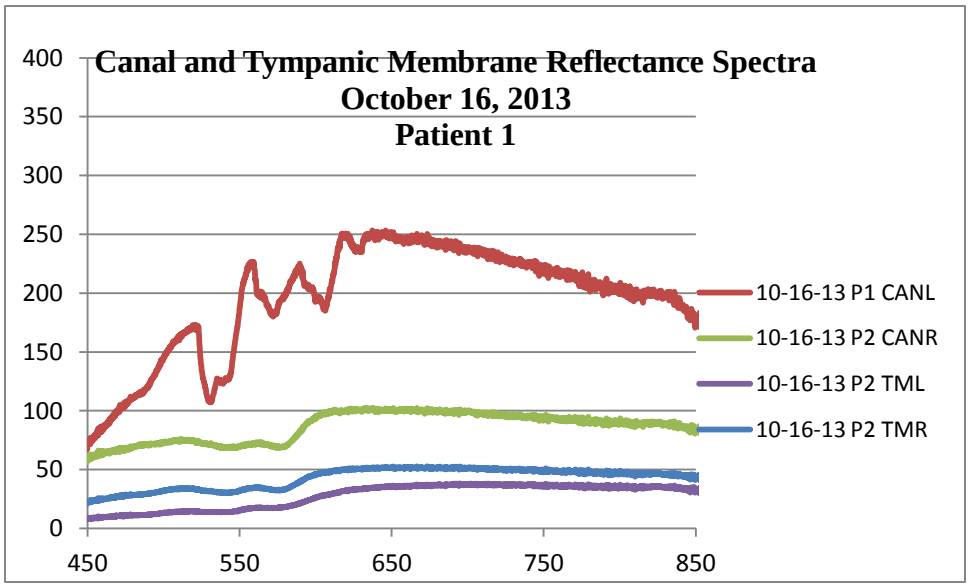

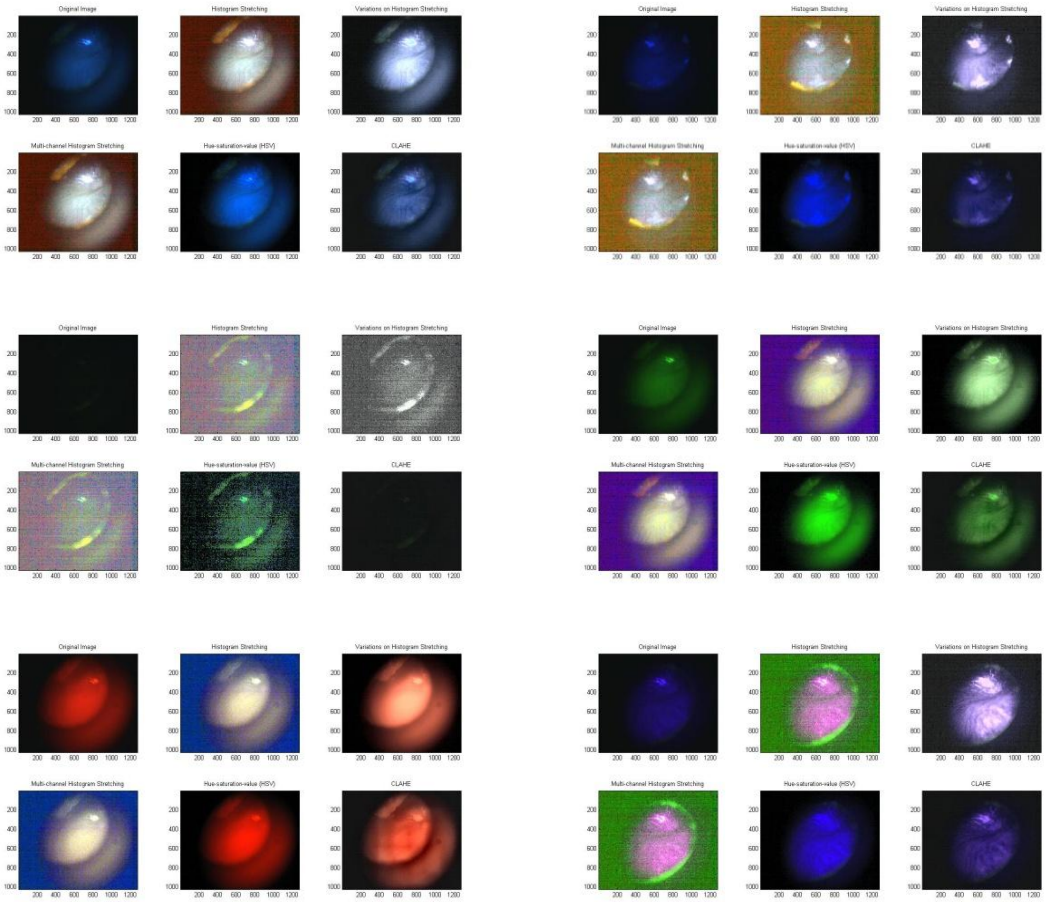

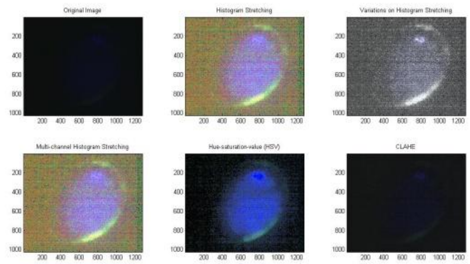
Original Image
Histogram Stretching
Variations on Histogram Stretching
Multi-channel Histogram Stretching
Hue-saturation-value (HSV)
CLAHE

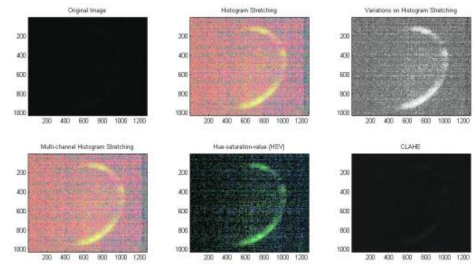
Original Image
Histogram Stretching
Variations on Histogram Stretching
Multi-channel Histogram Stretching
Hue-saturation-value (HSV)
CLAHE

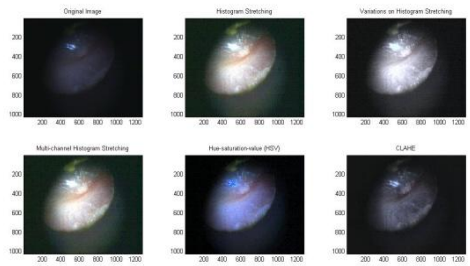
Original Image
Histogram Stretching
Variations on Histogram Stretching
Multi-channel Histogram Stretching
Hue-saturation-value (HSV)
CLAHE

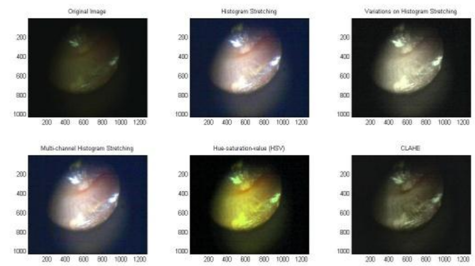
Original Image
Histogram Stretching
Variations on Histogram Stretching
Multi-channel Histogram Stretching
Hue-saturation-value (HSV)
CLAHE

10-16-2013 P1 Right

Images: BR500, BR, GBR,GR, RR, UV500R, UVR, UVR425, WBR, WBR2, WR

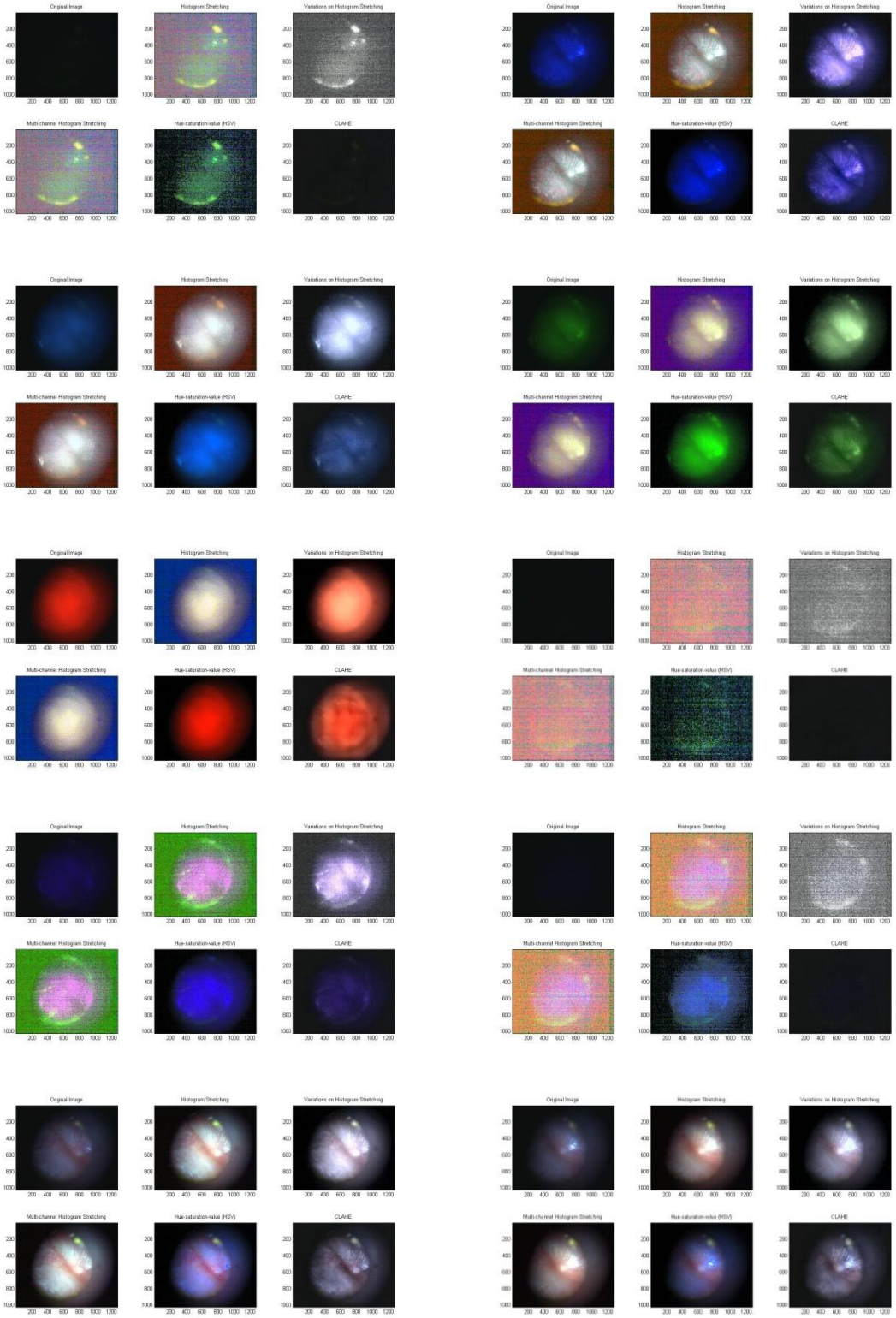

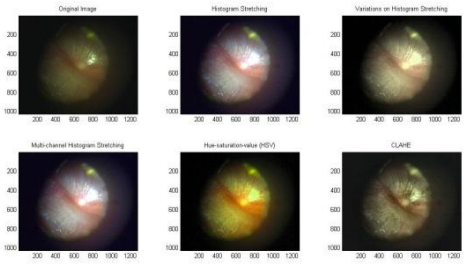
Original Image
Histogram Stretching
Variations on Histogram Stretching
Multi-channel Histogram Stretching
Hue-saturation-value (HSV)
CLAHE

10-16-2013 P2 Left

Images: BGL, BL, BL500, GL, RL, UVL 425, UVL500, UVL, WBL, WLBLEMP

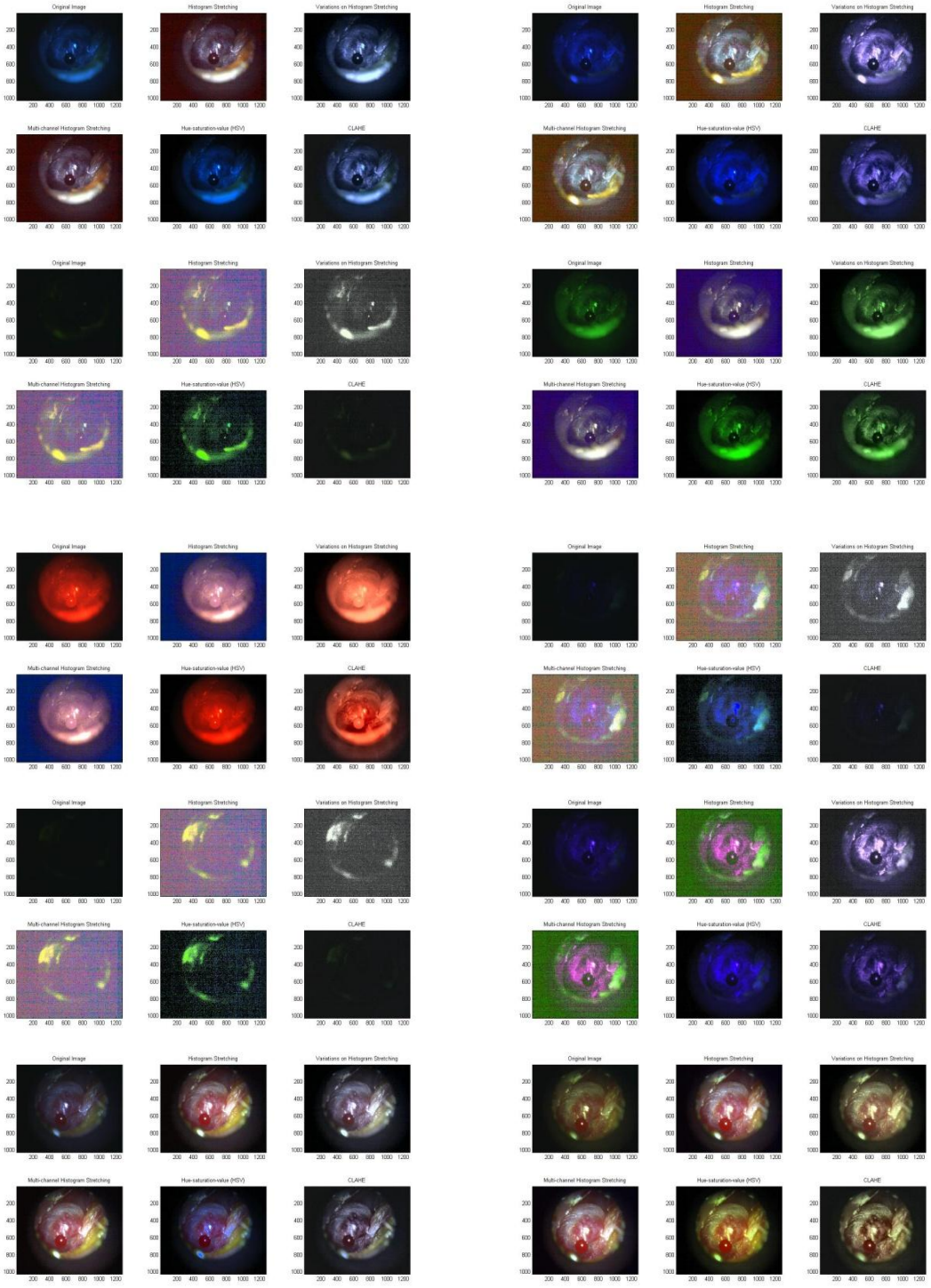

10-16-2013 P2 Right

Images: BGR, BR, BR500, GR, RR, UVR, UVR425, UVR500, WBR, WR

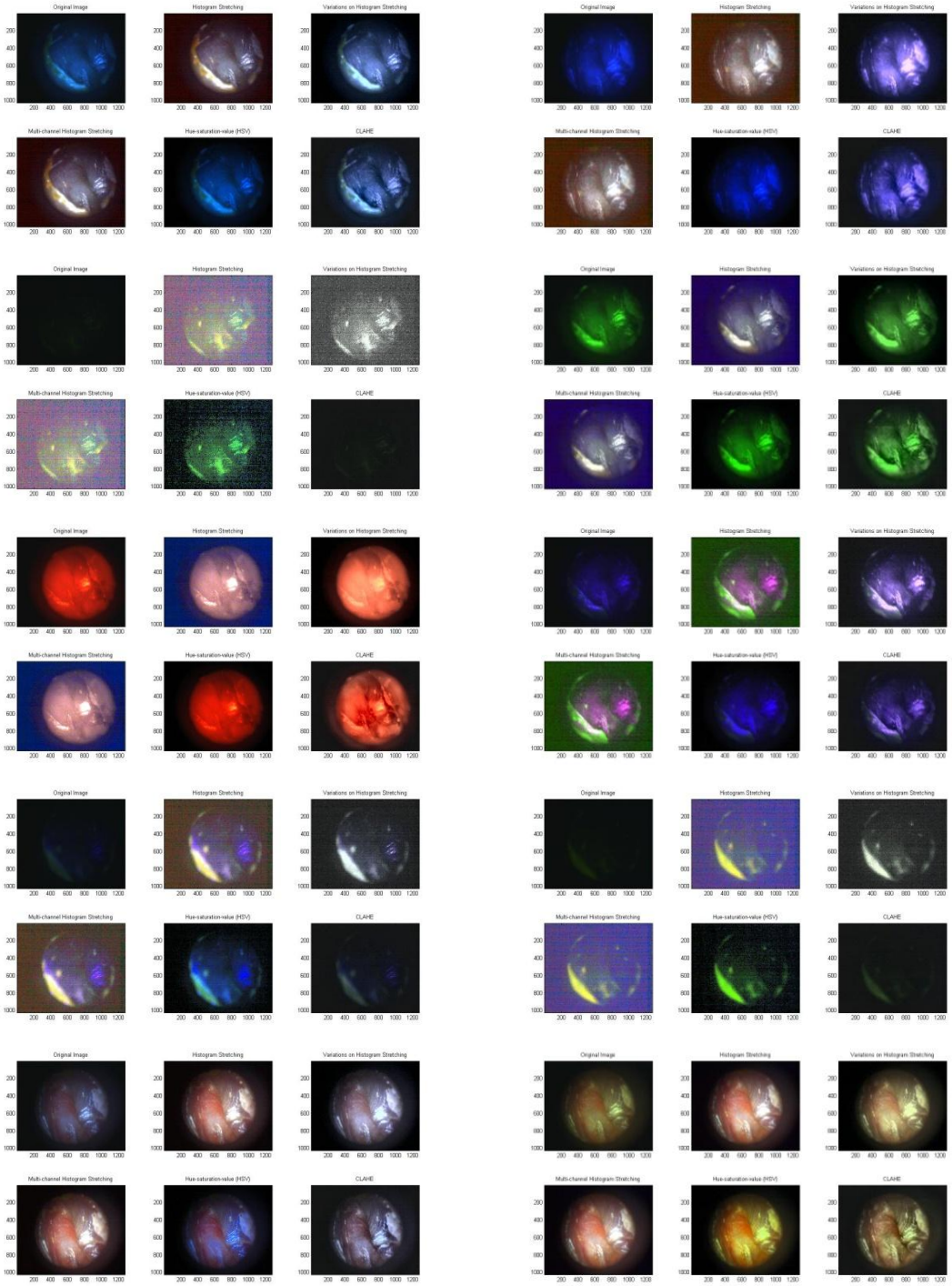

10-30-P1 Left

Images: B500L, BGL, BL, GL, RL, UVL, UVL425, UVL500, WBL, WL

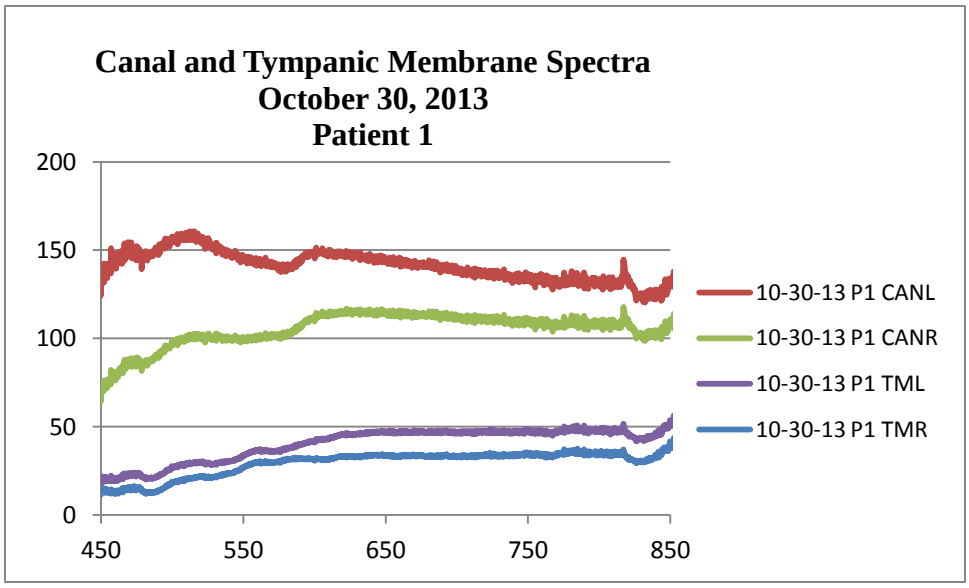

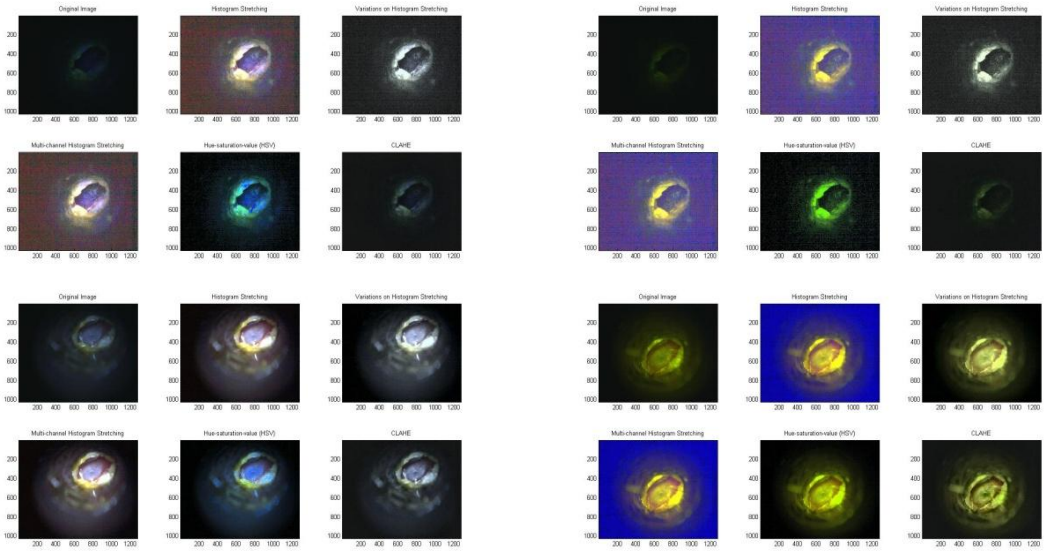
Original Image
Histogram Stretching
Variations on Histogram Stretching
Multi-channel Histogram Stretching
Hue-saturation-value (HSV)
CLAHE
Original Image
Histogram Stretching
Variations on Histogram Stretching
Multi-channel Histogram Stretching
Hue-saturation-value (HSV)
CLAHE
Original Image
Histogram Stretching
Variations on Histogram Stretching
Multi-channel Histogram Stretching
Hue-saturation-value (HSV)
CLAHE
Original Image
Histogram Stretching
Variations on Histogram Stretching
Multi-channel Histogram Stretching
Hue-saturation-value (HSV)
CLAHE

10-30-2013 P1 Right

Images: B500R, BR, GR, RR, UVR, UVR425, UVR500, WBR, WR

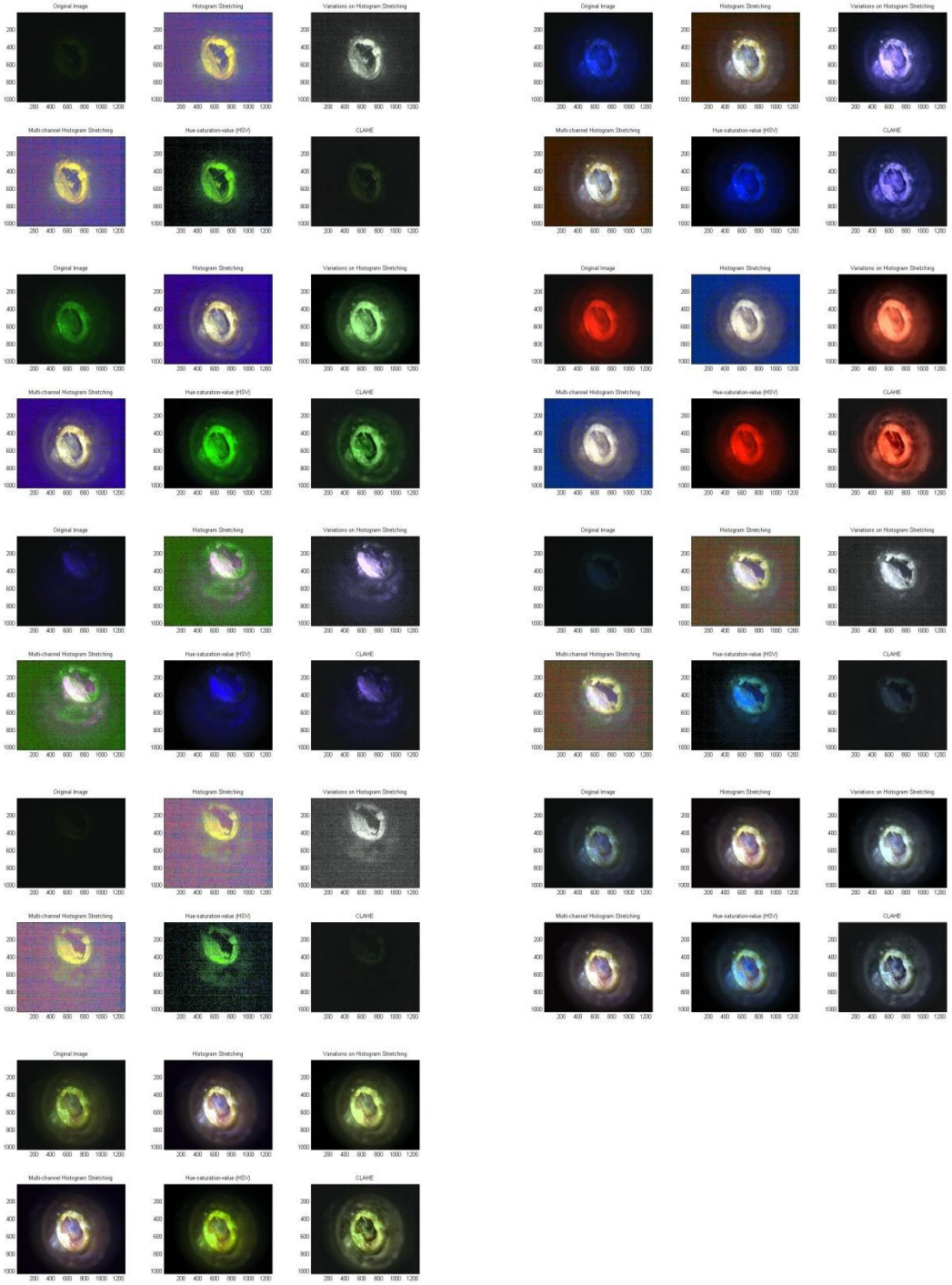

11-06-2013 P2 Left

Images: B500L, BG500, BGL, BL, GL, RL2, UVL, UVL425, UVL500, WBL, WL

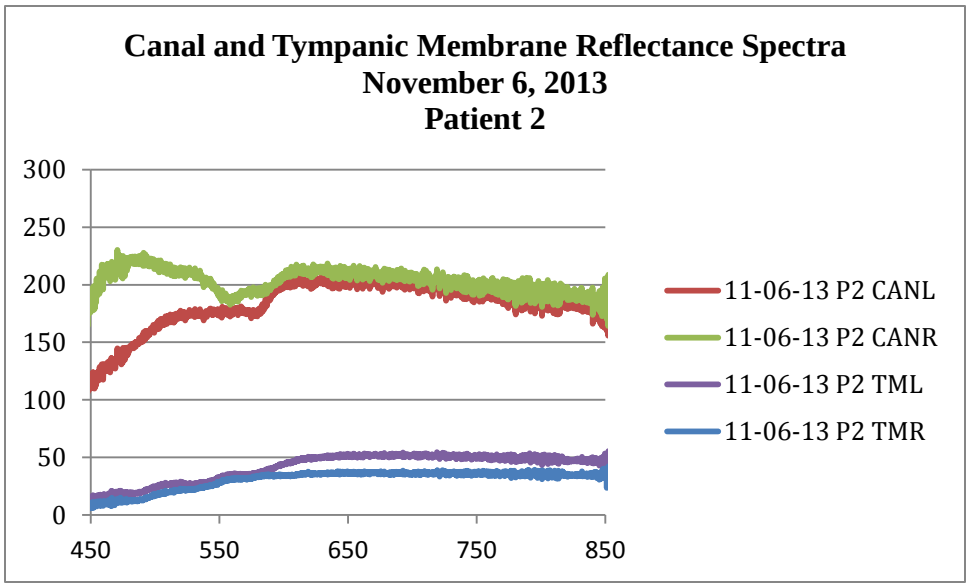

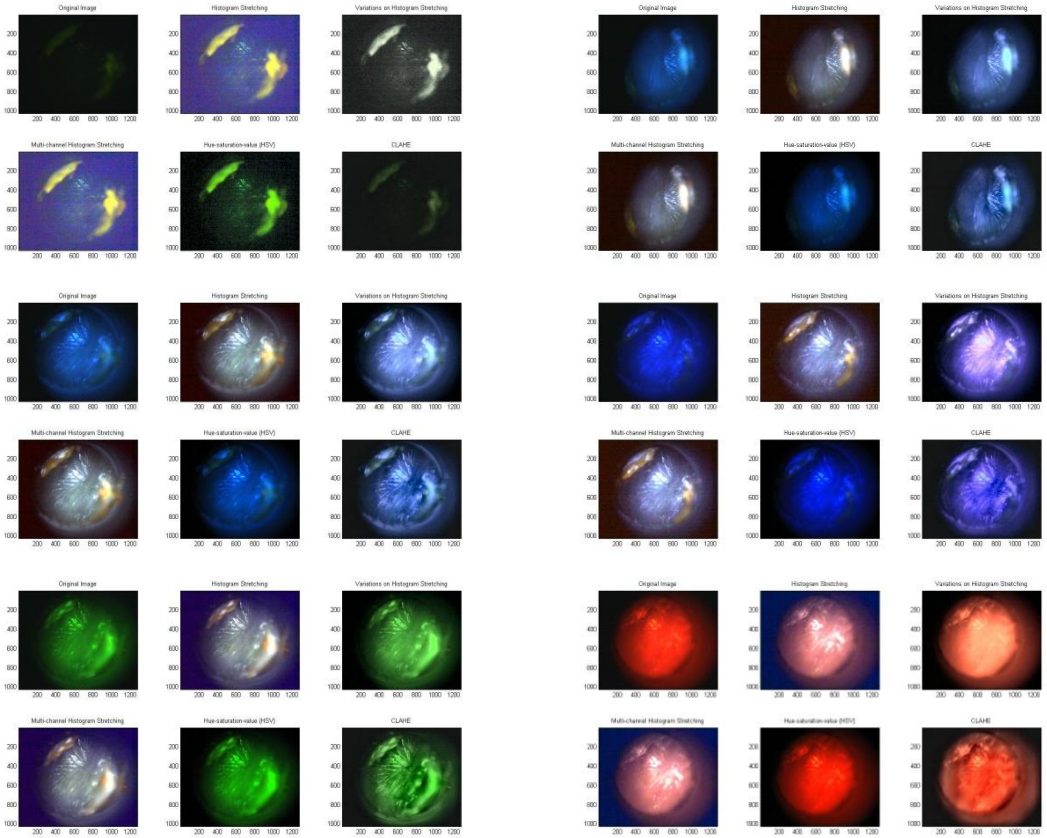

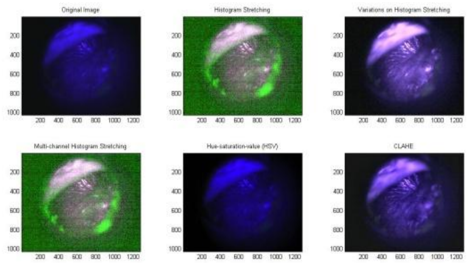
Original Image
Histogram Stretching
Variations on Histogram Stretching
Multi-channel Histogram Stretching
Hue-saturation-value (HSV)
CLAHE

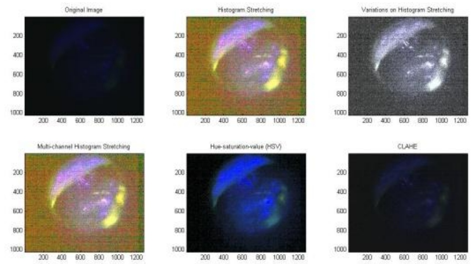
Original Image
Histogram Stretching
Variations on Histogram Stretching
Multi-channel Histogram Stretching
Hue-saturation-value (HSV)
CLAHE

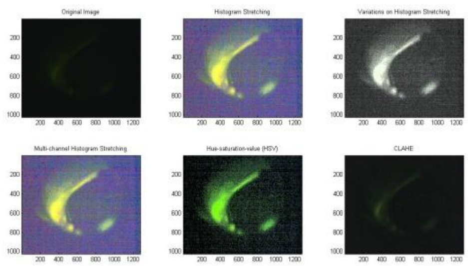
Original Image
Histogram Stretching
Variations on Histogram Stretching
Multi-channel Histogram Stretching
Hue-saturation-value (HSV)
CLAHE

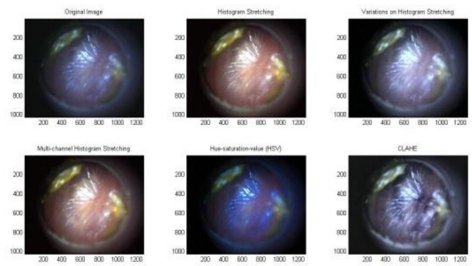
Original Image
Histogram Stretching
Variations on Histogram Stretching
Multi-channel Histogram Stretching
Hue-saturation-value (HSV)
CLAHE

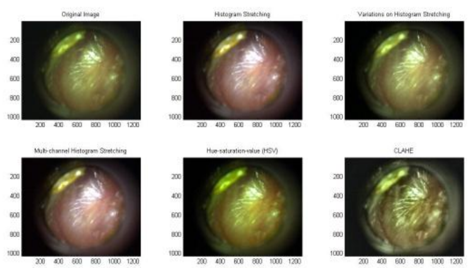
Original Image
Histogram Stretching
Variations on Histogram Stretching
Multi-channel Histogram Stretching
Hue-saturation-value (HSV)
CLAHE

11-06-2013 P2 Right

Images: B500R, BR, GR, RR, UV425R, UV500R, UVR, WBR

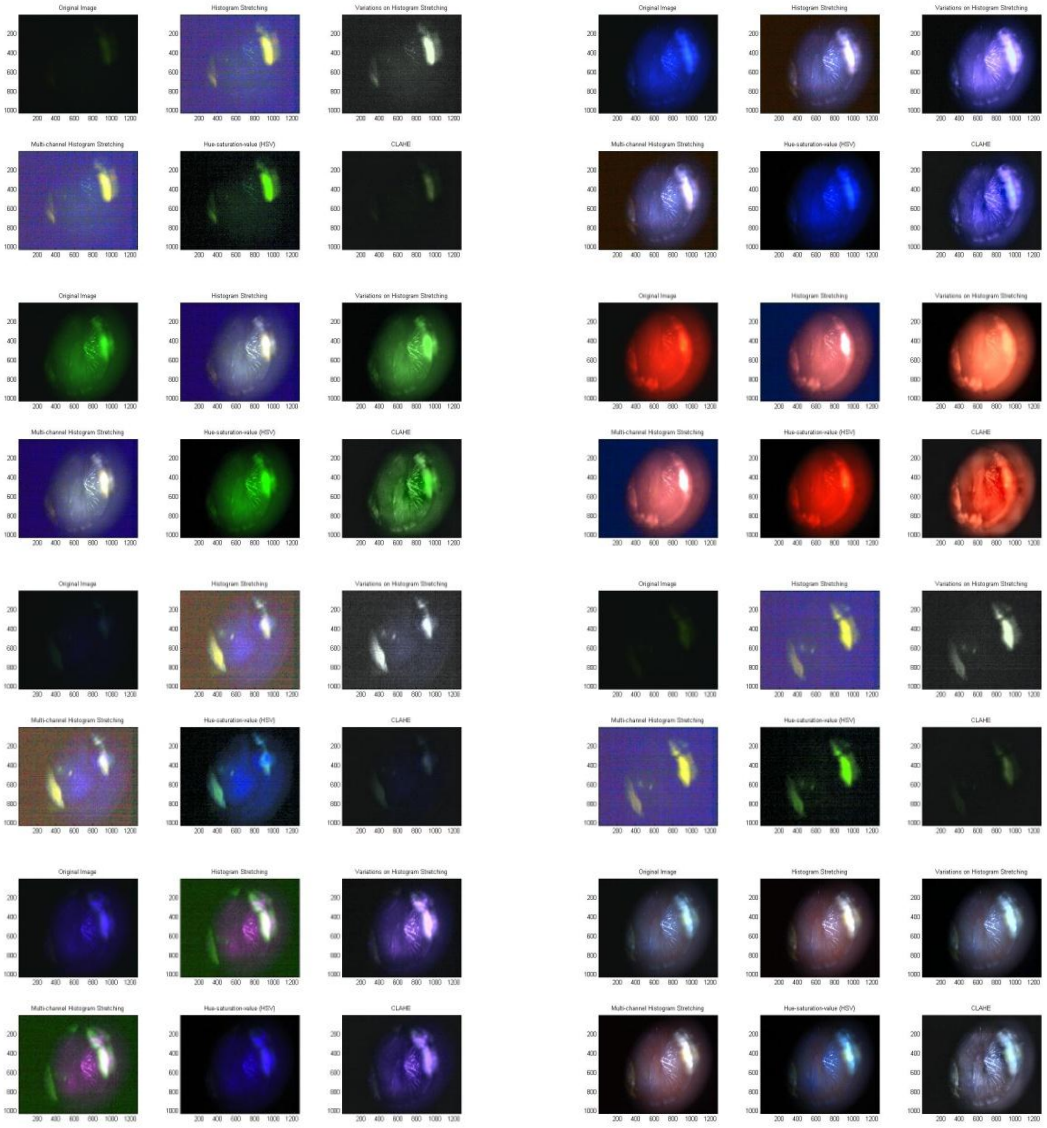

11-13-13 P1 Left

Images: BGL, BL, BL500, GL, RL, UVL, UVL425, UVL500, WBL

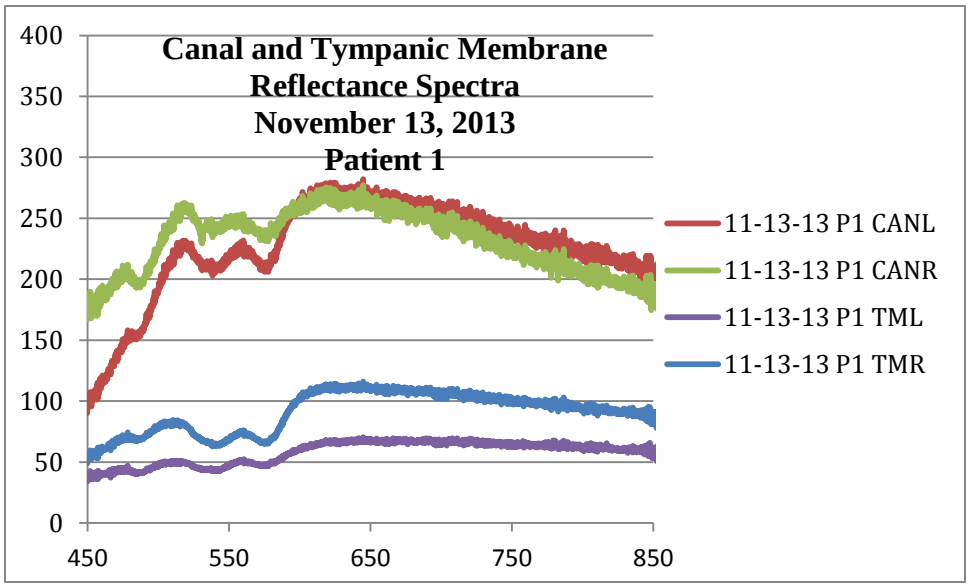

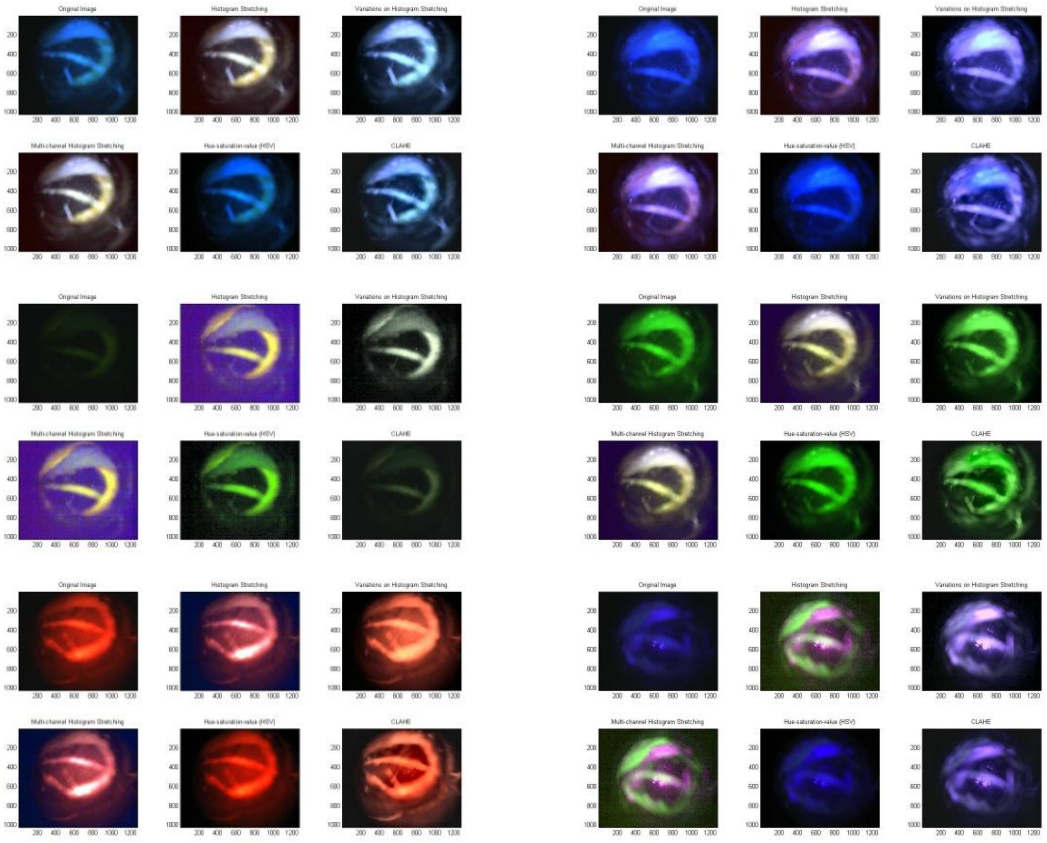

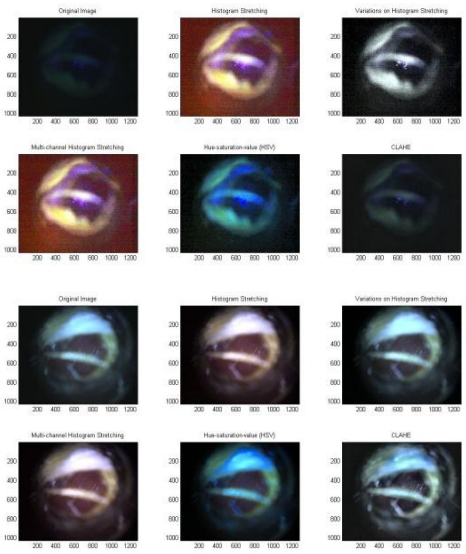
Original Image
Histogram Stretching
Variations on Histogram Stretching
Multi-channel Histogram Stretching
Hue-saturation-value (HSV)
CLAHE
Original Image
Histogram Stretching
Variations on Histogram Stretching
Multi-channel Histogram Stretching
Hue-saturation-value (HSV)
CLAHE

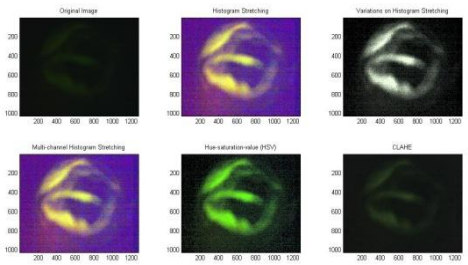
Original Image
Histogram Stretching
Variations on Histogram Stretching
Multi-channel Histogram Stretching
Hue-saturation-value (HSV)
CLAHE

11-13-13 P1 Right

Images: BGR, BR, GR, RR, UV500R, UVR, UVR425, WBR, WR2

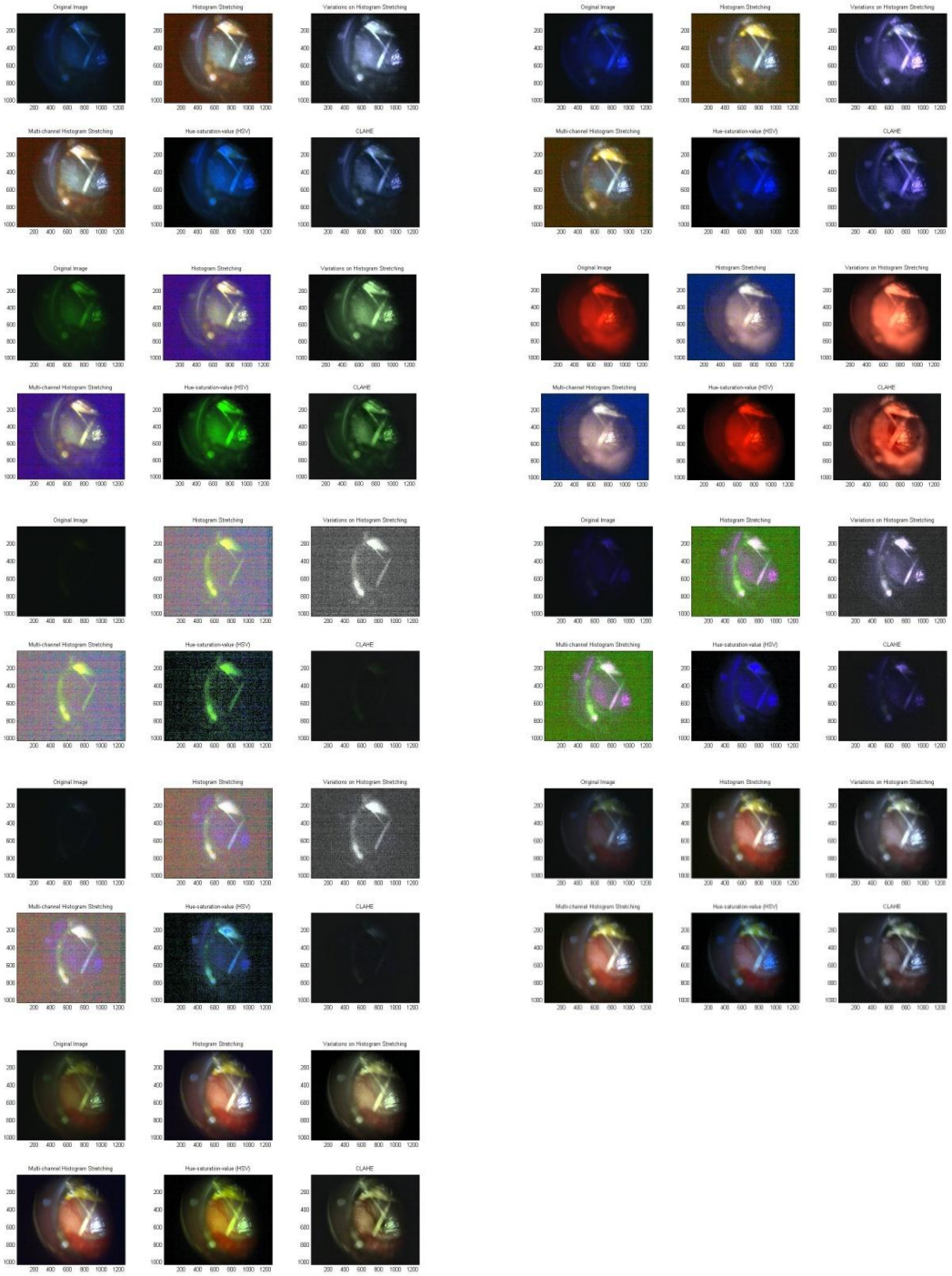

11-13-13 P2 Left

Images: BGL, BL, BL500, UVL425, UVL500, WB2L, WL2

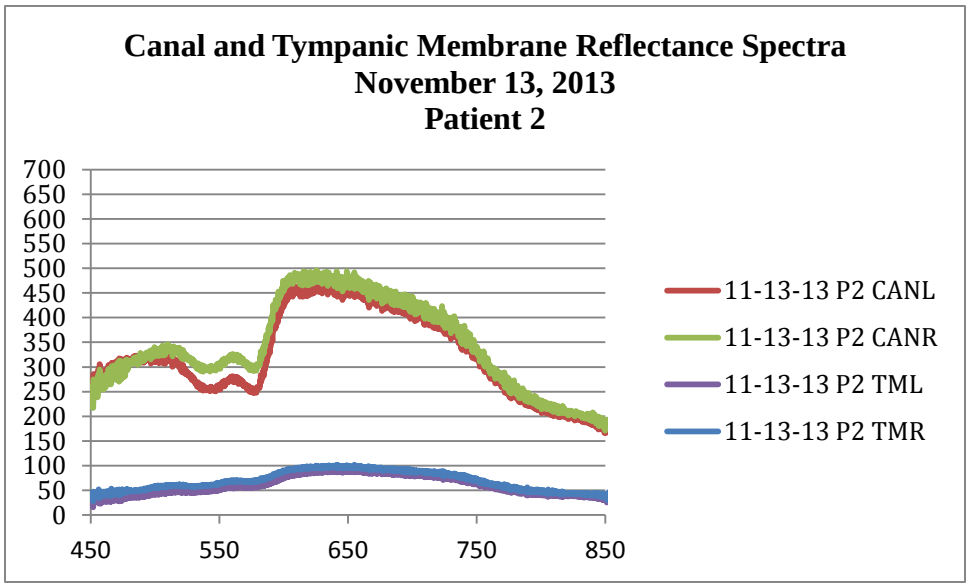

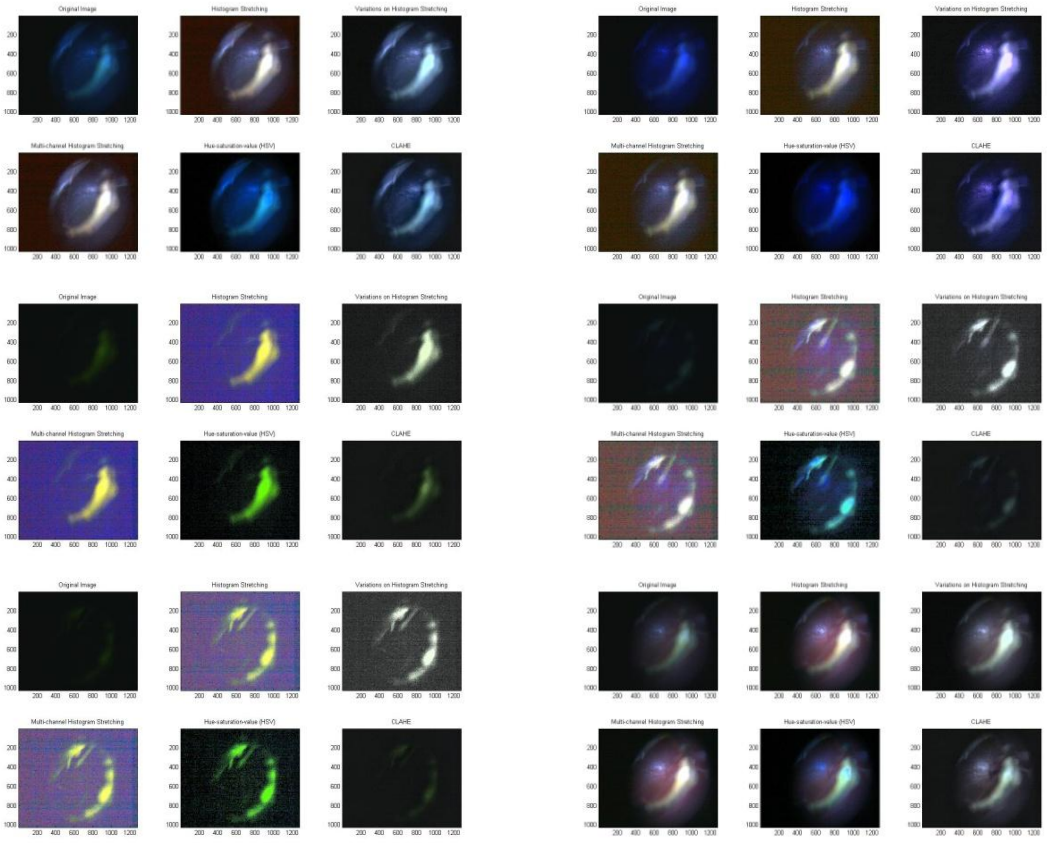

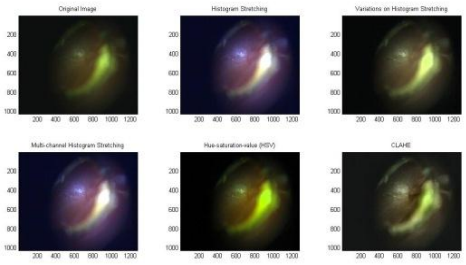
Original Image
Histogram Stretching
Variations on Histogram Stretching
Multi-channel Histogram Stretching
Hue-saturation-value (HSV)
CLAHE

11-13-13 P2 Right

Images: B500R, BGR, BR, GR, RR2, UVR, UVR425, UVR500, WBR, WR

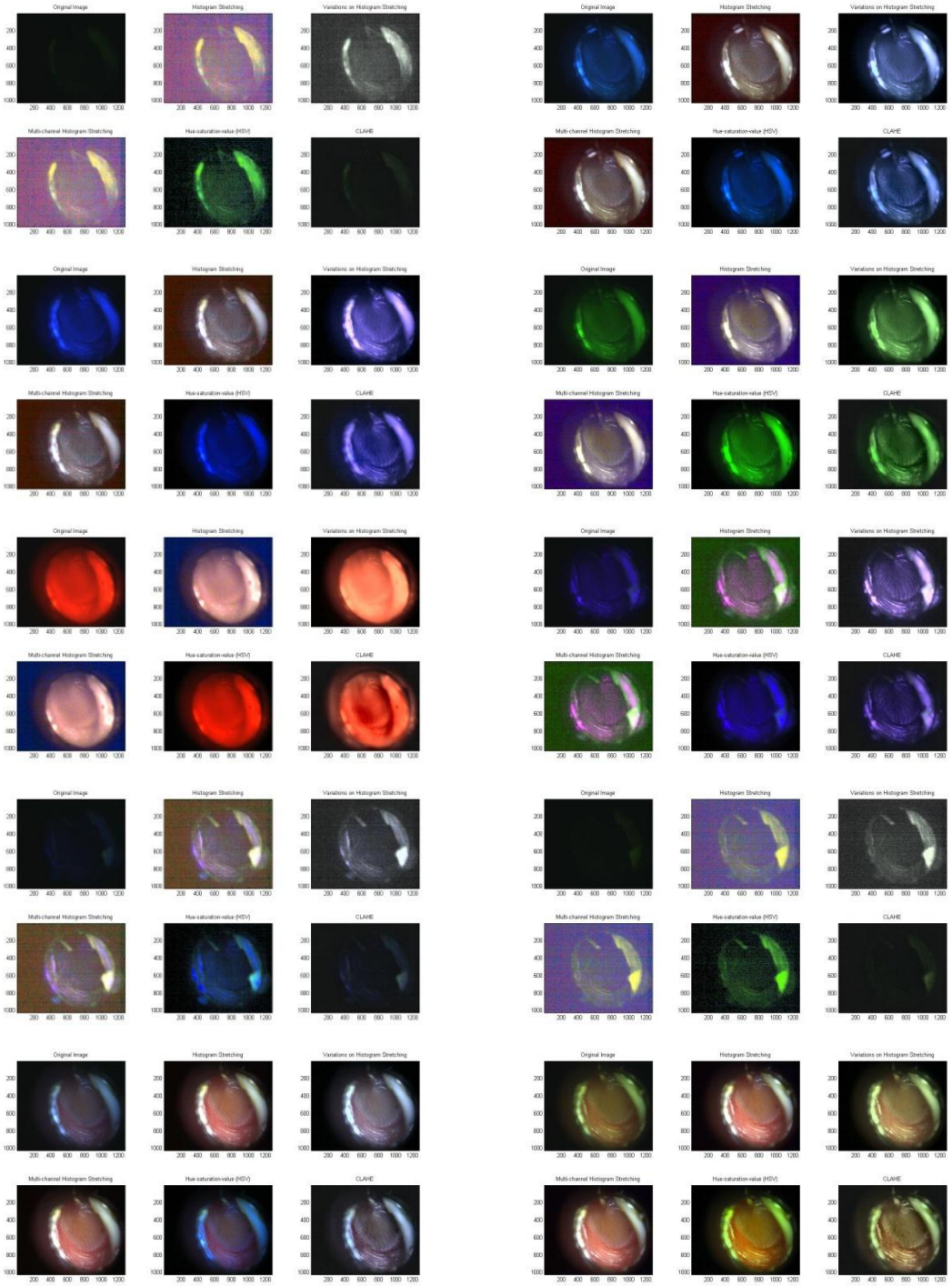

12-04-2013 P1 Left

Images: B500L, BGL, BL, GL, RL, UVL, UVL425, UVL500, WBL, WL

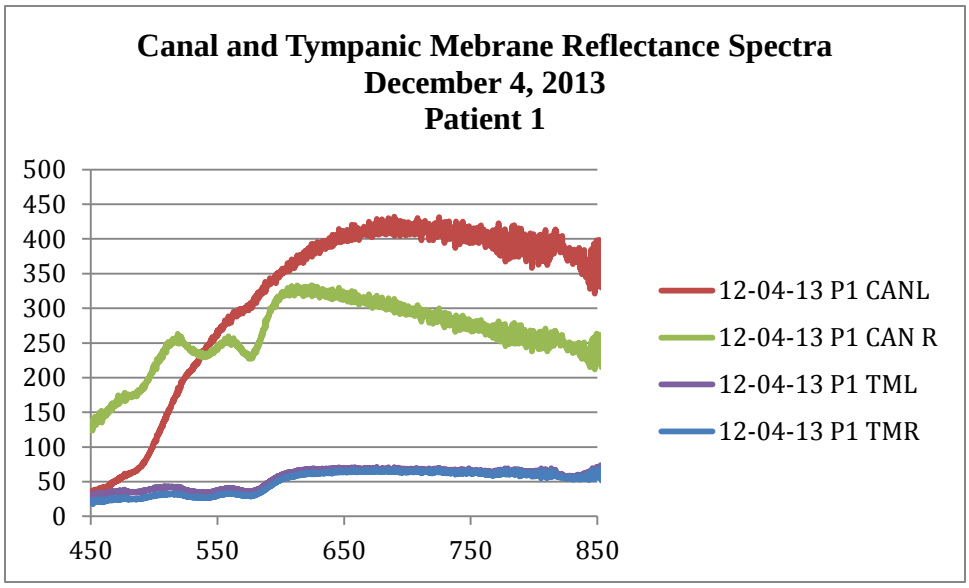

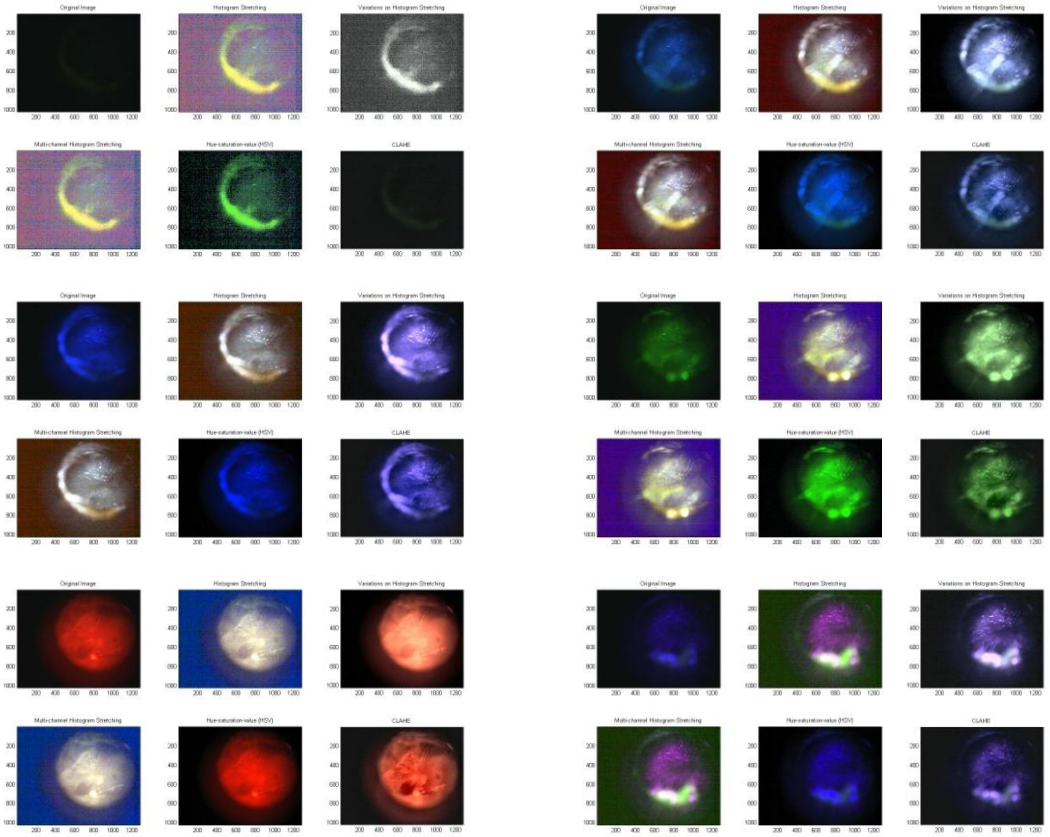

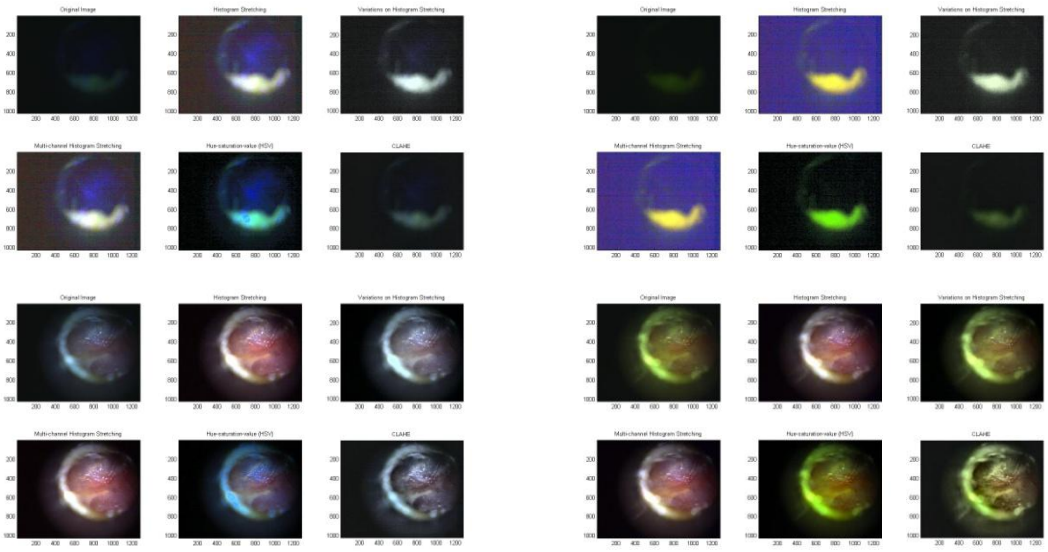
Original Image
Histogram Stretching
Variations on Histogram Stretching
Multi-channel Histogram Stretching
Hue-saturation-value (HSV)
CLAHE
Original Image
Histogram Stretching
Variations on Histogram Stretching
Multi-channel Histogram Stretching
Hue-saturation-value (HSV)
CLAHE
Original Image
Histogram Stretching
Variations on Histogram Stretching
Multi-channel Histogram Stretching
Hue-saturation-value (HSV)
CLAHE
Original Image
Histogram Stretching
Variations on Histogram Stretching
Multi-channel Histogram Stretching
Hue-saturation-value (HSV)
CLAHE

12-04-2013 P1 Right

Images: B500R, BGR, BR, GR, RR, UVR, UVR425, UVR500, WBR, WR

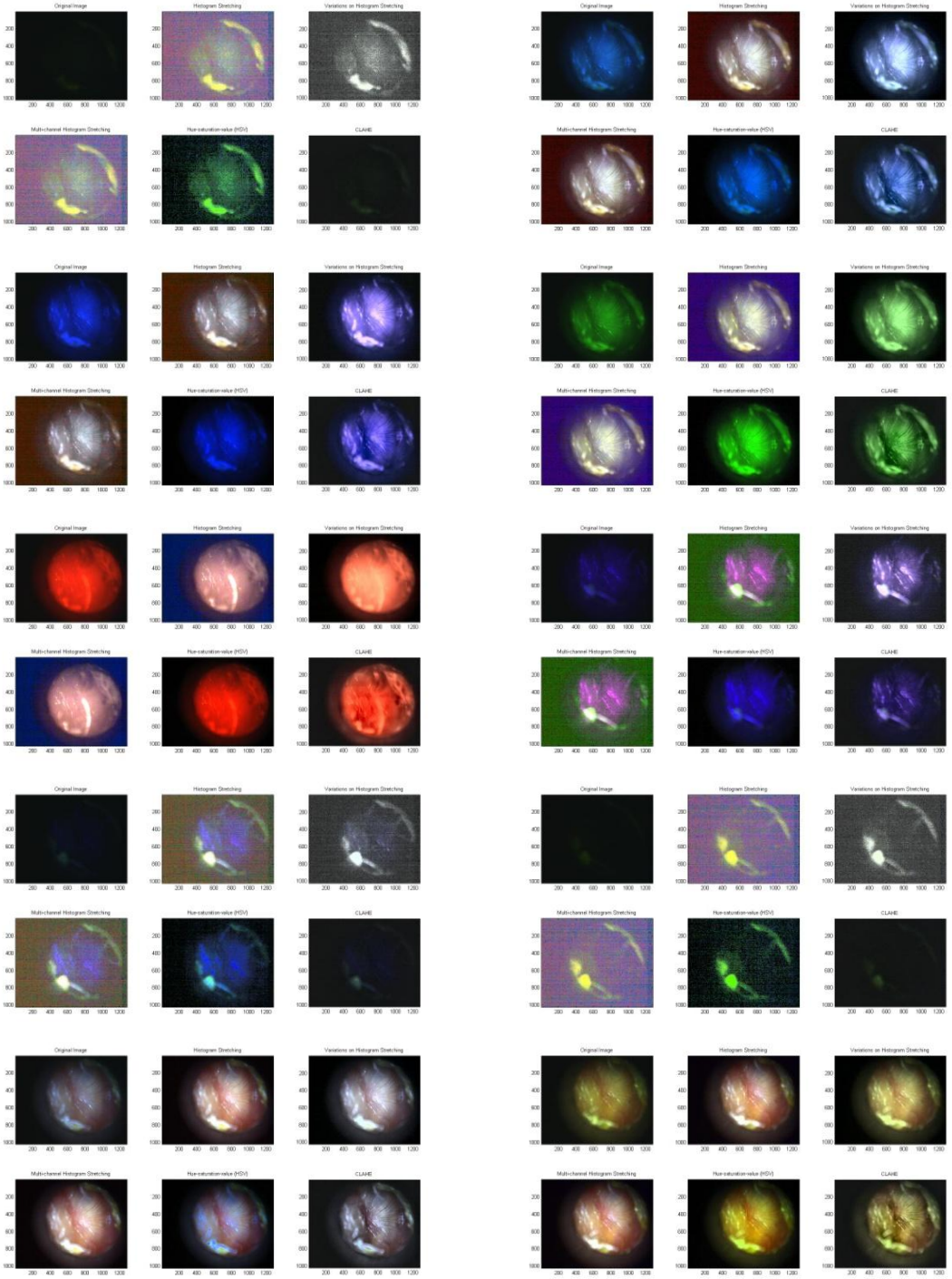

1-8-2014 P1 Right

Images: WBR, BR, WR, GR, UV500R, GBR, RR, UVR, UV425R, UV500R2

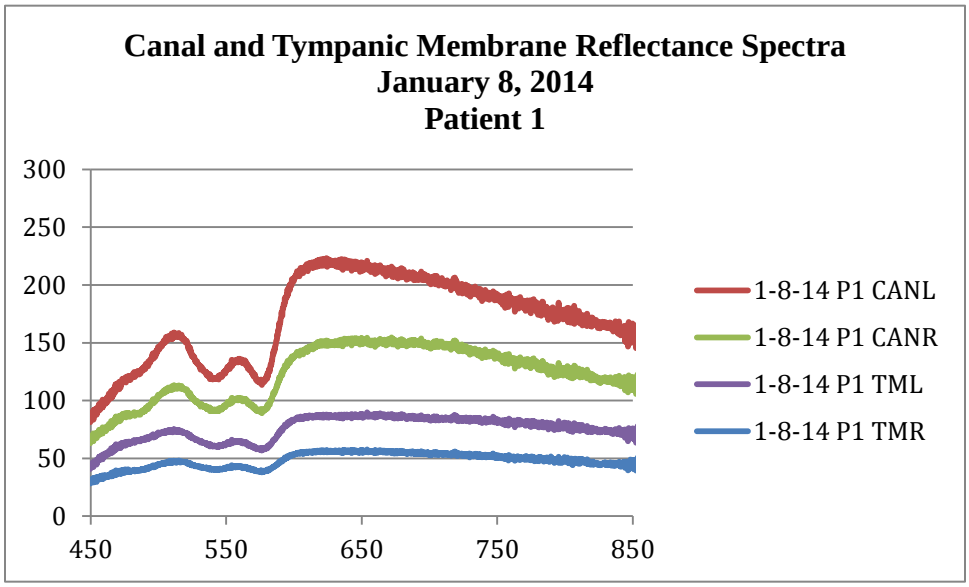

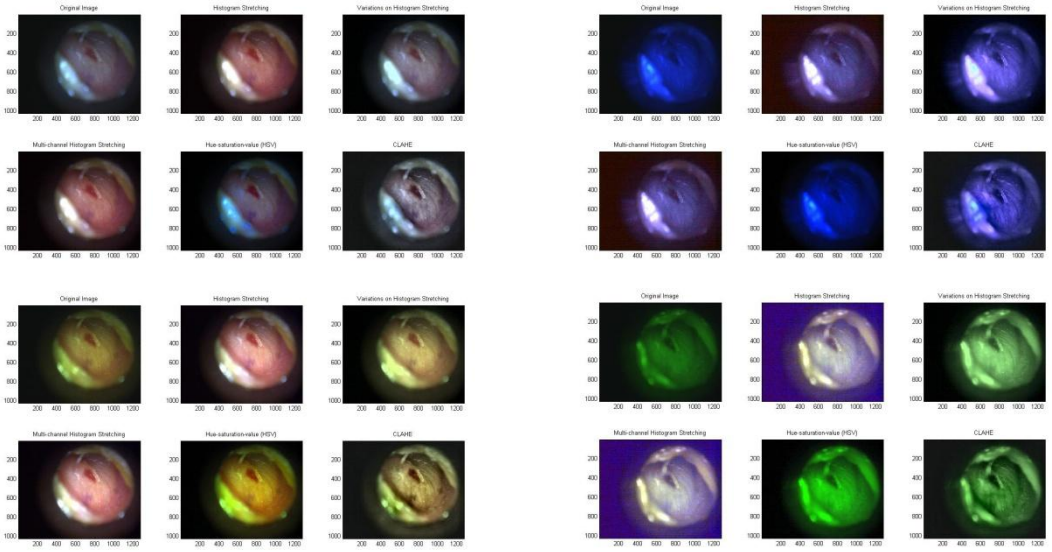

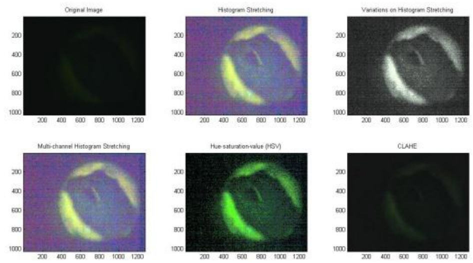
Original Image
Histogram Stretching
Variations on Histogram Stretching
Multi-channel Histogram Stretching
Hue-saturation-value (HSV)
CLAHE

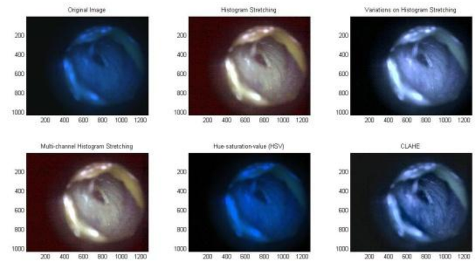
Original Image
Histogram Stretching
Variations on Histogram Stretching
Multi-channel Histogram Stretching
Hue-saturation-value (HSV)
CLAHE

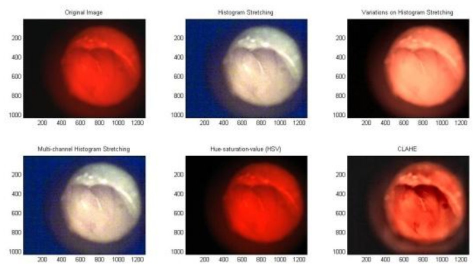
Original Image
Histogram Stretching
Variations on Histogram Stretching
Multi-channel Histogram Stretching
Hue-saturation-value (HSV)
CLAHE

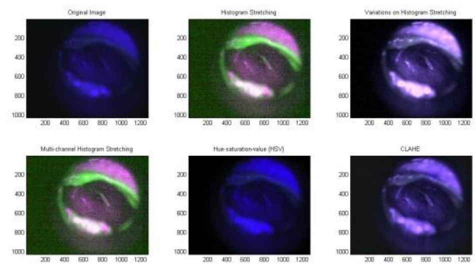
Original Image
Histogram Stretching
Variations on Histogram Stretching
Multi-channel Histogram Stretching
Hue-saturation-value (HSV)
CLAHE

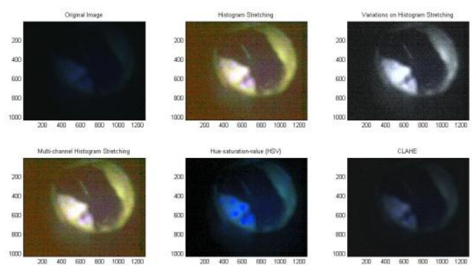
Original Image
Histogram Stretching
Variations on Histogram Stretching
Multi-channel Histogram Stretching
Hue-saturation-value (HSV)
CLAHE

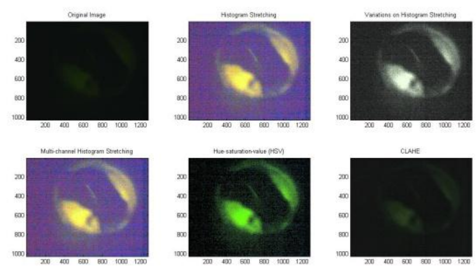
Original Image
Histogram Stretching
Variations on Histogram Stretching
Multi-channel Histogram Stretching
Hue-saturation-value (HSV)
CLAHE

1-8-2014 P1 Left

Images:WL, WBL,BL, B500L, BGL, GL, RL, UVL, UV425L, UV500L

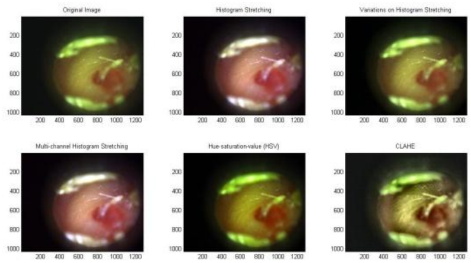

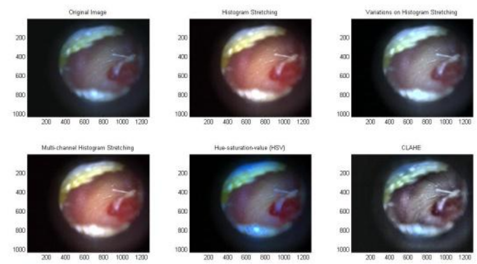

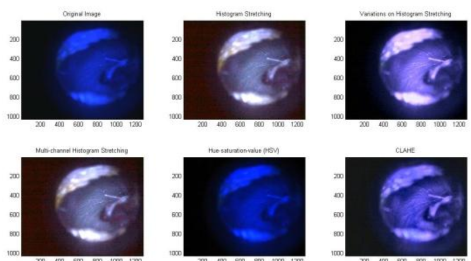

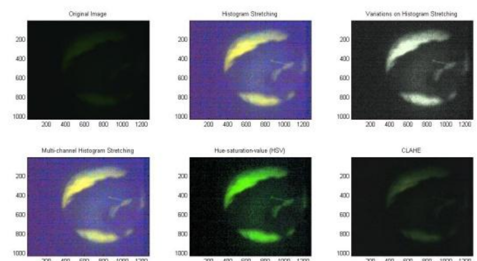

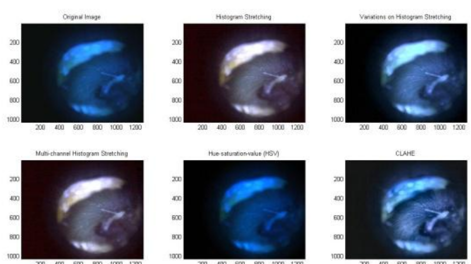

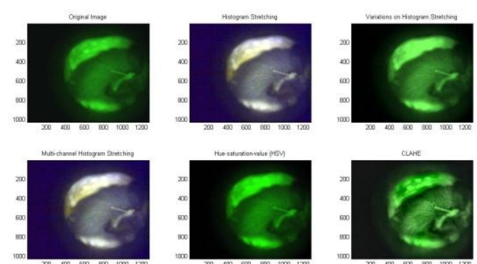

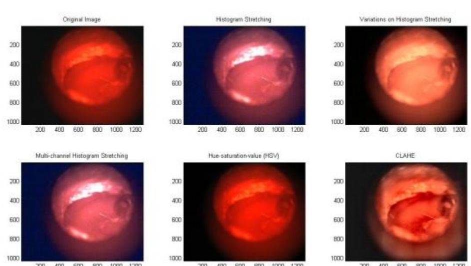

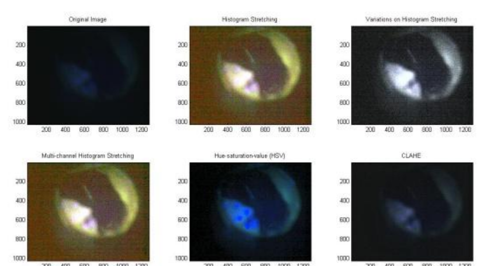

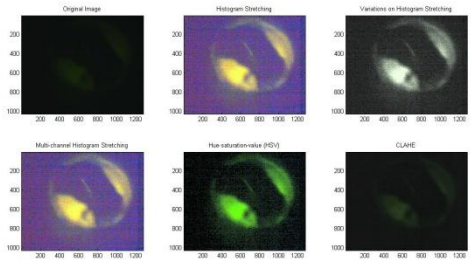
Original Image
Histogram Stretching
Variations on Histogram Stretching
Multi-channel Histogram Stretching
Hue-saturation-value (HSV)
CLAHE